AIRCRAFT DYNAMICS AND NON - LINEAR LANDING GEAR BEHAVIOUR AT TOUCH - DOWN

by

RAMAMOORTHY. R. P.

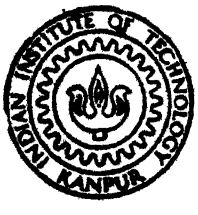

DEPARTMENT OF AEROSPACE ENGINEERING

INDIAN INSTITUTE OF TECHNOLOGY, KANPUR

MAY, 1989

AIRCRAFT DYNAMICS AND NON - LINEAR LANDING GEAR BEHAVIOUR AT TOUCH - DOWN

A Thesis Submitted
in Partial Fulfilment of the Requirements
for the Degree of
MASTER OF TECHNOLOGY

by
RAMAMOORTHY. R. P.

to the
DEPARTMENT OF AEROSPACE ENGINEERING
INDIAN INSTITUTE OF TECHNOLOGY, KANPUR
MAY, 1989

CERTIFICATE

This is to certify that the work entitled **Aircraft Dynamics and Non-Linear Landing Gear Behaviour at Touch-Down** is the record of the work carried out by Mr.Ramamoorthy.R.P. under my supervision and has not been submitted elsewhere for the award of a degree.

Dayanand yadav

April ,1989.

(*Dr. Dayanand Yadav*)
Assistant Professor
Dept.of Aerospace Engineering
Indian Institute of Technology,
Kanpur, India.

A C K N O W L E D G M E N T S

I would like to express my indebtedness to Dr.Dayanand Yadav for his invaluable guidance and inspiration throughout the tenure of this work.

I am grateful to Mr.Arun Kumar for furnishing the necessary data for my thesis.

Thanks are also extended to Aeronautical Development Agency (India), for supporting me financially for a few months during my work.

RAMAMOORTHY.R.P.

TABLE OF CONTENTS

Chapter		Page
	CERTIFICATE	i
	ACKNOWLEDGMENTS	ii
	TABLE OF CONTENTS	iii
	LIST OF FIGURES	vi
	LIST OF TABLES	xii
	NOMENCLATURE	xiii
	ABSTRACT	xviii
1.	INTRODUCTION	1
	1.1 Review of Past Work	3
	1.2 Scope of the Present Work	6
	1.3 Layout of the Thesis	8
2.	MODELING OF THE LANDING GEAR	9
	2.1 Mechanics of the Levered Landing Gear	9
	2.2 Analysis of the Heave Model	14
	2.2.1 Equations of Motion with Shock Strut Locked	15
	2.2.2 Equations of Motion with the Shock Strut Unlocked	18
	2.3 Analysis of the Heave-Pitch Model	20

2.3.1 Equations of Motion with Main Gear and Nose Gear Locked 22
2.3.2 Equations of Motion with Nose gear Locked and Main gear Unlocked 25
2.3.3 Equations of Motion with Main Gear Locked and Nose Gear Unlocked 27
2.3.4 Equations of Motion with Both Main Gear and Nose Gear Unlocked 31
2.4 Forces in the Shock Strut 33
2.4.1 Pneumatic Forces 33
2.4.2 Hydraulic Forces 34
2.4.3 Friction Forces 35
2.5 Forces on the Tyre 36
3. RESULTS AND DISCUSSIONS 38
3.1 Parametric Study of the Heave Model 40
3.1.1 Effect of Orifice Discharge Coefficient 40
3.1.2 Effect of Orifice Diameter 54
3.1.3 Effect of Polytropic Index 63
3.1.4 Effect of Initial Air Volume 63
3.1.5 Effect of Initial Air Pressure 76
3.2 Parametric Study of the Heave-Pitch Model 83
3.2.1 Effect of Pitching Moment of Inertia of the Aircraft 83
3.2.2 Effect of Landing Gear Location with Reapect to Aircraft Center of Gravity 96

4. CONCLUSIONS AND RECOMMENDATIONS 112

4.1 Conclusions 112

4.1.1 The Heave Model 112

4.1.2 The Heave-Pitch Model 113

4.2 Suggestions for Further Invesigation 114

REFERENCES 115

APPENDIX 117

LIST OF FIGURES

Figures		Page
2.1	Articulated landing gear	10
2.2a	Geometry of the levered landing gear	13
2.2b	Kinematics of the levered landing gear	13
2.3	Dynamic system of the heave model	16
2.4	Heave-pitch model	21
3.1a	Variation in displacement of the sprung mass with orifice discharge coefficient (0.2 & 0.4)	41
3.1b	Variation in displacement of the sprung mass with orifice discharge coefficient (0.6, 0.8 & 1.0)	42
3.1c	Variation in displacement of the unsprung mass with orifice discharge coefficient (0.2 & 0.4)	43
3.1d	Variation in displacement of the unsprung mass with orifice discharge coefficient (0.6, 0.8 & 1.0)	44
3.1e	Variation in velocity of the sprung mass with orifice discharge coefficient	45
3.1f	Variation in velocity of the unsprung mass with orifice discharge coefficient(0.2 & 0.4)	46

3.1g	Variation in velocity of the unsprung mass with orifice discharge coefficient(0.6, 0.8 & 1.0)	47
3.1h	Variation in acceleration of the sprung mass with orifice discharge coefficient(0.2 & 0.4)	48
3.1i	Variation in acceleration of the sprung mass with orifice discharge coefficient(0.6 & 0.8 & 1.0)	49
3.1j	Variation in acceleration of the unsprung mass with orifice discharge coefficient(0.2 & 0.4)	50
3.1k	Variation in acceleration of the unsprung mass with orifice discharge coefficient (0.6, 0.8 & 1.0)	51
3.2a	Variation in displacement of the sprung mass with orifice diameter	56
3.2b	Variation in displacement of the unsprung mass with orifice diameter	57
3.2c	Variation in velocity of the sprung mass with orifice diameter	58
3.2d	Variation in velocity of the unsprung mass with orifice diameter	59
3.2e	Variation in acceleration of the sprung mass with orifice diameter	60
3.2f	Variation in acceleration of the unsprung mass with orifice diameter	61

3.3a Variation in displacement of the sprung mass with polytropic index 64

3.3b Variation in displacement of the unsprung mass with polytropic index 65

3.3c Variation in velocity of the sprung mass with polytropic index 66

3.3d Variation in velocity of the unsprung mass with polytropic index 67

3.3e Variation in acceleration of the sprung mass with polytropic index 68

3.3f Variation in acceleration of the unsprung mass with polytropic index 69

3.4a Variation in displacement of the sprung mass with initial air volume 70

3.4b Variation in displacement of the unsprung mass with initial air volume 71

3.4c Variation in velocity the sprung mass with initial air volume 72

3.4d Variation in velocity of the unsprung mass with initial air volume 73

3.4e Variation in acceleration of the sprung mass with initial air volume 74

3.4f Variation in acceleration of the unsprung mass with initial air volume 75

3.5a Variation in displacement of the sprung mass with initial air pressure 77

3.5b Variation in displacement of the unsprung mass with initial air pressure 78

3.5c Variation in velocity of the sprung mass with initial air pressure 79

3.5d Variation in velocity of the unsprung mass with initial air pressure 80

3.5e Variation in acceleration of the sprung mass with initial air pressure 81

3.5f Variation in acceleration of the unsprung mass with initial air pressure 82

3.6a Variation in displacement of the sprung mass with the pitching moment of inertia 84

3.6b Variation in pitching response of the sprung mass with the pitching moment of inertia 85

3.6c Variation in displacement of the nose wheel with the pitching moment of inertia 86

3.6d Variation in displacement of the main wheel with the pitching moment of inertia 87

3.6e Variation in velocity of the sprung mass with the pitching moment of inertia 88

3.6f Variation in velocity of pitching of the sprung mass with the pitching moment of inertia 89

3.6g Variation in velocity of the nose wheel with the pitching moment of inertia 90

3.6h Variation in velocity of the main wheel with the pitching moment of inertia 91

3.6i Variation in acceleration of the sprung mass with the pitching moment of inertia 92

3.6j Variation in acceleration of pitching of the sprung mass with the pitching moment of inertia 93

3.6k Variation in acceleration of the nose wheel with the pitching moment of inertia 94

3.6l Variation in acceleration of the main wheel with the pitching moment of inertia 95

3.7a Variation in displacement of the sprung mass with the distance of aircraft c.g. from the main gears 97

3.7b Variation in pitching response of the sprung mass with the distance of aircraft c.g. from the main gears 98

3.7c Variation in displacement of the nose wheel with the distance of aircraft c.g. from the main gears 99

3.7d Variation in displacement of the main wheel with the distance of aircraft c.g. from the main gears 100

3.7e Variation in velocity of the sprung mass with the distance of aircraft c.g. from the main gears 101

3.7f	Variation in velocity of pitching of the sprung mass with the distance of aircraft c.g. from the main gears	102
3.7g	Variation in velocity of the nose wheel with the distance of aircraft c.g. from the main gears	103
3.7h	Variation in velocity of the main wheel with the distance of aircraft c.g. from the main gears	104
3.7i	Variation in acceleration of the sprung mass with the distance of aircraft c.g. from the main gears	105
3.7j	Variation in acceleration of pitching of the sprung mass with the distance of aircraft c.g. from the main gears	106
3.7k	Variation in acceleration of the nose wheel with the distance of aircraft c.g. from the main gears	107
3.7l	Variation in acceleration of the main wheel with the distance of aircraft c.g. from the main gears	108
A1	Load-deflection curve for the main wheel	121
A2	Load-deflection curve for the nose wheel	122

LIST OF TABLES

Table		Page
1	Variation in the peak values of the shock strut forces and tyre forces and the shock strut stroke with C_d	52
2a	Variation in the extreme values of displacement and acceleration of the sprung mass with C_d	53
2d	Variation in the extreme values of displacement and acceleration of the unsprung mass with C_d	53
3	Variation in the peak values of the shock strut forces and tyre forces and the shock stroke with orifice diameter	55
4a	Variation in the extreme values of displacement and acceleration of the sprung mass with orifice diameter	62
4b	Variation in the extreme values of displacement and acceleration of the unsprung mass with orifice diameter	62
5a	Variation in the extreme values of displacements with the distance of the main gear from the aircraft center of gravity	109
5b	Variation in the extreme values of acceleration of the airframe with the distance of the main gear from the aircraft center of gravity	110
5c	Variation in the extreme values of acceleration of the wheels with the distance of the main gear from the aircraft center of gravity	110

NOMENCLATURE

A_a	Pneumatic area
A_h	Hydraulic area
A_n	Orifice area (main or recoil)
A_o	Distance between the axle of the main wheel and the point of attachment of the main gear with the airframe
$A_1 \ldots A_6$	Geometrical parameters describing the configuration of the landing gear in the fully extended condition
A_7	Term defined in equation (2.2)
B_2, B_3	Terms defined in equation (2.23) and (2.58)
$B_4 \ldots B_8$	Terms defined in equation (2.24)
C_d	Orifice discharge coefficient (main or recoil)
F_a	Pneumatic force in the shock strut
F_{fj}	Journal friction force in the shock strut
F_{fs}	Seal friction force in the shock strut
F_h	Hydraulic force in the shock strut
F_{ha}	Horizontal reaction from the wheel axle on the trailing arm
F_{hg}	Horizontal ground reaction on the wheel
F_n	Normal load on the shock strut
F_s	Force on the Shock strut

F_{va}	Vertical reaction from the wheel axle on the trailing arm
F_{vg}	Vertical ground reaction on the tyre
F_1	Normal force on the upper bearing of the shock strut
F_2	Normal force on the lower bearing of the shock strut
g	Acceleration due to gravity
h	Vertical distance of aircraft center of gravity from ground level
I_w	Polar moment of inertia of the wheel assembly
I_{yy}	Pitching moment of inertia of the aircraft about its center of gravity
L	Lift force acting on the aircraft
l_{ac}	Distance of the aerodynamic center of the aircraft measured in the forward direction from its center of gravity
l_m	Distance between aircraft center of gravity and the main wheel
l_n	Distance between aircraft center of gravity and the nose wheel
l_x, l_z	Terms defined in equation (2.15)
l_1	Axial distance between upper and lower bearings on extended shock strut
l_2	Axial distance between lower bearing of the shock strut and the pin joint of the piston

m	Coefficient depending on various regimes of tyre deflection
p	Term defined in equation (2.9)
p_a	Instantaneous air pressure in the shock strut
p_{ao}	Initial air pressure in the shock strut
$[\ P\ ]$	Matrix defined in equations (2.59) and (2.66)
$P_{11}...P_{44}$	Elements of P matrix
q_1, q_2	Terms defined in equation (2.9)
q_3, q_4	Terms defined in equations (2.9) and (2.56)
q_5	Term defined in equation (2.15)
r	Constant corresponding to various regimes of tyre deflection
r_d	Radius of the tyre in the deflected condition
$\{\ R\ \}$	Matrix defined in equations (2.59) and (2.66)
$R_{11}...R_{44}$	Elements of R matrix
s	stroke of the shock strut
s_o	Extended length of the shock strut
s_t	length of the shock strut at any instant
V_{a_o}	Initial air volume in the shock strut
V_{h_o}	Horizontal velocity of the aircraft
V_{o_o}	Initial oil volume in the shock strut
W	Portion of the aircraft weight acting on the landing gear in heave model
	Total weight of the aircraft in the heave-pitch model
W_a	Weight of airframe and nose wheel assembly
W_b	Weight of airframe and main wheel assembly

W_1	Weight of sprung mass
W_2	Weight of unsprung mass in heave model
W_3	Weight of nose wheel assembly
W_4	Weight of main wheel assembly
x	Horizontal travel of the wheel axle in the levered gear
$y_A..y_E$	Lateral distance of the shock strut joints A...E from aircraft center line
z_1	Vertical displacement of the sprung mass
z_2	Vertical displacement of the unsprung mass in the heave model
z_3	Vertical displacement of nose wheel axle
z_4	Vertical displacement of main wheel axle
z_m	Vertical displacement of the attachment point of the main gear
z_n	Vertical displacement of the attachment point of the nose gear
$\{ Z \}$	Displacement vector as used in equations (2.59) and (2.66)
β	Bulk modulus of oil
δ	Angle as defined in equation (2.2)
ϕ_t	Inclination of the axis of the shock strut with the vertical at any instant of time t
μ_g	Coefficient of ground friction

μ_{j1}, μ_{j2}	Coefficients of friction of upper and lower bearings of the shock strut
μ_s	Coefficient of seal friction
θ_o	Inclination of the trailing arm in the airborne configuration of the landing gear
θ_t	Inclination of the trailing arm from the vertical at any instant of time t
ρ	Mass density of hydraulic fluid
subscript m	For the main gear
subscript n	For the nose gear
$\dot{(\ )}$	First derivative with respect to time
$\ddot{(\ )}$	Second derivative with respect to time

A B S T R A C T

An analysis has been presented for determining the dynamic response of an articulated non-linear landing gear at touch-down. The analysis with the aircraft modeled as a rigid lumped mass in heave has been extended to a heave-pitch model with an articulated nose landing gear and telescopic main landing gears. In developing the system equations oil compressibility effects, kinematics of the articulation of the gear, drag loads on the tyre and pneumatic, hydraulic and frictional forces in the shock strut have been included. A parametric study of the orifice discharge coefficient, polytropic index of air compression process, orifice diameter, initial air volume and initial air pressure on the heave model and the pitching moment of inertia and the landing gear layout configuration on the heave- pitch model of the aircraft have been carried out. Numerical results have been obtained for a light fighter - trainer aircraft by numerically integrating the coupled non-linear differential equations of motion.

CHAPTER 1

INTRODUCTION

In order to cater to the requirements of landing impact and ground roll, the landing gear of an aircraft functionally consists of a wheel unit and a shock absorber unit. In the past, the shock absorbing characteristics of an aircraft were developed by means of extensive trial and error drop testing. However, the drop testing does not properly simulate the aerodynamic forces on the aircraft. Moreover, the expense and time required for such an approach emphasizes the need for suitable theoretical methods and appropriate computer simulation for the analysis of the landing gear behavior. Such a rational method finds application in :

- -determining the behavior of a given landing gear to varying impact conditions.
- -developing new landing gear configurations to suit given impact condition.
- -determination of wheel spin-up and spring-up loads which takes into account the shock absorbing characteristics.
- -determination of dynamic loads in flexible aircraft structures during landing.
- -estimation of airframe structural fatigue and fatigue of undercarriage load attachment points.

Apart from the effect of vibration on airframes, it is

also necessary to consider the influence of vibration environment on crew and passengers. In some cases, the cockpit vibration in the vertical plane can degrade the pilot's ability to read the instruments accurately and perform correct control operations. Simulation studies suggest that simultaneous exposure to vertical acceleration greater than 0.6g at 3 Hz and horizontal acceleration greater than 0.1g at 2 Hz may cause some loss of visual acuity [1]. It is known that cockpit vibration levels are greater than that experienced at aircraft mass center due to the pitching motion. Thus pilots will be more influenced by vibration than passengers. With regards to the effect of critical frequencies on human beings, human response to both harmonic and random vibrations is most critical between 1 Hz and 5 Hz and it is in this range that most air-frame vibrations are excited [2].

Since many aspects of landing impact problems are so intimately connected with the mechanics of landing gear, the subject of landing gear behavior has received analytical treatment at various times. Many of the earlier investigations in order to reduce the mathematical complexity of the analysis, were limited to consideration of highly simplified linear systems, which have little relation to the actual landing gears. Some of the later works, consider with varying degrees of simplification, more realistic non-linear systems.

Taxiing induced vibrations in large aircraft due to run-way unevenness has also been recognized as a significant factor in metal fatigue damage, dynamic stressing of airframes as well as crew and passenger discomfort. Such

taxiing loads applied to an airframe should not be ignored since their cumulative effects represents a considerable proportion of fatigue damage. The fatigue life of the undercarriage at its point of attachment with airframe as well as associated structural components should also be considered as an important design case. Many investigators have studied the effects of runway induced vibrations on landing gear.

Based on geometrical disposition, landing gears are classified as telescopic or non-articulated, levered or articulated and semi-levered or semi-articulated [3]. Though there are a number of aircrafts with articulated and semi-articulated landing gears, most of the published literature deals only with the behaviour of telescopic landing gears. the present work analyses heave and pitch models of an aircraft with articulated landing gears.

1.1 REVIEW OF PAST WORK

Since the dynamic conditions present during landing impact are often critical, from very early days considerable emphasis was given to the accurate prediction of landing gear behavior in the landing run.

Schlaefke [4] analyzed a telescopic landing gear in which the spring was considered to be linear and for the first time assumed the damping to be proportional to the square of the spring compression velocity. From the study, he drew a disputable conclusion that the realization of quadratic damping law would offer no advantage over linear damping.

Milwitzky and Cook [5] made a theoretical study of behavior of a telescopic oleo-pneumatic landing gear during the process of landing impact. The analysis treated the motions of landing gear prior to and subsequent to the beginning of shock strut deflection. In the first phase of landing impact, a single degree of freedom system was solved in order to determine the conditions at the instant of initial shock strut deflection, after which a two degrees of freedom system was solved. The analysis considered such factors as hydraulic (velocity squared) resistance of orifice, the forces due to air compression and internal friction in the shock strut, non- linear force-deflection characteristics of the tyre, wing lift, the inclination of landing gear and the effect of wheel spin-up and drag loas. In addition to this exact treatment, investigations were also made to determine the extent to which the basic equations of motion could be be simplified and yet yield acceptable results. Most of the specific solutions were obtained by "linear procedure" which assumes the changes in the variables to be linear over finite time intervals. A few of the specific solutions were also obtained by "quadratic procedure" and the generalised solutions of equations of motions were obtained with the well known Runge- Kutta method.

An analog simulation of landing impact and initial ground run was performed by Wahi [6]. He included in his work the internal friction in shock strut, wing lift, inclination of landing gear and effects of wheel spin-up and drag loads. The discharge coefficient was treated as function of Reynold's

number, orifice shape and orifice orientation. An iterative procedure was adopted for the solution. His later paper [7] included the effects of hydraulic fluid compressibility, gas solubility, and its entrainment in oil, and the varying nature of polytropic exponent during compression stroke.The model chosen by Wahi was a heave model in which the pitching of the aircraft was not accounted for.

Nightingale [8] described an approximate method for predicting landing gear performance from a `step-by-step' calculation by assuming a load-stroke curve for an articulated landing gear. Equations were developed for a telescopic landing gear with a vertical strut and later modified to include telescopic landing gears with inclined strut and levered landing gear. A simple model was considered for the analysis. The aircraft was modeled as a single mass, supported by an oleo-pneumatic shock strut and a tyre in series. The tyre was taken to be an undamped linear spring and the landing was assumed to be fully airborne. The effects of surface friction and the mass of wheel were not considered in the analysis.

Others also have analysed the behavior of articulated landing gear as extension of telescopic landing gear. In all these works, a single degree of freedom system was solved neglecting the unsprung mass. Mechanical advantage and velocity ratio were obtained from layout drawings of the gear and were used for obtaining landing impact transients. The kinematic relation between wheel axle travel and shock strut deflection were not introduced in these mathematical models.

Jayarami Reddy et al [9] developed dynamic equations

with kinematic relations as a part of analysis for an articulated landing gear. He considered in his work velocity squared damping, seal and journal friction and treated the tyre as an undamped non-linear spring. On impact only the tyre was assumed to compress and hence a single degree of freedom system was solved. Once the force in the shock-strut exceeded its pre-load, the shock-strut became active and a two degrees of freedom system was solved. A fourth order Runge-Kutta method was used for solving the coupled non-linear equations of motion. A semi- levered suspension type landing gear was also analysed by the same authors [10]. This investigation included the effects of oil compressibility and considered the wheel spin-up as a function of slip ratio. Both these works assumed only a heave model in which the pitching motion of the aircraft was not considered.

1.2 SCOPE OF THE PRESENT WORK

The present work develops an analysis for the determination of the response of an aircraft at touch-down. Initially the aircraft is idealised to a single rigid mass supported on a levered landing gear. The hydraulic, pneumatic and friction forces of the shock strut and the linkage dynamics of the gear have been taken into account for the study. Other factors included are the wing lift forces and the drag loads on the wheel during its spin-up.

Due to the complicated nature of the thermodynamic process occurring in the shock strut at impact no consensus exist on the exact value of the polytropic index of air

compression at these condition. The coefficient of orifice discharge and the area of orifice also varies with the shock strut stroke due to the presence of metering pin and is different for compression stroke and expansion stroke. Therefore the variation in the dynamic response of aircraft to different values of these parameters are investigated.

To make this model more realistic the pitching motion of the aircraft is included in the second model. The aircraft considered is assumed to possess a levered nose gear and telescopic main landing gear. Since the main gears are usually located fairly close to the nodal points of the fundamental bending mode of the wing, the landing gear performance is not significantly affected by the elastic deformtion of the wing. In the case of large supersonic transports which have large slender bodies, elastic modes in the longitudinal direction may also be considerable For smaller aircrafts the airframe may be assumed to be rigid without significant loss of accuracy. The flexible modes may also be incorporated in this study by the simultaneous solution of the equations of motion of the landing gear coupled with those equations representing the additional degrees of freedom of the structure.

Rolling and yawing of the aircraft is not included in developing the system response. The pilot's input to the system is also not considered because of lack of reliable information regarding pilot's action at touch down.

The effects of the variations in the pitching radius of gyration and the location of landing gear with reference to

the center of gravity of the aircraft is also studied.

By changing the parameters described above a spectrum of responses is developed. In all these cases the following quantities were determined :

a. translation, velocity and acceleration of the wheels.

b. vertical translation, velocity and acceleration of the center of gravity of the aircraft.

c. pitching of the aircraft about its center of gravity.

The dynamic response so obtained can be used for determining the load factors, ground clearance and other standards specified by the international agencies to determine whether any damage has occurred.

1.3 LAYOUT OF THE THESIS

The general layout of the thesis is presented below. Idealization of the aircraft and the details of the development of system equations are dealt in chapter 2. A parametric study on the landing gears of the aircraft and its effects on the aircraft response during landing impact are covered in chapter 3. Chapter 4 presents the conclusions drawn from the study and suggestion for further investigations in this area.

CHAPTER - 2

MODELING OF THE LANDING GEAR

The accuracy with which the behaviour of any dynamic system is predicted depends to a large extent on the model chosen to idealize the physical system. The present work analyses the response of an aircraft with articulated nose gear and telescopic main gears. Two models have been considered for the analysis. First, a heave model is studied for a levered gear with linkage dynamics included as a part of the analysis. This is extended to a heave-pitch model for the aircraft which includes the full kinematics of the articulated nose gear and conventional telescopic main gears. The landing gears are assumed to be infinitely rigid in bending and the external lift forces are assumed to act throughout the impact and ground-roll. The analysis also includes the oil compressibility effects, pneumatic, hydraulic and friction forces in the shock strut.

2.1 MECHANICS OF THE LEVERED LANDING GEAR

The type of articulated landing gear analyzed is shown in fig 2.1. The shock strut (ED) of the gear is hinged at both ends and hence experiences only axial loads. The trailing arm

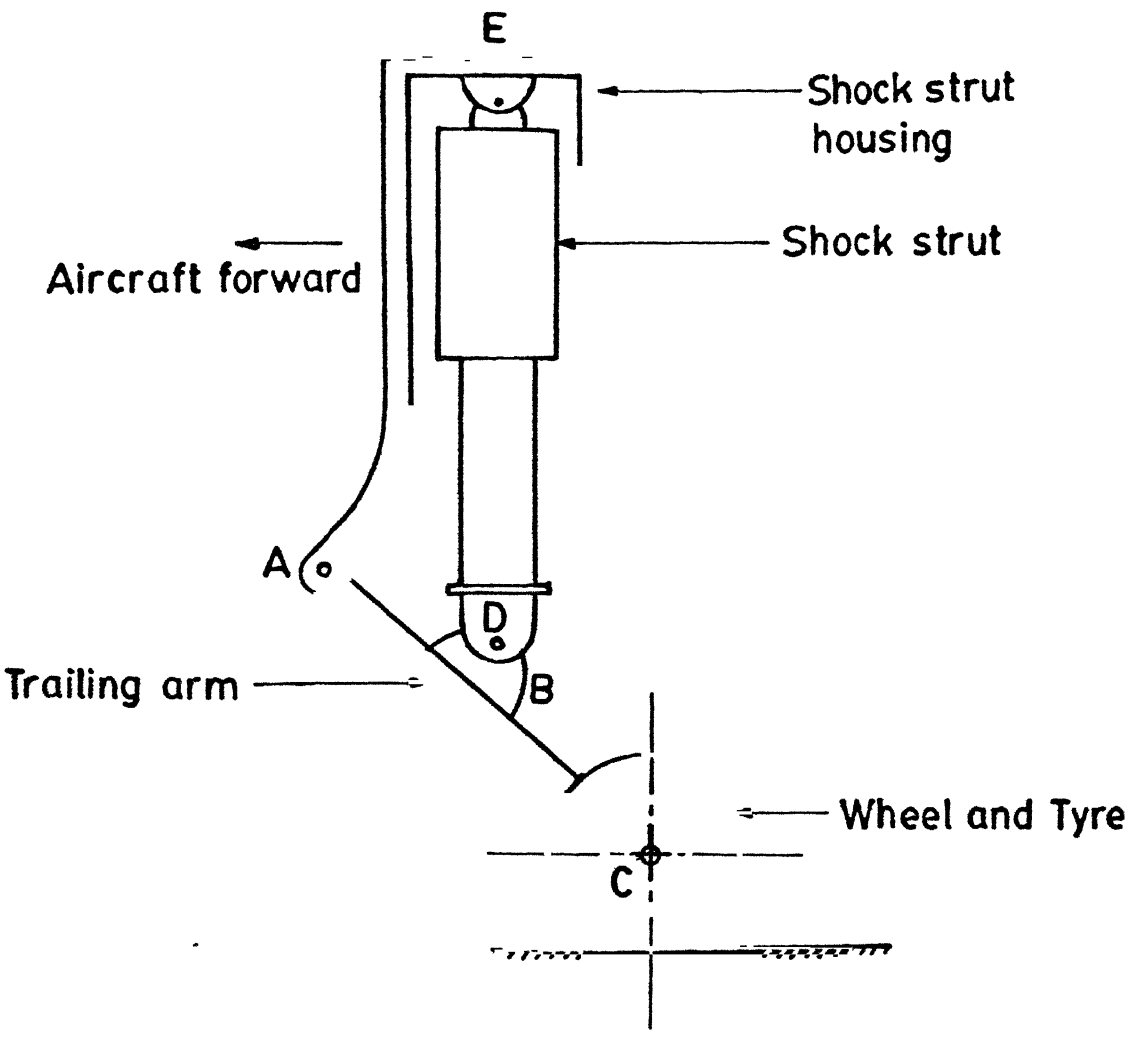

FIG. 2·1 ARTICULATED LANDING GEAR

(AC) has the wheel axle at its lower end (C). The housing of the shock strut is mounted on the aircraft which has a fork hinge (A) at its bottom for receiving the upperend of the trailing arm and fork end (E) at its top for receiving the cylinder eye end of the shock strut. The piston eye end (D) is hinged to the trailing arm through a rigid link (BD). The hinges at A and E are thus fixed with references to the airframe.

Figure 2.2a shows the geometric layout of the landing gear in the fully extended condition when the aircraft is airborne. During the process of landing, the trailing arm moves from its original position AC to the deflected position AC' in an arc of circle with A as center, shifting the axis of the shock strut from ED to ED' (fig 2.2b). The relative motion between the aircraft mass and the wheel compresses the shock strut (ED) producing the necessary resistance in the form of pneumatic, hydraulic and friction forces.

The inclination of the trailing arm with the vertical θ_t at any instant of time t is

$$\theta_t = \text{Cos}^{-1}\left[\frac{A_6 - (z_1 - z_2)}{A_5}\right] \qquad \ldots(2.1)$$

where

$A_1..A_6$ = geometrical parameters describing the configuration of the landing gear in the fully extended condition

z_1 = vertical displacement of the aircraft mass

z_2 = vertical travel of wheel axle

The extended length of the shock strut s_o is obtained from the geometry. Thus,

$$s_o = \left\{ [A_7 \, \mathrm{Sin}(\theta_o+\delta)-A_1]^2 + [A_7 \, \mathrm{Cos}(\theta_o+\delta)+A_5)]^2 + [y_D - y_E]^2 \right\}^{1/2} \quad \ldots(2.2)$$

where

$$A_7 = \left\{ A_2^2 + A_4^2 \right\}^{1/2}$$

$$\delta = \mathrm{Tan}^{-1} [A_4 / A_2]$$

$y_A \ldots y_E$ = lateral distance of the shock strut joints A...E from the center line of the aircraft

θ_o = inclination of the trailing arm from the vertical in the airborne configuration of the landing gear

The compressed length of the shock strut s_t at any instant of time t can be obtained from equation (2.2) by using the current value θ_t for the inclination of the trailing arm in place of θ_o

$$s_t = \left\{ [A_7 \, \mathrm{Sin}(\theta_t+\delta)-A_1]^2 + [A_7 \, \mathrm{Cos}(\theta_t+\delta)+A_5)]^2 + [y_D - y_E]^2 \right\}^{1/2} \quad \ldots(2.3)$$

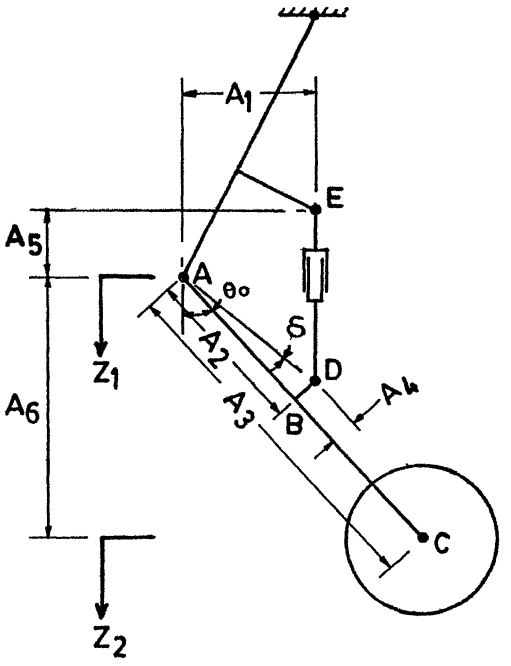

FIG. 2·2a GEOMETRY OF THE LEVERED LANDING GEAR

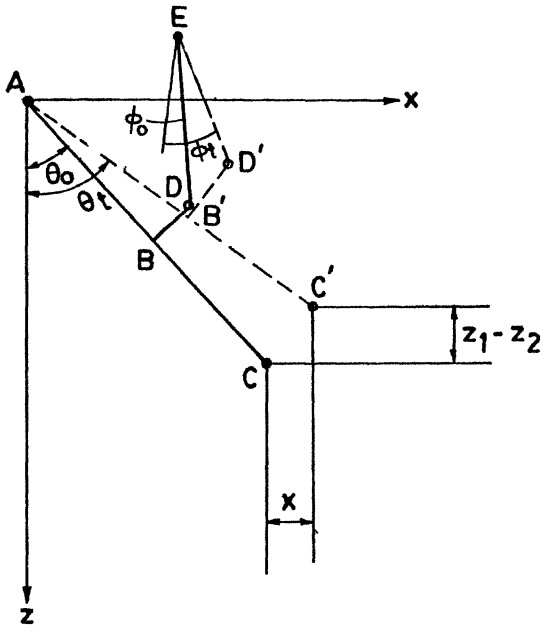

FIG 2 2b KINEMATICS OF THE LEVERED LANDING GEAR

The shock strut stroke is therefore $s = s_o - s_t$ ...(2.4)

Differentiating equation (2.4), the telescoping velocity of the shock strut is obtained. Thus,

$$\dot{s} = \frac{A_7(z_1 - z_2)\left\{ A_5 \operatorname{Sin}(\theta_t + \delta) + A_4 \operatorname{Cos}(\theta_t + \delta) \right\}}{A_3 \operatorname{Sin} \theta_t \; s_t} \qquad \ldots(2.5)$$

From the geometry, the horizontal travel x of the wheel axle is

$$x = A_3 (\operatorname{Sin} \theta_t - \operatorname{Sin} \theta_o) \qquad \ldots(2.6)$$

Differentiation of the above expression gives the horizontal velocity and acceleration of the wheel as

$$\dot{x} = q_1(\dot{z}_1 - \dot{z}_2) \qquad \ldots(2.7)$$

$$\ddot{x} = q_1(\ddot{z}_1 - \ddot{z}_2) - q_2(\dot{z}_1 - \dot{z}_2)^2 \qquad \ldots(2.8)$$

where

$$q_1 = \operatorname{Cot} \theta_t \qquad \ldots(2.9)$$

$$q_2 = 1/A_3 \operatorname{Sin}^3 \theta_t$$

2.2 ANALYSIS OF THE HEAVE MODEL

The dynamic system considered for the analysis is shown in figure 2.3.Oleo-pneumatic struts are inflated to some finite

air pressure in the fully extended position. The strut doesn't begin to deflect in an impact until sufficient force is developed to overcome the preload F_{s0} due to the extended air pressure and internal friction. Since the struts are comparatively rigid in bending and compression , initially the shock strut is locked and the tyre alone compresses with the system behaving as a single degree of freedom system. Once, the preload is exceeded, the shock strut becomes operational and the system is converted to one with two degrees of freedom.

2.2.1 Equations of Motion with Shock Strut Locked

In the locked condition of the shock strut, the aircraft and the wheel moves as a whole and hence the system is modeled as a single degree of freedom system.

Equation of motion for this model in the vertical direction is

$$\frac{W}{g}\ddot{z} + L - W + F_{vg} = 0 \qquad \ldots(2.10)$$

where

W = portion of aircraft weight acting on the landing gear

L = aerodynamic lift force on the aircraft

F_{vg} = vertical ground reaction on the tyre

z = vertical translation of the aircraft and the wheel mass

From the force equilibrium of the sprung mass in the vertical direction, the vertical component of the force in the

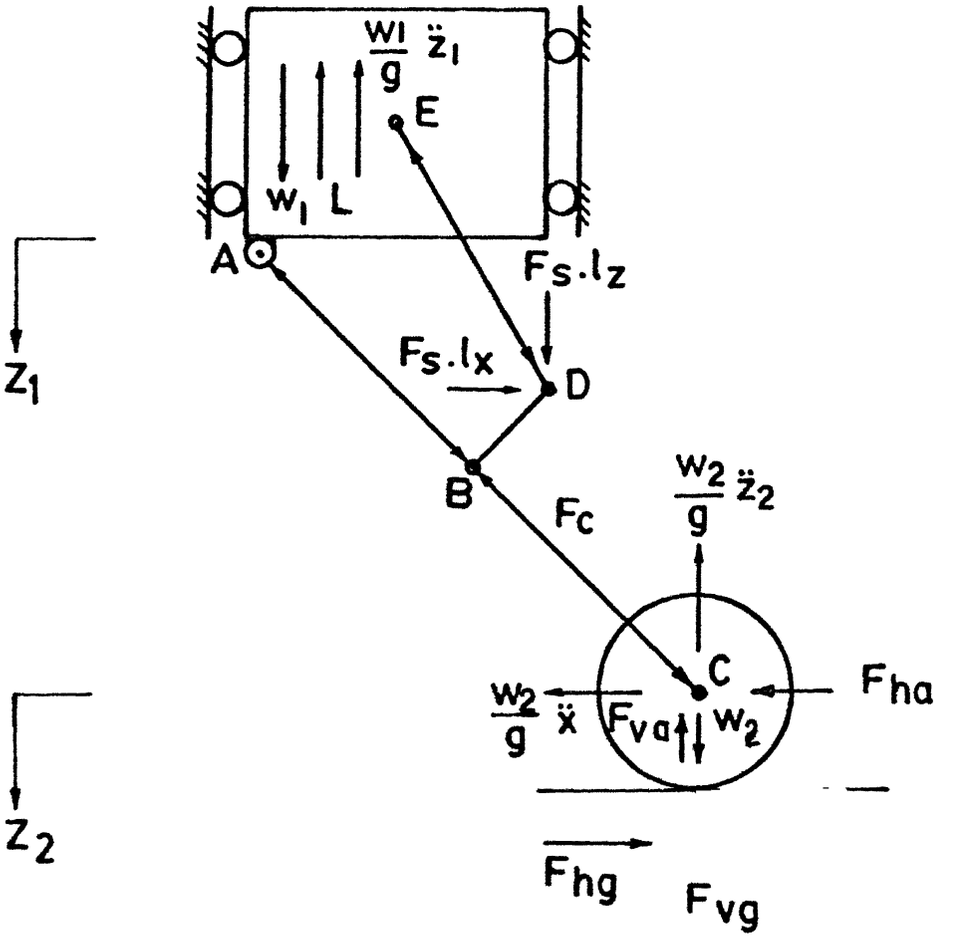

FIG. 2-3 DYNAMIC SYSTEM OF THE HEAVE MODEL

trailing arm F_{va} is obtained as

$$F_{va} = W_i - L - \frac{W_i}{g} \ddot{Z} \qquad \ldots(2.11)$$

where W_i is the weight of the upper sprung mass

In the locked configuration of the landing gear the horizontal component of the force in the trailing arm F_{ha} can be determined from the force equilibrium of the wheel as

$$F_{ha} = - F_{hg} \qquad \ldots(2.12)$$

where F_{hg} is the horizontal ground reaction on the wheel due to ground friction.

The inclination of the axis of the shock strut ϕ_t with the vertical at any instant of time t is

$$\phi_t = \text{Tan}^{-1} \left[\frac{A_7 \, \text{Sin}(\theta_t + \delta) - A_4}{A_7 \, \text{Cos}(\theta_t + \delta) + A_5} \right] \qquad \ldots(2.13)$$

The force F_s in the shock strut is obtained from the balance of moments about the hinge A of the trailing arm. Thus,

$$F_s = \frac{F_{va} - F_{ha} \, q_4}{q_5} \qquad \ldots(2.14)$$

where

q_4 quantity defined in equation (2.9)

$$q_5 = \frac{A_7 \, [\, l_z \text{Sin}(\theta_t + \delta) - l_x \text{Cos}(\theta_t + \delta) \,]}{A_8 \, \text{Sin} \, \theta_t}$$

l_z = Cos ϕ_t

l_x = Sin ϕ_t

The force F_s in the shock strut is monitored continuously. The system transits from one to two degrees of freedom system when the force in the shock strut exceeds its preload F_{s0}. The state at which $F_s = F_{s0}$ gives the initial condition for the solution of the two degrees of freedom system.

2.2.2 Equations of Motion With shock Strut Unlocked

Once the shock strut becomes operational, the sprung mass and the unsprung mass displace separately therefore the system is modeled as one with two degrees of freedom.

Vertical equilibrium of the sprung mass is

$$F_{va} + L - W_1 + \frac{W_1}{g} \ddot{z}_1 = 0 \qquad \ldots(2.16)$$

Equation of motion of the unsprung mass in the vertical and horizontal directions are

$$F_{va} + W_2 - F_{vg} - \frac{W_2}{g} \ddot{z}_2 = 0 \qquad \ldots(2.17)$$

$$F_{hg} = \frac{W_2}{g} \ddot{x} - F_{ha} \qquad \ldots(2.18)$$

Substituting for $\ddot{x}$ from equation (2.8)in equation (2.18) yields

$$F_{ha} = q_3 (\ddot{z}_1 - \ddot{z}_2) + q_4 \qquad \ldots(2.19)$$

where

$$q_3 = \frac{W_2}{g} q_1$$

$$q_4 = -\left[\frac{W_2}{g} q_2 (\dot{z}_1 - \dot{z}_2) + F_{hg} \right] \quad \ldots(2.20)$$

q_1 , q_2 quantities defined in equation (2.9)

From the moment equilibrium of the trailing arm about the hinge A, the vertical component of the force in the trailing arm F_{va} can be obtained as

$$F_{va} = q_5 F_3 + q_4 F_{ha} \quad \ldots(2.21)$$

Eliminating F_{ha} from equations (2.19) and (2.21) yields on simplification

$$F_{va} = B_2 + B_3 (\ddot{z}_1 - \ddot{z}_2) \quad \ldots(2.23)$$

where

$$B_2 = q_5 F_3 + q_4 q_4$$

$$B_3 = q_4 q_3$$

Let

$$B_4 = B_2 + L - W_1$$

$$B_5 = B_2 + W_2 - F_{vg}$$

$$B_6 = B_3 + W_1 / g \quad \ldots(2.24)$$

$$B_7 = B_3 + W_2 / g$$

$$B_8 = B_3^2 - B_6 B_7$$

Substitution of equations (2.22) and (2.24) in the equations of motion (2.16) and (2.17) yields on simplification

$$\ddot{z}_1 = [B_7 B_4 - B_3 B_5] / B_8 \quad \ldots(2.25)$$

$$\ddot{Z}_2 = [\, B_2 B_4 - B_5 B_3]/B_1 \qquad \ldots(2.26)$$

The coupled non-linear differential equations (2.25) and (2.26) are the system equations of motion which are solved numerically by standard routines.

2.3 ANALYSIS OF THE HEAVE-PITCH MODEL

The heave model considered in section 2.2 is improved to a heave pitch model by considering the operations of the nose and the main wheels separately so as to account for the pitching motion of the aircraft. Figure 2.4 shows the model used for the analysis.

The combination of aircraft and landing gear consists of four degrees of freedom due to the rigid body translation and rotation of the upper sprung mass and the vertical displacement of the lower unsprung masses of nose and main gears. All motion is assumed to be restricted to the vertical plane through the center of gravity of the aircraft.

According to the force in the shock strut in the main and nose gear, four distinct possibilities exists.

1. Both main and nose gears are locked.
2. Nose gear is locked and the main gear is unlocked.
3. Main gear is locked and the nose gear is unlocked.
4. Both main and nose gears are unlocked.

These four cases are considered one by one in the following sections for developing the equations of motion.

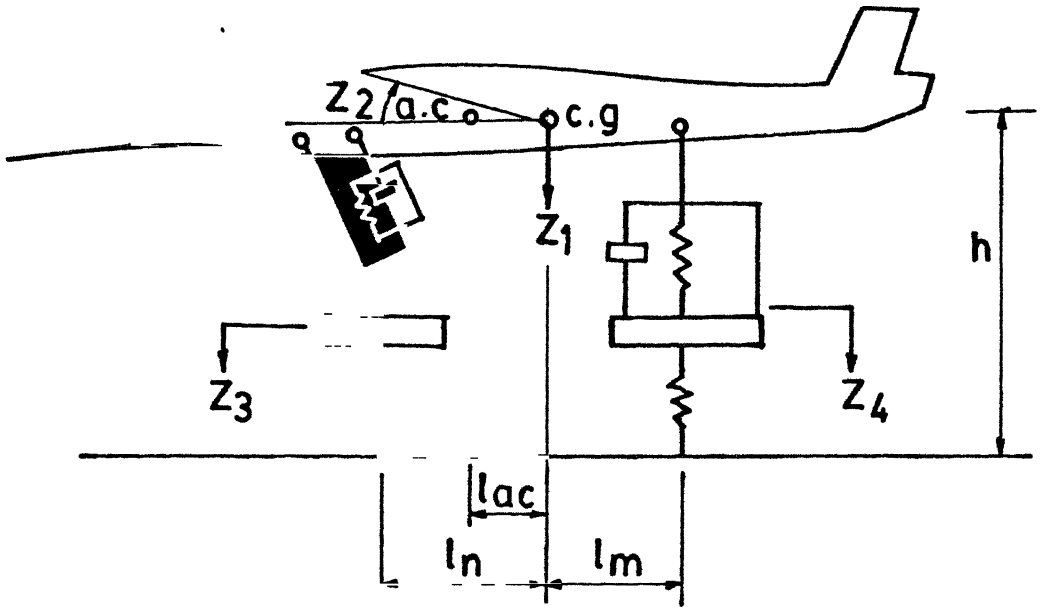

FIG. 2·4 THE HEAVE-PITCH MODEL

2.3.1 Equations of Motion with Main Gear and Nose Gear Locked

When the forces in the shock strut are less than their preloads, only the two tyres compress and hence the system has two degrees of freedom with the unsprung mass moving along with the airframe.

The equation of motion of the system in the vertical direction is

$$\frac{W}{g}\ddot{z}_1 + L - W + F_{vg_m} + F_{vg_n} = 0 \qquad \ldots(2.27)$$

where

W = $W_1 + W_3 + W_4$ (total weight of the aircraft)

W_1 = weight of the sprung mass

W_3 = unsprung weight of the nose wheel

W_4 = unsprung weight of the main wheel

L = lift acting on the aircraft

z_1 = vertical displacement of the sprung mass

F_{vg_n}, F_{vg_m} = vertical ground reaction on the wheels

subscript m for the main gear

subscrpit n for the nose gear

Since the shock struts are locked the displacements z_3 of the nose wheel and z_4 of the main wheel are obtained from the geometry. Thus,

$$\begin{aligned} z_3 &= z_1 - l_n z_2 \\ z_4 &= z_1 + l_m z_2 \end{aligned} \qquad \ldots(2.28)$$

where

l_n = distance between aircraft c.g and the nose wheel

l_m = distance between aircraft c.g and the main wheel

z_2 = angle of pitching of the aircraft

Differentiating twice, the acceleration of the nose wheel and the main wheel are obtained as

$$\begin{aligned} \ddot{z}_3 &= \ddot{z}_4 - l_n \ddot{z}_2 \\ \ddot{z}_4 &= \ddot{z}_4 + l_m \ddot{z}_2 \end{aligned} \qquad \ldots(2.29)$$

Equation of motion of pitching of the aircraft is

$$I_{yy}\ddot{z}_2 - F_{vg_n} l_n - L\, l_{ac} + F_{vg_m} l_m + F_{hg_m}(h - z_4) + F_{hg_n}(h - z_4) = 0 \qquad \ldots(2.30)$$

where

I_{yy} = pitching moment of inertia of the aircraft about its c.g.

l_{ac} = distance of the aerodynamic center of the aircraft measured in the forward direction from the aircraft c.g.

F_{hg} = horizontal ground reaction on tyre

h = height of the aircraft c.g.from the ground level

The horizontal equilibrium equation of the nose wheel is

$$F_{ha_n} = -F_{hg_n} \qquad \ldots(2.31)$$

where F_{ha} is the horizontal component of the force in the trailing arm.

Considering the sprung mass separately the vertical and the rotational equlibrium equations are

$$\frac{W_t}{g}\ddot{z}_t + L - W_t + F_{va_n} + F_{s_m} = 0 \qquad \ldots(2.32)$$

$$I_{yy}\ddot{z}_2 - F_{va_n} l_n - L\, l_{ac} + F_{s_m} l_m + F_{hg_m}(A_o + l_m z_2) - F_{ha_n}(A_s \cos\theta_o - l_n z_2) = 0 \qquad \ldots(2.33)$$

where

F_s = force in the shock strut

A_o = distance of the point of attachment of the main gear from the axle of the main wheel

Eliminating F_{sm} from equations (2.32) and (2.33), the vertical component of force in the trailing arm is

$$F_{va_n} = W_t\left\{1 - \frac{\ddot{z}_t}{g}\right\} - L\left\{\frac{l_{ac} + l_m}{l}\right\} - F_{ha_n}\left\{\frac{A_s \cos\theta_o - l_n z_2}{l}\right\} + F_{hg_m}\left\{\frac{A_o + l_m Z_2}{l}\right\} + I_{yy}\frac{\ddot{z}_2}{l} \qquad \ldots(2.34)$$

The moment equilibrium of the forces in the trailing arm about the hinge A gives the force F_{sn} in the shock strut of the nose gear. Thus

$$F_{s_n} = \frac{F_{va_n} - F_{ha_n} q_4}{q_5} \qquad \ldots(2.35)$$

where q_4, q_5 are terms defined in equations (2.9) and (2.15)

The force F_{s_m} in the shock strut of the main gear is obtained by substituting for F_{va_n} from equation (2.34) in equation (2.32)

The system has one increased degree of freedom when the force in any of the shock strut exceeds its preload. The state at which F_s exceeds F_{s0} gives the initial condition for the new system.

2.3.2 Equations of Motion with the Nose Gear Locked and the Main Gear Unlocked

The three degrees of freedom system in this case is attained when the main shock strut alone is operating.

The vertical displacements of the attachment points z_n and z_m of the nose gear and the main gear respectively due to translation and rotation of the airframe are

$$\begin{aligned} z_n &= z_4 - (l_n + A_s \operatorname{Sin} \theta_0) z_2 \\ z_m &= z_4 + l_m z_2 \end{aligned} \qquad \ldots(2.36)$$

Differentiating once the corresponding velocities are

$$\begin{aligned} \dot{z}_n &= \dot{z}_4 - (l_n + A_s \operatorname{Sin} \theta_0) \dot{z}_2 \\ \dot{z}_m &= \dot{z}_4 + l_m \dot{z}_2 \end{aligned} \qquad \ldots(2.37)$$

The shock strut stroke s_m and the strut telescoping velocity $\dot{s}_m$ of the main gear are given by

$$\begin{aligned} s_m &= z_m - z_4 \\ \dot{s}_m &= \dot{z}_m - \dot{z}_4 \end{aligned} \qquad \ldots(2.38)$$

Since $F_s = F_s(s,\dot{s})$, the force F_{s_m} of the main shock strut can be determined.

The airframe mass and the mass of the nose wheel acts as a single unit. Hence the vertical equilibrium equation of the airframe is

$$\frac{W_a}{g}\ddot{z}_1 + L - W_a + F_{vg_n} + F_{s_m} = 0 \qquad \ldots(2.39)$$

where $W_a = W_1 + W_2$

Equation of motion of rotation of the airframe is

$$I_{yy}\ddot{z}_2 - F_{vg_n} l_n - L\, l_{ac} + F_{s_m} l_m + F_{hg_m}(A_0 + l_m z_2) + F_{hg_n}(h - z_1) = 0 \qquad \ldots(2.40)$$

Acceleration $\ddot{z}_s$ of the nose wheel in the vertical direction is

$$\ddot{z}_s = \ddot{z}_1 - l_n \ddot{z}_2 \qquad \ldots(2.41)$$

Vertical equilibrium equation of the main wheel is

$$\frac{W_4}{g}\ddot{z}_4 - W_4 + F_{vg_m} - F_{s_m} = 0 \qquad \ldots(2.42)$$

The equations of motion (2.39) to (2.42) are solved simultaneously. The force in the nose gear shock strut is given by equation (2.40), where F_{va_n} is obtained from (2.32) and F_{ha_n} from (2.31). By successively calculating the values of F_{s_n}, the state at which $F_{s_n} > F_{so_n}$ can be estimated leading to the initial condition for four degrees of freedom system.

2.3.3 Equations of Motion with the Main Gear Locked and the Nose Gear Unlocked

When the shock strut in the nose gear is operating, the linkage geometry relations developed in equations (2.1) to (2.7) for the heave model are valid except that z_1 and z_2 correspond to z_n and z_s respectively. Thus,

$$\theta_t = \text{Cos}^{-1}\left[\frac{A_6 - (z_n - z_s)}{A_3} \right] \qquad \ldots(2.43)$$

$$s_o = \left\{ [A_7 \text{ Sin}(\theta_o+\delta)-A_4]^2 + [A_7 \text{ Cos}(\theta_o+\delta)+A_5)]^2 + [y_D - y_E]^2 \right\}^{1/2} \qquad \ldots(2.44)$$

$$s_t = \left\{ [A_7 \text{ Sin}(\theta_t+\delta)-A_4]^2 + [A_7 \text{ Cos}(\theta_t+\delta)+A_5)]^2 + [y_D - y_E]^2 \right\}^{1/2} \qquad \ldots(2.45)$$

$$s_n = s_o - s_t \qquad \ldots(2.46)$$

$$\dot{s} = \frac{A_7(\dot{z}_n - \dot{z}_s)\left\{ A_5 \text{ Sin}(\theta_t+\delta) + A_4 \text{Cos}(\theta_t+\delta) \right\}}{A_3 \text{ Sin } \theta_t \; s_t} \qquad \ldots(2.47)$$

$$x = A_3 (\text{Sin } \theta_t - \text{Sin } \theta_o) \qquad \ldots(2.48)$$

$$\begin{aligned} \dot{x} &= q_1(\dot{z}_n - \dot{z}_s) \\ \ddot{x} &= q_1(\ddot{z}_n - \ddot{z}_s) - q_2(\dot{z}_n - \dot{z}_s)^2 \end{aligned} \qquad \ldots(2.49)$$

where the terms used are the the same as those defined in equations (2.1) to (2.7) and (2.36) and (2.37).

Using s_n and $\dot{s}_n$, the force F_{s_n} of the nose gear can be determined.

The equation of motion of the sprung mass in the vertical direction is

$$\frac{W_b}{g}\ddot{z}_4 + L - W_b + F_{vg_m} + F_{va_n} = 0 \qquad \ldots(2.50)$$

where $W_b = W_4 + W_4$

Rotational equilibrium equation for the airframe is

$$I_{yy}\ddot{z}_2 - F_{va_n} l_n - L\, l_{ac} + F_{vg_m} l_m + F_{hg_m}(h - z_4) - F_{ha_n}(A_s \cos\theta_t - l_n z_2) = 0 \qquad \ldots(2.51)$$

Vertical equilibrium equation of the nose wheel is

$$\frac{W_s}{g}\ddot{z}_s - W_s + F_{vg_n} - F_{va_n} = 0 \qquad \ldots(2.52)$$

Since the main wheel and the airframe acts as a single mass, the acceleration of the main mass is

$$\ddot{z}_4 = \ddot{z}_4 + l_m \ddot{z}_2 \qquad (2.53)$$

The horizontal equilibrium equation of the nose wheel is

$$F_{ha_n} = \frac{W_s}{g} \ddot{x} - F_{hg_n} \qquad \ldots(2.54)$$

Substituting for x from equation (2.49) in equation (2.54) yields

$$F_{ha_n} = q_3 (\ddot{z}_n - \ddot{z}_s) + q_4 \qquad \ldots(2.55)$$

where

$$\begin{aligned} q_3 &= \frac{W_s}{g} q_1 \\ q_4 &= -\left[\frac{W_s}{g} q_2 (\dot{z}_n - \dot{z}_s)^2 + F_{hg} \right] \end{aligned} \qquad \ldots(2.56)$$

Balance of moments of the forces in the trailing arm about the hinge A yields the expression for F_{va_n} as in equation (2.22). Thus,

$$F_{va_n} = B_2 + B_3 (\dot{z}_n - \dot{z}_s) \qquad \ldots(2.57)$$

where

$$\begin{aligned} B_2 &= q_5 F_{s_n} + q_1 q_4 \\ B_3 &= q_1 q_3 \end{aligned} \qquad \ldots(2.58)$$

Substituting for F_{va_n} from equation (2.57) and F_{ha_n} from equation (2.55) in the equations of motion (2.50) to (2.53) and rearranging in a matrix form yields

$$[\,P\,]\ \{\ddot{z}\} + \{R\} = \{0\} \qquad \ldots(2.59)$$

where the elements of the P matrix are :

$$P_{11} = B_3 + W_b / g$$

$$P_{12} = -B_3 (l_n + A_3 \text{Sin } \theta_o)$$

$$P_{13} = -B_3$$

$$P_{14} = 0$$

$$P_{21} = B_3 l_n + q_3 (A_3 \text{Cos } \theta_t - l_n z_2)$$

$$P_{22} = -B_3 l_n (l_n + A_3 \text{Sin } \theta_o) - I_{yy} - q_3 (A_3 \text{Cos } \theta_t - l_n z_2)(l_n + A_{33} \text{Sin } \theta_o)$$

$$P_{23} = -[B_3 l_n + q_3 (A_3 \text{COS } \theta_t - l_n z_2)]$$

$$P_{24} = 0$$

$$P_{31} = B_3$$

$$P_{32} = -B_3 (l_n + A_3 \text{Sin } \theta_o)$$

$$P_{33} = -(B_3 + W_3 / g)$$

$$P_{34} = 0$$

$$P_{41} = 1$$

$$P_{42} = l_m$$

$$P_{43} = 0$$

$$P_{44} = -1$$

and the elements of the R matrix are :

$$R_{11} = B_2 + L - W_b + F_{vg_m}$$

$$R_{21} = B_2 l_n + L\, l_{ac} - F_{vg_m} l_m - F_{hg_m} (h - z_1) + q_1 (A_3 \text{Cos } \theta_t - l_n z_2)$$

$$R_{31} = B_2 - F_{vg_n} + W_3$$

$$R_{41} = 0$$

The force F_{s_m} in the main shock strut can be obtained

from the equilibrium equations of the sprung mass in the vertical direction.

$$F_{s_m} = W_4 - L - F_{va_n} - \frac{W_4}{g}\ddot{z}_4 \qquad \ldots(2.60)$$

The system is converted to four degrees of freedom system when the preload in the main shock strut is exceeded.

2.3.4 Equations of Motion with Both Main Gear and Nose Gear Unlocked

When both the shock struts are operating, the forces in them can be determined directly. The strokes in the shock struts are

$$\begin{aligned} s_m &= z_m - z_4 \\ s_n &= s_o - s_t \end{aligned} \qquad \ldots(2.61)$$

The strut telescoping velocities of the main and nose gear are obtained from equations (2.38) and (2.47) respectively. Since $F_s = F_s(s,\dot{s})$, the force in the main gear and the nose gear F_{s_m} and F_{s_n} can be determined.

The equations of motion of the sprung and unspung masses are

$$\frac{W_4}{g}\ddot{z}_4 + L - W_4 + F_{va_n} + F_{s_m} = 0 \qquad \ldots(2.62)$$

$$I_{yy}\ddot{z}_2 - F_{va_n} l_n - L\, l_{ac} + F_{s_m} l_m + F_{hg_m}(A_o - S_{M_1} + l_m z_2) - F_{ha_n}(A_3 \cos\theta_t - l_n z_2) = 0 \qquad \ldots(2.63)$$

$$\frac{W_s}{g}\ddot{z}_s - W_s + F_{vg_n} - F_{va_n} = 0 \qquad \ldots(2.64)$$

$$\frac{W_4}{g}\ddot{z}_4 - W_4 + F_{vg_m} - F_{a_m} = 0 \qquad \ldots(2.65)$$

Substituting for F_{ha_n} from equation (2.55) and F_{va_n} from equation (2.57), the equations of motion (2.62) to (2.65) can be written in the form

$$[\,P\,]\ \{\ddot{Z}\} + \{R\} = \{0\} \qquad \ldots(2.66)$$

where the elements of the P matrix are :

$P_{11} = B_s + W_1 / g$

$P_{12} = -B_s(l_n + A_s \sin\theta_o)$

$P_{13} = -B_s$

$P_{14} = 0$

$P_{21} = B_s l_n + q_s(A_s \cos\theta_t - l_n z_2)$

$P_{22} = -B_s l_n(l_n + A_s \sin\theta_o) - I_{yy} + q_s(A_s \cos\theta_t - l_n z_2)(l_n + A_s \sin\theta_o)$

$P_{23} = -[B_s l_n + q_s(A_s \cos\theta_t - l_n z_2)]$

$P_{24} = 0$

$P_{31} = B_s$

$P_{32} = -B_s(l_n + A_s \sin\theta_o)$

$P_{33} = -(B_s + W_s / g)$

$P_{34} = 0$

$P_{41} = 0$

$P_{42} = 0$

$P_{43} = 0$

$P_{44} = W_4 / g$

The elements of the R matrux are :

$$R_{11}=B_2 + L - W_1 + F_{a_m}$$

$$R_{21}=B_2 l_n + L\, l_{ac} - F_{a_m} l_m - F_{hg_m}(A_0 + l_m z_2) + q_4 (A_3 \cos\theta_1 - l_n z_2)$$

$$R_{31}=B_2 - F_{vg_n} + W_3$$

$$R_{41}=-[\, W_4 + F_{a_m} - F_{vg_m}\,]$$

2.4 FORCES IN THE SHOCK STRUT

The total force in the shock strut is due to hydraulic resistance, air compression and internal friction. As the strut compresses, the hydraulic fluid is forced through the orifice to the the lower chamber providing the non-linear damping.When the fluid enters the lower chamber, it pushes the separator down and compressing the air in the processes. The polytropic compression of air provides the non-linear springing.

2.4.1 Pneumatic force

The pneumatic force in the shock strut is determined by the initial air pressure, initial air and oil volumes, pneumatic area oil, bulk modulus and the air compression processes.

The pneumatic force in a shock strut is given by

$$F_a = p_{a_o} A_a \left\{ \frac{V_{a_o}}{V_{a_o} - A_a s + V_{o_o} \left\{ \frac{p_a - p_{a_o}}{\beta} \right\}} \right\}^n \quad \ldots(2.67)$$

where

V_{a_o} = initial air volume

V_{o_o} = initial oil volume

p_{a_o} = initial air pressure

p_a = instantaneous air pressure

n = polytropic exponent of the air compression processes

β = bulk modulus of oil

2.4.2 Hydraulic force

The hydraulic resistance F_h due to the telescoping of the strut is given by

$$F_h = \frac{\dot{s}}{|\dot{s}|} \frac{\rho A_h^2}{2(C_d A_n)^2} \dot{s}^2 \quad \ldots(2.68)$$

where

ρ = mass density of fluid

A_h = hydraulic area

C_d = coefficient of discharge

A_n = net orifice area

$\dot{s}$ = strut telescoping velocity

2.4.3 Friction forces

The journal friction F_{fj} can be written as

$$F_{fj} = \frac{\dot{s}}{|\dot{s}|} \left\{ \mu_{j1} |F_1| + \mu_{j2} |F_2| \right\} \qquad \ldots(2.69)$$

where

μ_{j1} = coefficient of friction of upper bearing (attached to the inner cylinder) on the shock strut

μ_{j2} = coefficient of friction of lower bearing (attached to the outer cylinder) on the shock strut

F_1 = normal force on the upper bearing

F_2 = normal force on the lower bearing

$\dot{s}$ = strut telescoping velocity

From the balance of moments

$$F_1 = \left\{ \frac{l_2 - s}{l_1 + s} \right\} F_n \quad \text{and} \quad F_2 = \left\{ \frac{l_1 + l_2}{l_1 + s} \right\} F_n$$

so that

$$F_{fj} = \frac{\dot{s}}{|\dot{s}|} |F_n| \left\{ \frac{l_2 - s}{l_1 + s} (\mu_{j_1} + \mu_{j_2}) + \mu_{j2} \right\} \qquad \ldots(2.70)$$

where

F_n = normal load on the shock strut

l_1 = axial distance between upper and lower bearings on fully extended shock strut

l_2 = axial distance between lower bearing and point of attachment of shock strut

The seal friction force F_{fs} is given by

$$F_{fs} = \frac{\dot{s}}{|\dot{s}|} \mu_s F_a \qquad ...(2.71)$$

where

μ_s = coefficient of seal friction

F_a = pneumatic force in the shock strut

The total axial force in the shock strut is obtained as

$$F_s = F_a + F_h + F_{fj} + F_{fs} \qquad ...(2.72)$$

2.5. FORCES ON THE TYRE

The exponential force-deflection of the tyre, neglecting hysteresis can be represented by

$$F_{vg} = m\, z^r \qquad ...(2.73)$$

where

F_{vg} = vertical force applied to the tyre at the ground

m , r = constants corresponding to various regimes of tyre deflection process

z = radial deflection of tyre

The drag load F_{hg} in the tyre ground interface is given by

$$\begin{aligned} F_{hg} &= \mu_g F_{vg} \quad \text{before wheel spin-up} \\ &= 0 \quad \text{after wheel spin-up} \end{aligned} \qquad ...(2.74)$$

where μ_g is the coefficient of skid-friction between tyre and ground

The wheel spin-up time can be obtained from simple impulse momentum relationship.Thus,

$$\int_0^{t_{su}} \mu_g F_{vg}\, dt = \frac{I_w V_{h_o}}{r_d^2} \qquad \ldots(2.75)$$

where

I_w = moment of Inertia of the wheel assembly about its axle

V_{h_o} = horizontal velocity of landing of the aircraft

r_d = radius of the deflected shape of the tyre

CHAPTER 3

RESULTS AND DISCUSSIONS

The dynamic response of an aircraft during landing have been obtained. The equations of motion developed in chapter 2 requires the numerical value of several quantities which may not be known to a designer before hand A parametric study is therefore carried out to determine the relative accuracy with which any parameter has to be known in advance in order to determine their influence on the aircraft behaviour.

The coefficient of orifice discharge plays the most significant role in any mathematical modeling of the landing gear. The dynamic loads on the aircraft can vary over 25% with the variations in C_d [6]. Due to lack of sufficient experimental data on the air compression process in the shock strut, the exact value of the polytropic index is also not known in advance. Hence these two parameters were varied to study their effect on the landing gear performance. The study also includes the effect of orifice diameter, initial air volume and initial air pressure. Besides the variation of the parameters of the shock strut for the heave model, the relative locations of the nose and main landing gears with respect to the aircraft center of gravity and the radius of gyration of the aircraft for the heave-pitch model are also examined.

The equations of motion of the masses developed in sections 2.2.2 and 2.2.3 forms a set of coupled non-linear differential equations equal in number to the number of degrees of freedom of the airframe-landing gear system. These equations are solved by numerical integration. The method used for accomplishing this is the Gear method, which is a modification of Variable Order Variable Step Adam's method. The equations of motion are reduced to a system of first order differential equations which are solved using a standard routine D02EBF in DEC 1090 mainframe.

To start with, the programme reads in all the relevant physical characteristics of the aircraft, the landing gears and the initial conditions of the system. Using these informations the forces on the tyre and the geometry of the landing gear at any instance are determined. A distinction must be made at this point between the case when the force in the shock strut is greater than its pre-load and the case when it is less than its pre-load. In the latter case the force in the shock strut is treated as an unknown and an additional constraint is imposed on the system that there is no relative motion between the sprung and the unsprung masses as the shock strut is locked.

The output information includes the displacement, velocity and acceleration of the system co-ordinates and the hydraulic, pneumatic and frictional forces in the shock strut. The output so obtained are plotted inorder to present the results in a graphical and tabular form for easy inference.

The aircraft and the landing gear data used for generating the results are placed in the Appendix.

3.1 PARAMETRIC STUDY OF THE HEAVE MODEL

3.1.1 Effect of Orifice Discharge Coefficient

The influence of orifice discharge coefficient on the behaviour of the landing gear for the heave model are shown in figures 3.1a to 3.1k. Results are presented for a range of values of C_d from 0.2 to 1.0, when all other conditions are assumed identical. The negative values of the displacement of the unsprung mass indicates an airborne state of the model. A decrease in C_d increases the force in the shock strut due to a higher hydraulic force (Table 1). Due to the larger force acting upwards on the sprung mass, the following observations can be justified.

(a). A decrease in the maximum downward displacement as C_d decreases. (figures 3.1a and 3.1b and Tables 2a and 2b)

(b). The aircraft ballooning back into air for the lower values of C_d (figures 3.1c and 3.1d), the duration being greater for C_d = 0.2 compared to C_d = 0.4.

(c). A higher maximum upward acceleration with a decrease in the value of C_d (figures 3.1h and 3.1i and Table 2a and 2b)

It can also be noted from the graphs that the downward acceleration of the sprung and unsprung masses are constant during the period the aircraft is fully airborne (figures 3.1h and 3.1j). Therefore the variation of the velocity of the masses are linear during this time (figures 3.1e and 3.1f).

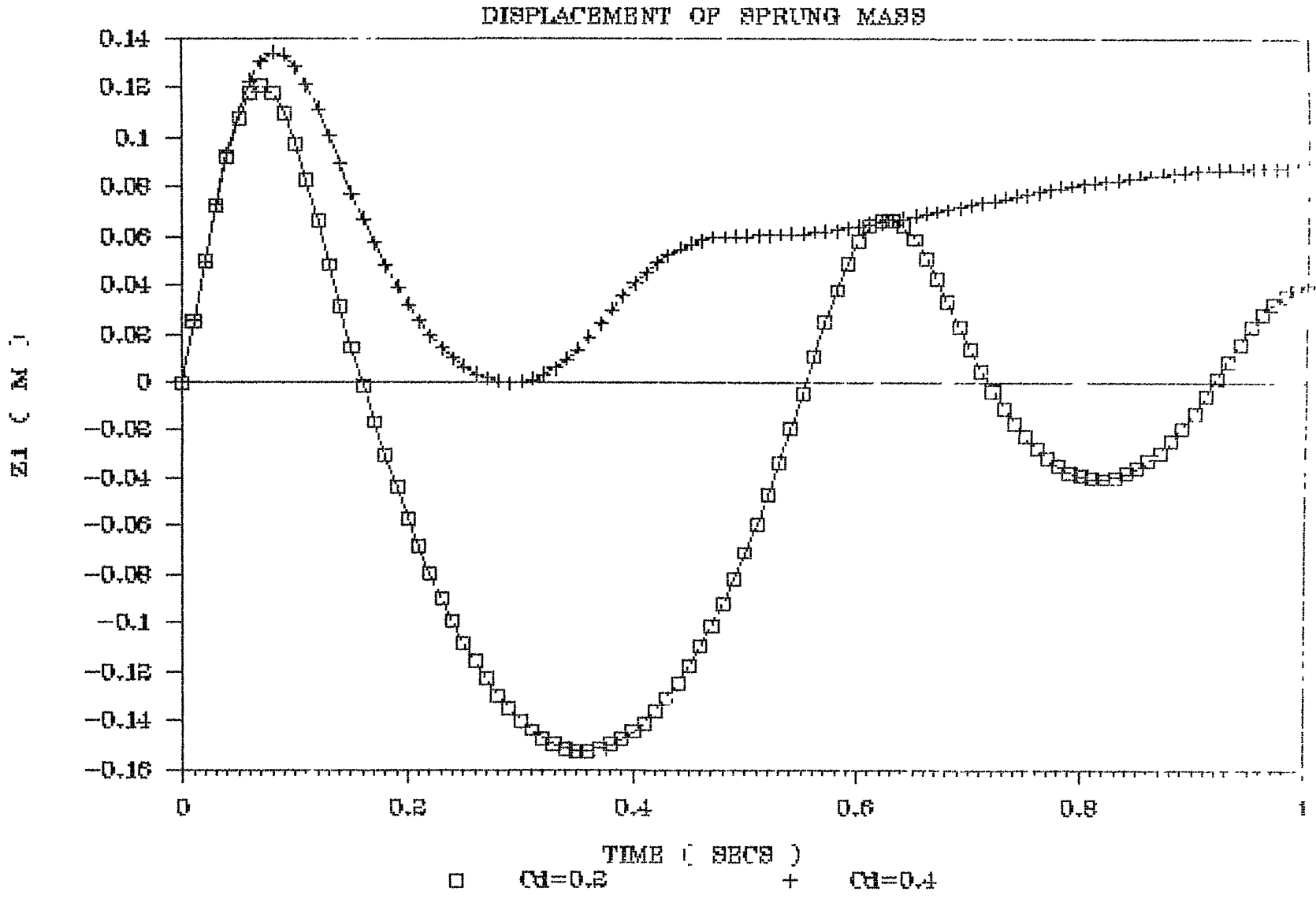

FIG 3.1a VARIATION IN DISPLACEMENT OF THE SPRUNG MASS WITH ORIFICE DISCHARGE COEFFICIENT (0.2 & 0.4)

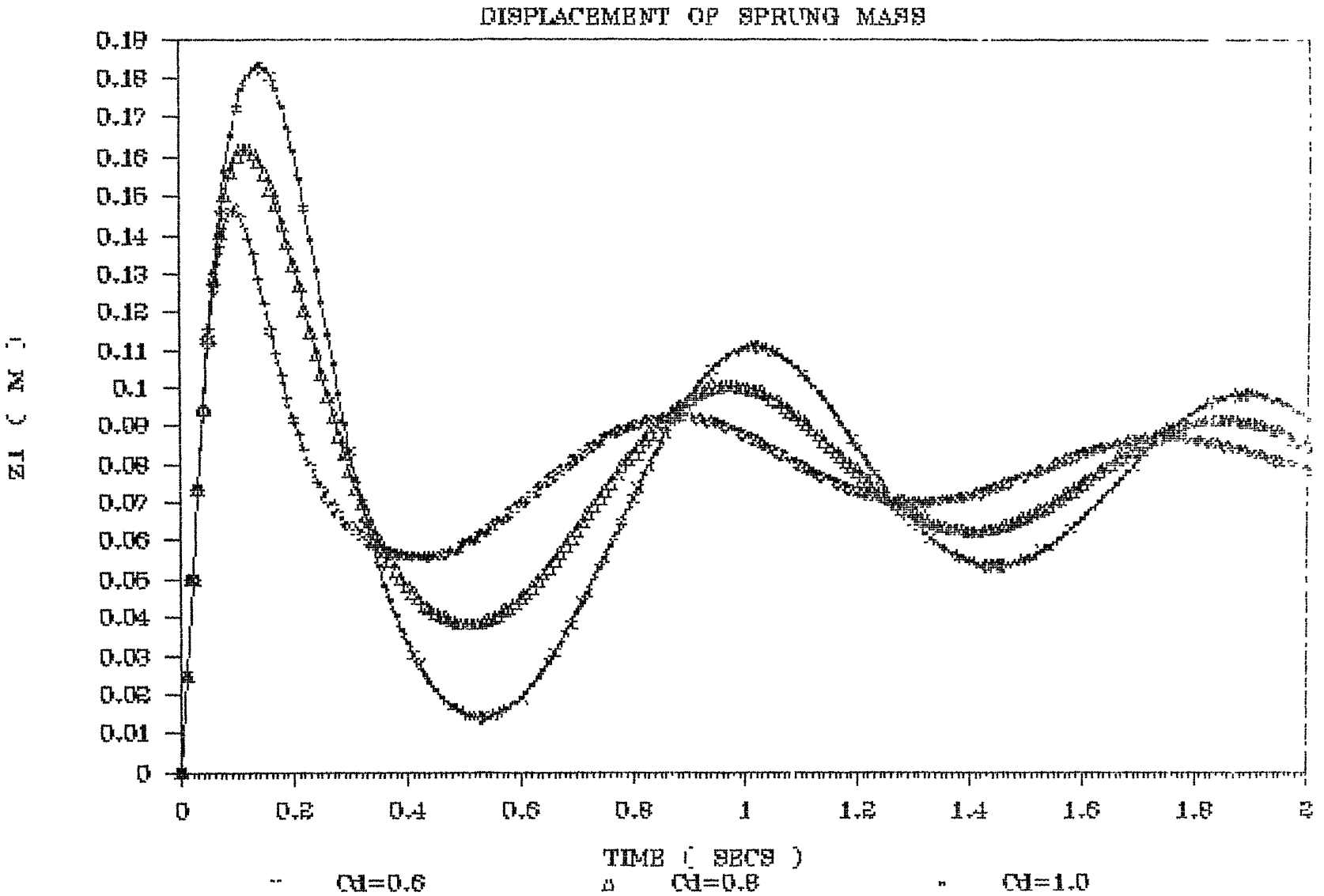

FIG 3.1b VARIATION IN DISPLACEMENT OF THE SPRUNG MASS WITH ORIFICE DISCHARGE COEFFICIENT (0.6, 0.8 & 1.0)

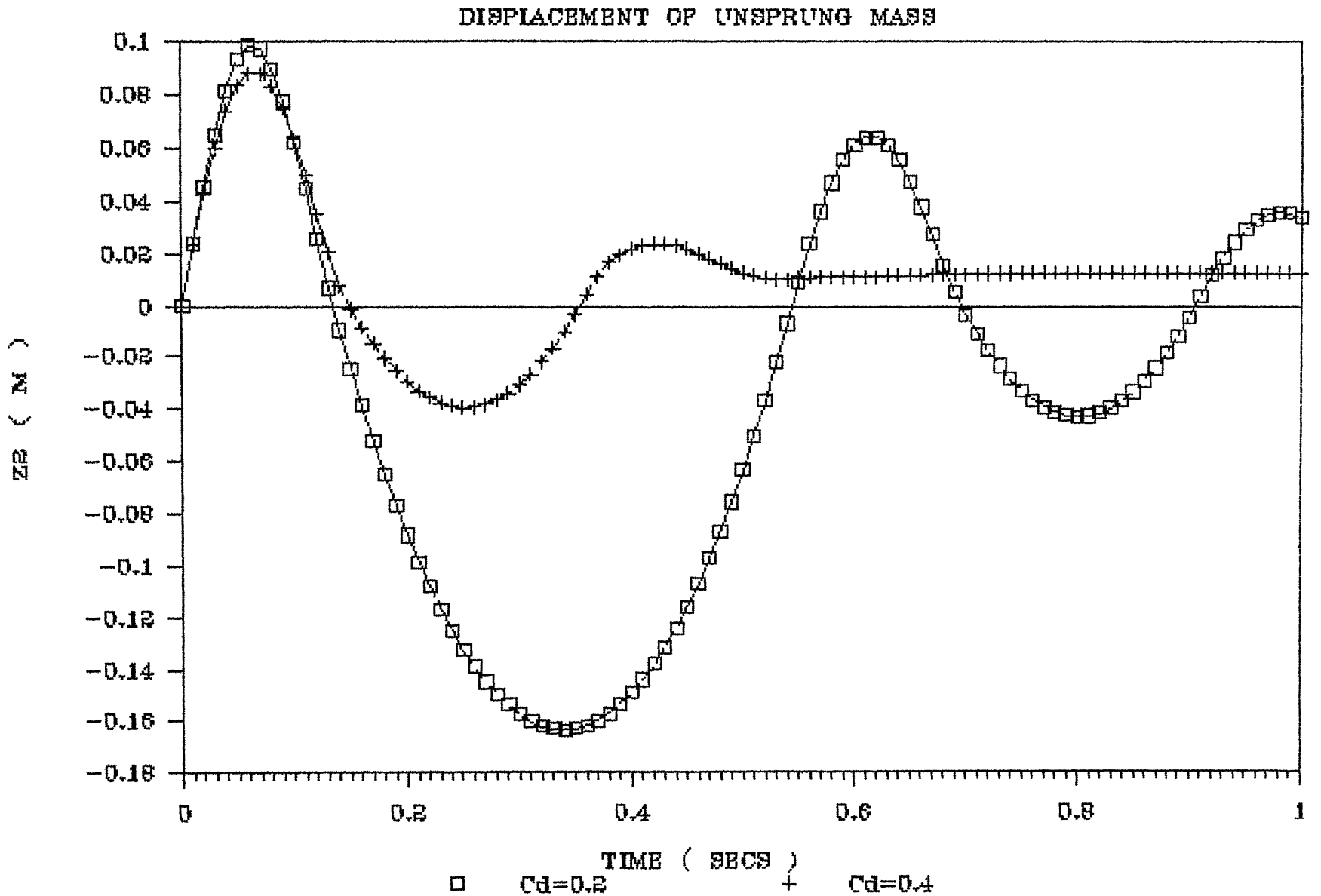

FIG 3.1c VARIATION IN DISPLACEMENT OF THE UNSPRUNG MASS WITH ORIFICE DISCHARGE COEFFICIENT (0.2 & 0.4)

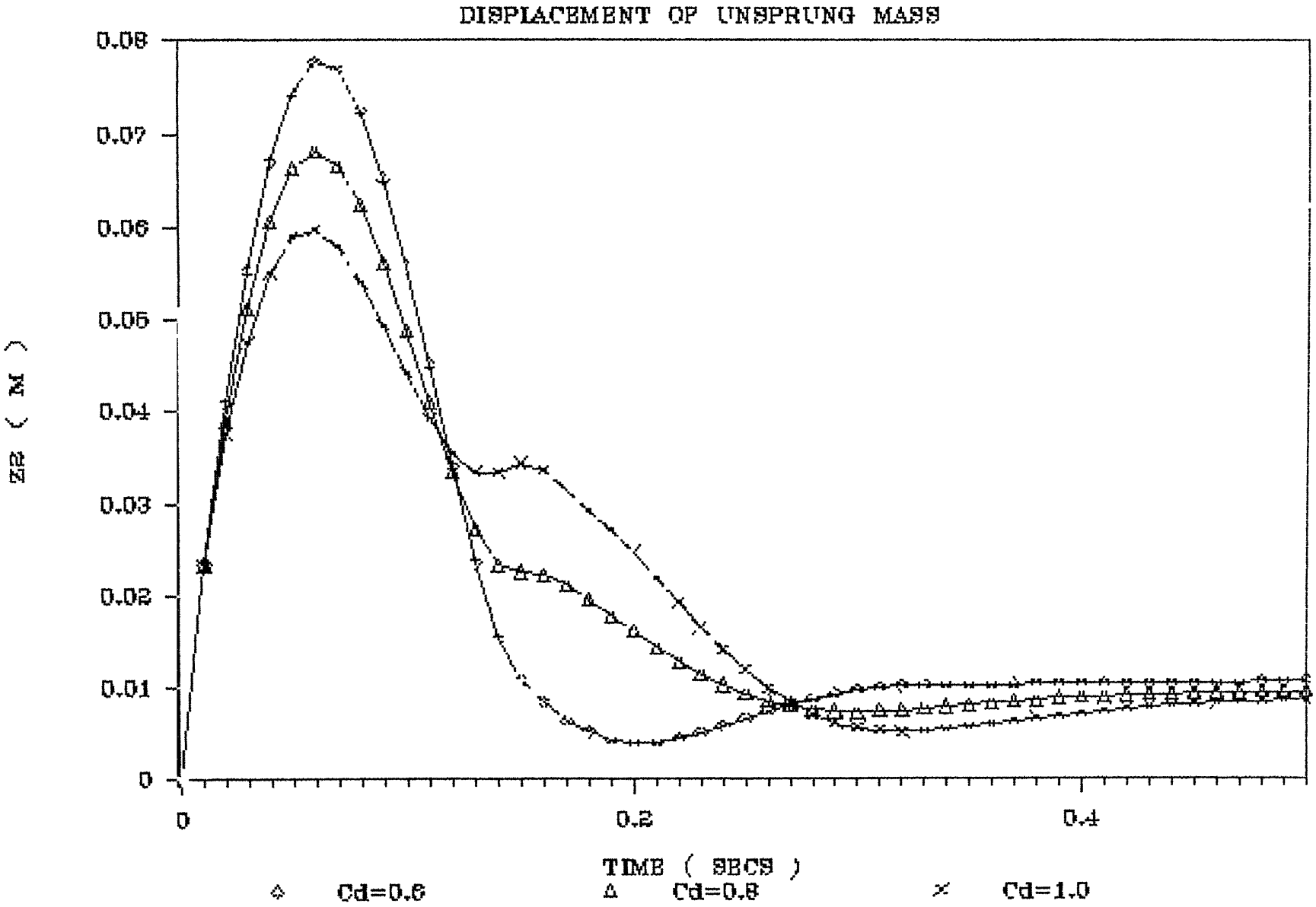

FIG 3.1d VARIATION IN DISPLACEMENT OF THE UNSPRUNG MASS WITH ORIFICE DISCHARGE COEFFICIENT (0.6, 0.8 &1.0)

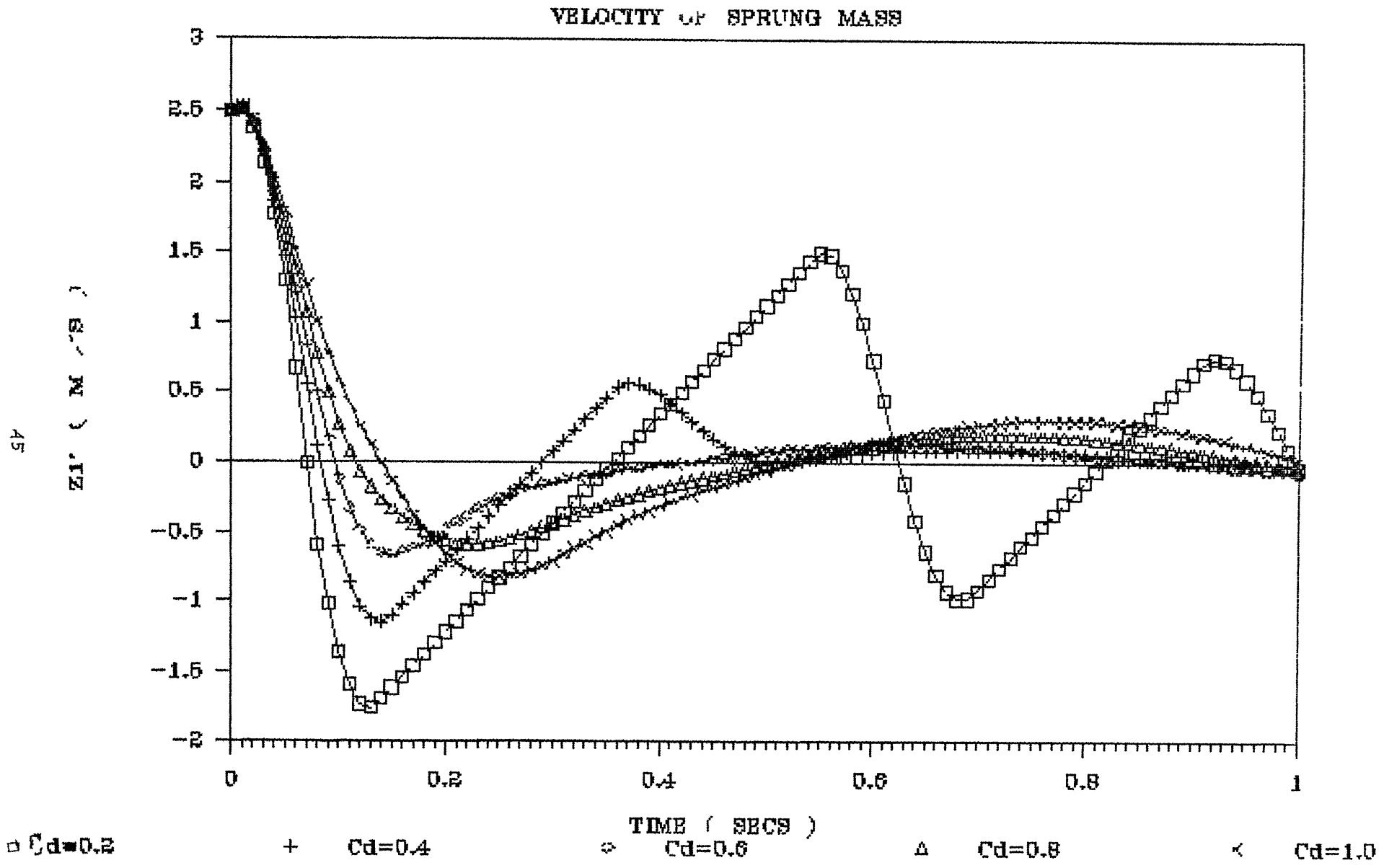

FIG 3.1e VARIATION IN VELOCITY OF THE SPRUNG MASS WITH ORIFICE DISCHARGE COEFFICIENT

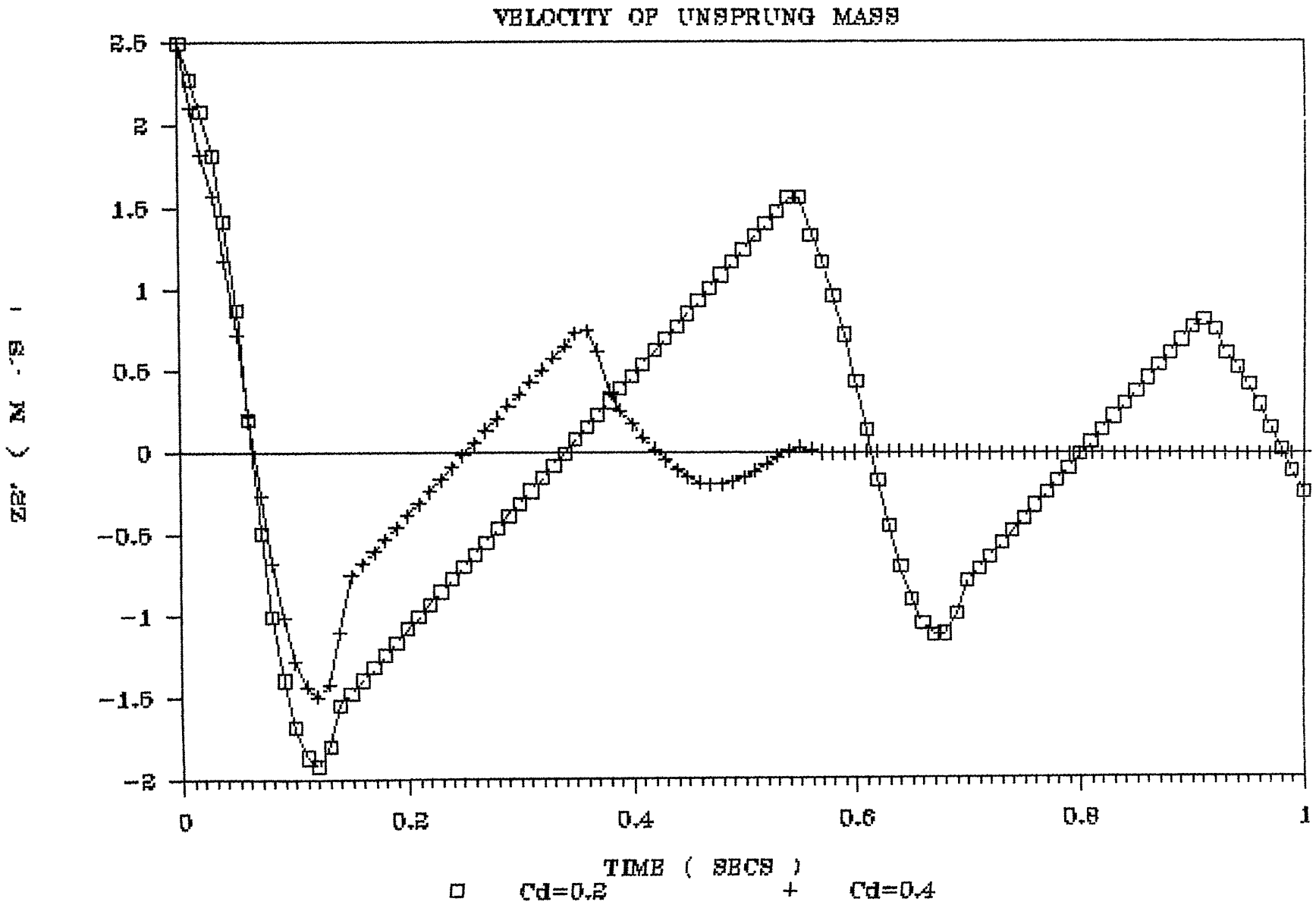

FIG 3.1f VARIATION IN VELOCITY OF THE UNSPRUNG MASS WITH ORIFICE DISCHARGE COEFFICIENT (0.2 & 0.4)

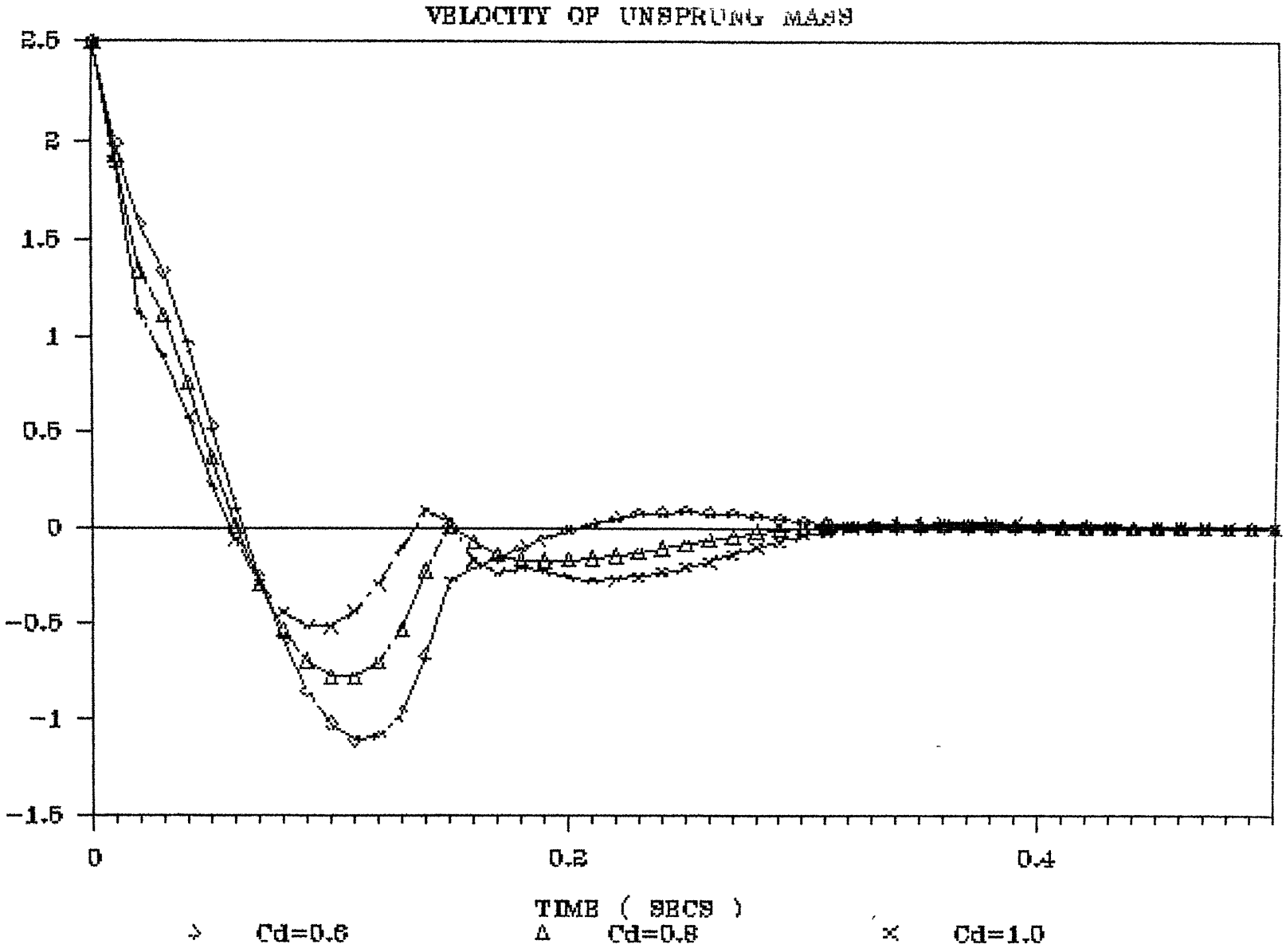

FIG 3.1g VARIATION IN VELOCITY OF THE UNSPRUNG MASS WITH ORIFICE DISCHARGE COEFFICIENT (0.6, 0.8 & 1.0)

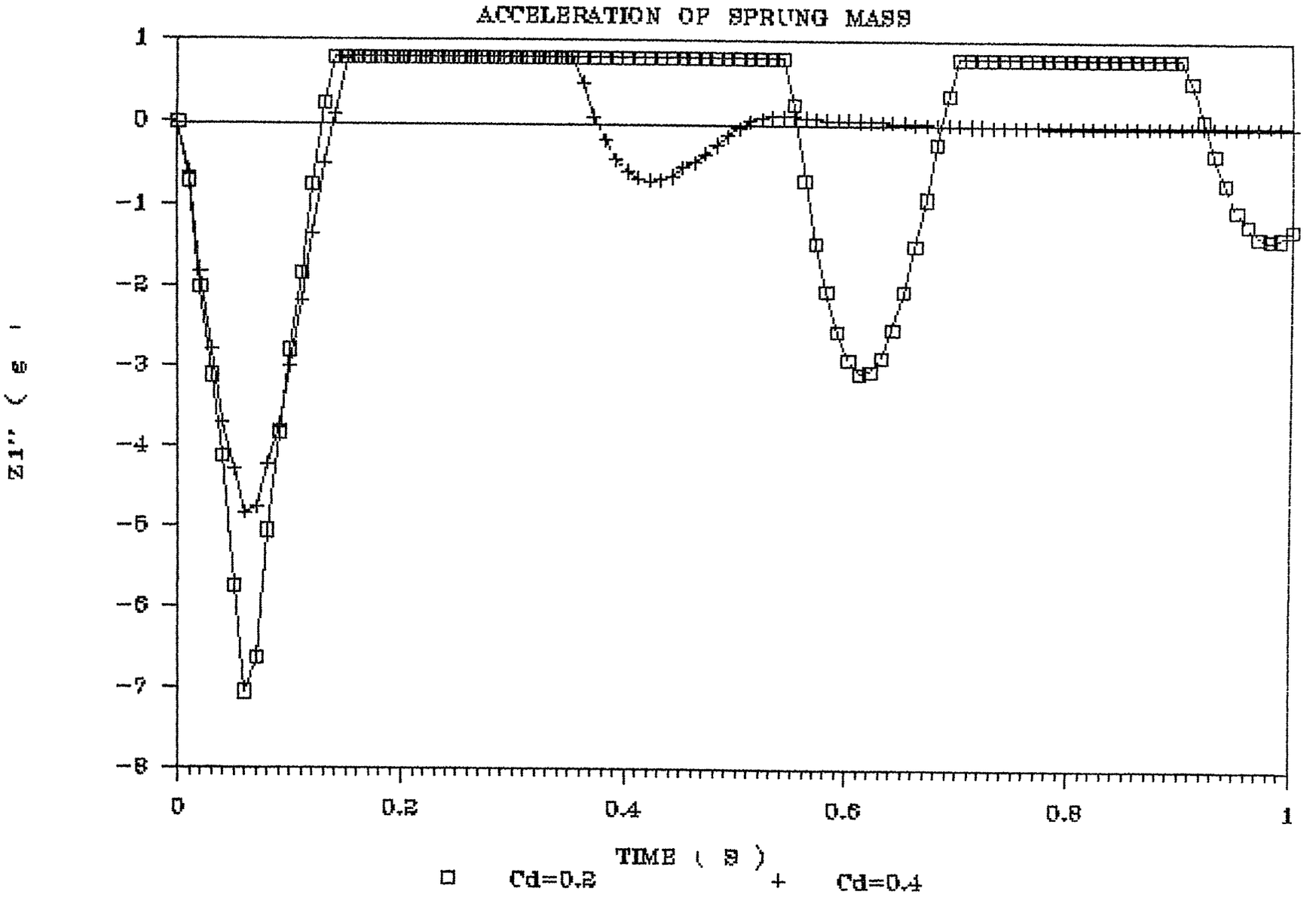

FIG 3.1h VARIATION IN ACCELERATION OF THE SPRUNG MASS WITH ORIFICE DISCHARGE COEFFICIENT (0.2 & 0.4)

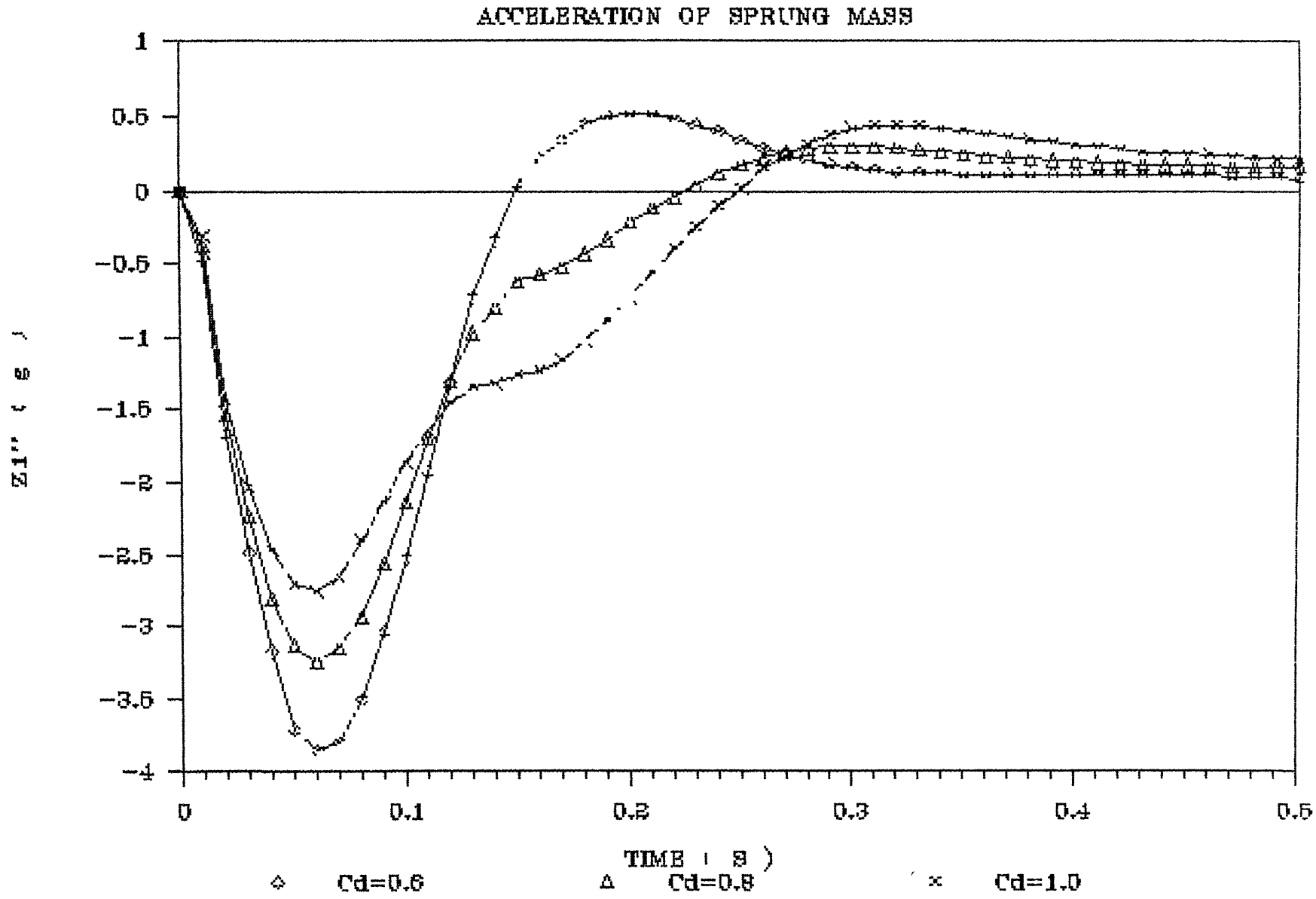

FIG 3.11 VARIATION IN ACCELERATION OF THE SPRUNG MASS WITH ORIFICE DISCHARGE COEFFICIENT (0.6,0.8 & 1.0)

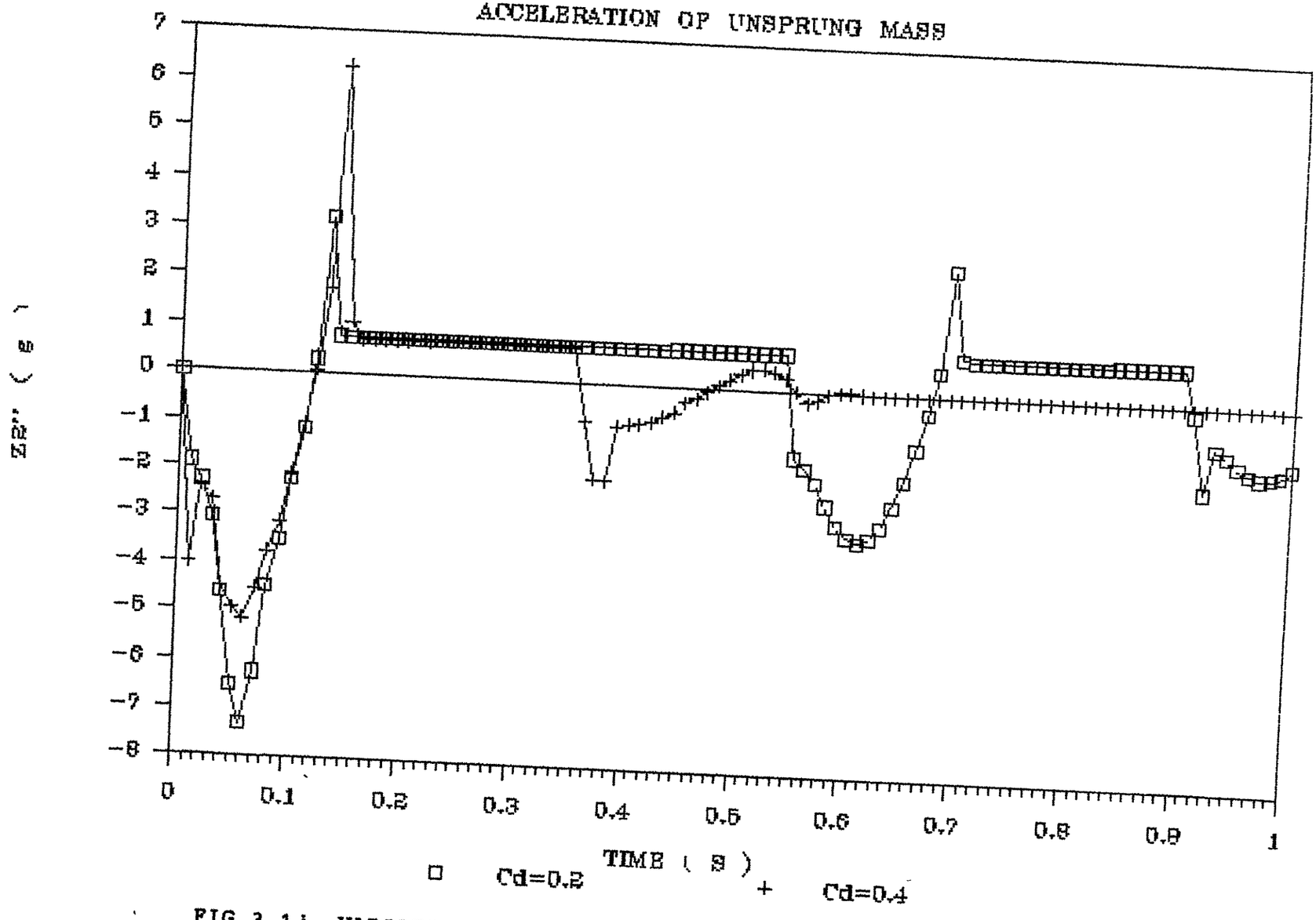

FIG 3.1j VARIATION IN ACCELERATION OF THE UNSPRUNG MASS WITH ORIFICE DISCHARGE COEFFICIENT (0.2 & 0.4)

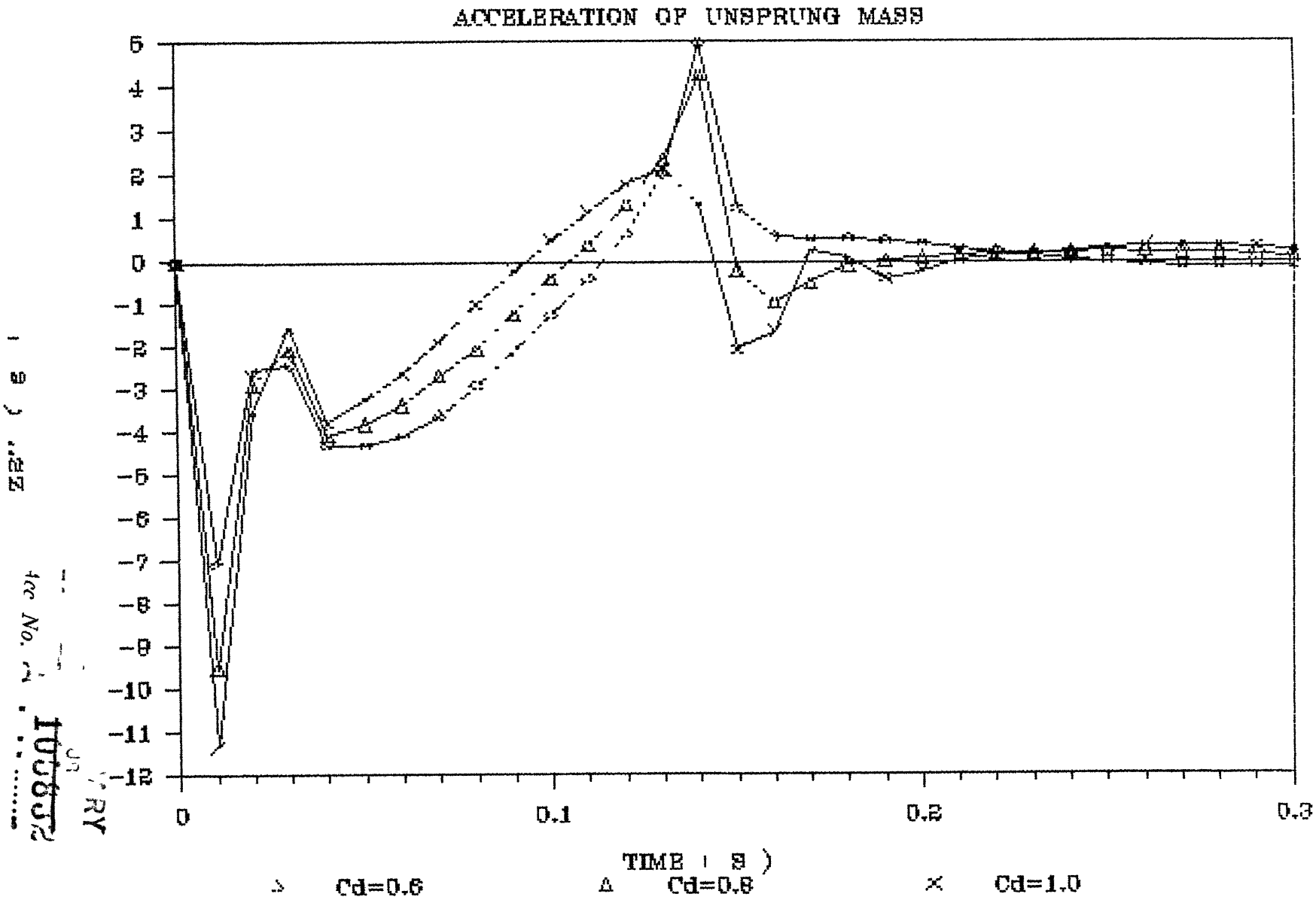

FIG 3.1k VARIATION IN ACCELERATION OF THE UNSPRUNG MASS WITH ORIFICE DISCHARGE COEFFICIENT (0.6,0.8 & 1.0)

Due to the higher force acting downwards on the unsprung mass, their peak downward displacements increase with decreasing C_d (figures 3.1c and 3.1d).

Table 1 gives the maximum values of pneumatic, hydraulic and the total force in the shock strut, the shock strut stroke and the force on the tyre.

C_d	F_a Newtons	F_h Newtons	F_s Newtons	F_t Newtons	s cm
0.2	11345.0	105110.0	113600.0	61492.0	3.149
0.4	13514.0	74056.0	83679.0	43992.0	4.167
0.6	18836.0	59290.0	69989.0	36123.0	5.707
0.8	25817.0	50112.0	61633.0	31459.0	6.800
1.0	33438.0	42436.0	54548.0	27534.0	7.494

TABLE 1. Variation in the peak values of the shock strut forces and tyre forces and the shock strut stroke with orifice discharge coefficient

Because of the increased force in the shock strut with decreasing C_d, the ground reaction also increases with deceasing orifice discharge coefficient. The rate of decrease of the tyre and the shock strut forces however is higher for lower values of C_d. Inorder to provide the higher pneumatic force, the maximum strut closure increases with C_d, hence some extra allowance should be made in the strut. *for variations in*

Tables 2a and 2b shows the extreme positive and negative displacement and acceleration of the two masses for different values of C_d.

	Maximum Displacement (cm)		Maximum Acceleration (g)	
C_d	Up	Down	Up	Down
0.2	15.5	12.1	7.2	0.8
0.4	0.0	13.4	4.8	0.8
0.6	.	14.7	3.9	0.5
0.8	.	16.2	3.2	0.4
1.0	.	18.3	2.7	0.4

TABLE 2a Variation in the extreme values of displacement and acceleration of the sprung mass with orifice discharge coefficient.

	Maximum Displacement (cm)		Maximum Acceleration (g)	
C_d	Up	Down	Up	Down
0.2	16.8	9.9	13.2	6.3
0.4	3.8	8.9	6.8	3.4
0.6	.	7.8	8.6	5.0
0.8	.	6.8	10.1	4.0
1.0	.	5.0	11.5	2.0

TABLE 2b Variation in the extreme values of displacement and acceleration of the unsprung mass with orifice discharge coefficient.

Comparison of the figures and the values in Table 1 and Tables 2a and 2b show that magnitude of orifice coefficient has significant effect on the landing gear behaviour. The accurate prediction of the numerical value of C_d is therefore necessary for obtaining reliable results.

3.1.2 Effect of Orifice Diameter

A decrease in orifice diameter essentially increases the hydraulic force in the shock strut (Table 3). Its effect is therefore similar to that of decreasing C_d. Figures 3.2.a to 3.2.f and Tables 4a and 4b show the variation in the dynamic response of the aircraft for orifice diameters of 44 mm, 52 mm and 60mm.

Table 3 gives the maximum values of pneumatic, hydraulic and the total force in the shock strut, the shock strut stroke and the force on the tyre.

D_n mm	F_a Newtons	F_h Newtons	F_s Newtons	F_t Newtons	s cm
4.4	14032.0	71613.0	81359.0	42663.0	4.365
5.2	18530.0	59729.0	70388.0	36353.0	5.642
6.0	25265.0	50741.0	62194.0	31742.0	6.735

TABLE 3 Variation in the peak values of the shock strut forces and tyre forces and the shock strut stroke with orifice diameter

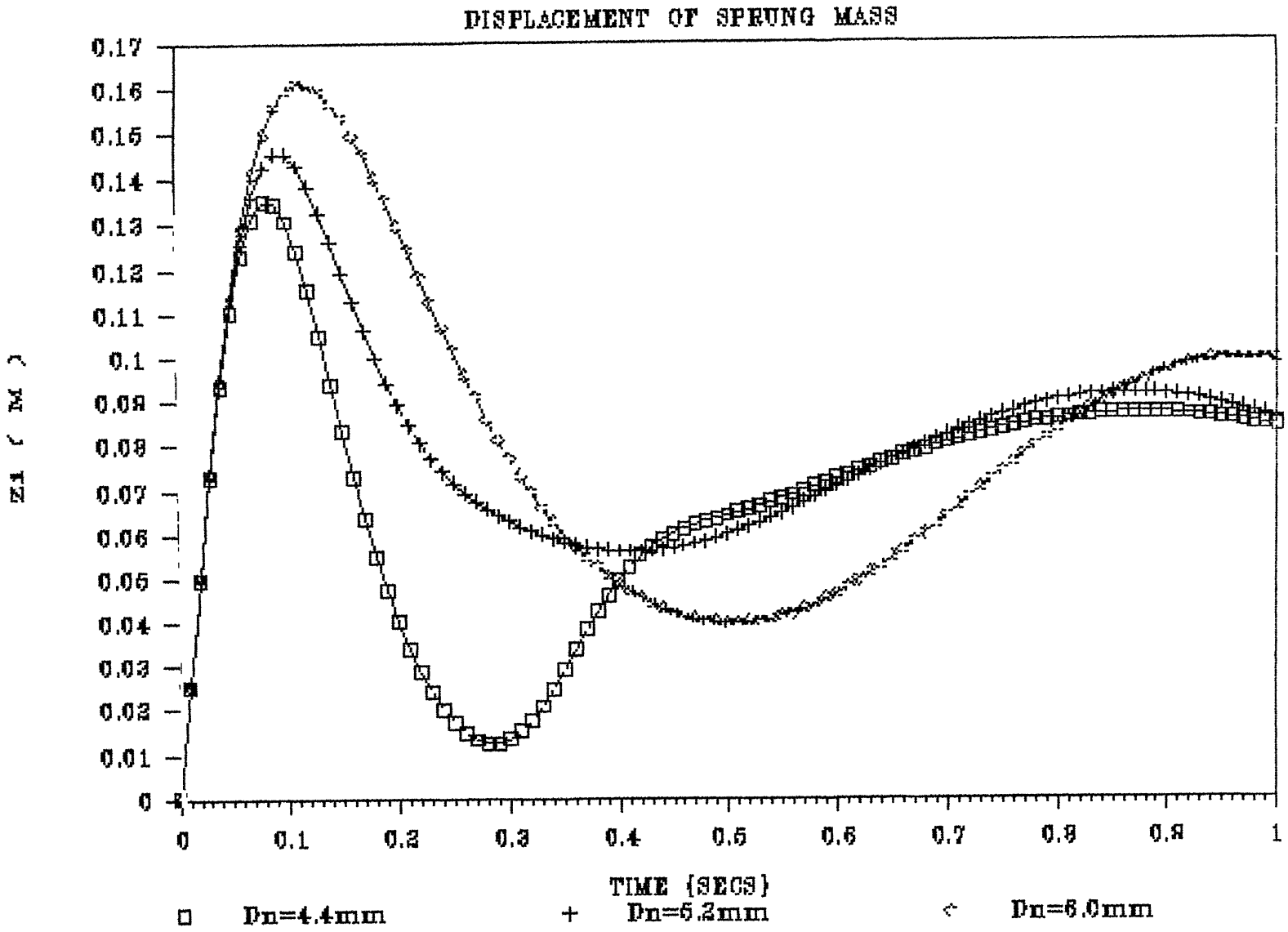

FIG 3.2a VARIATION IN DISPLACEMENT OF THE SPRUNG MASS WITH ORIFICE DIAMETER

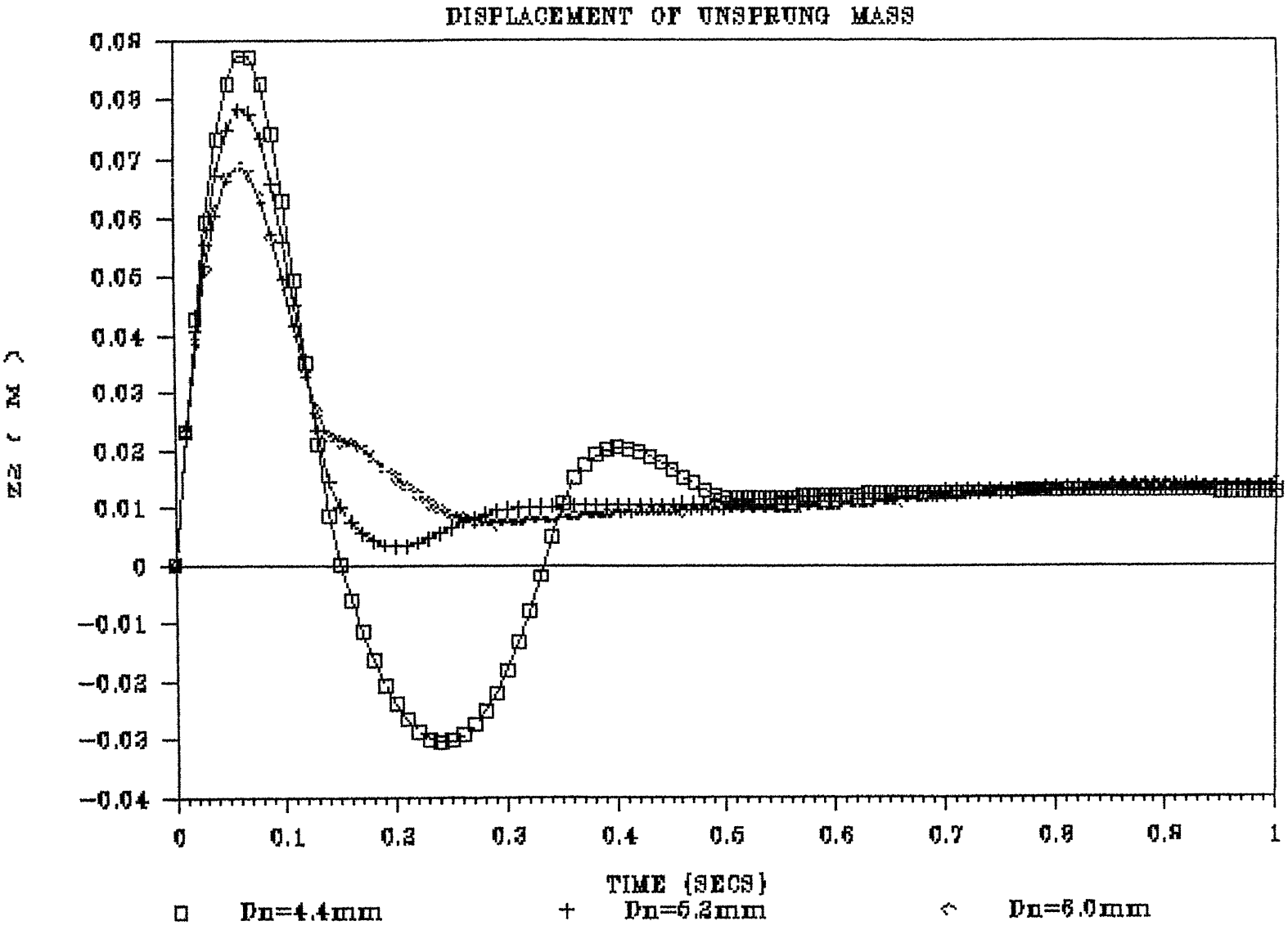

FIG 3.2b VARIATION IN DISPLACEMENT OF THE UNSPRUNG MASS WITH ORIFICE DIAMETER

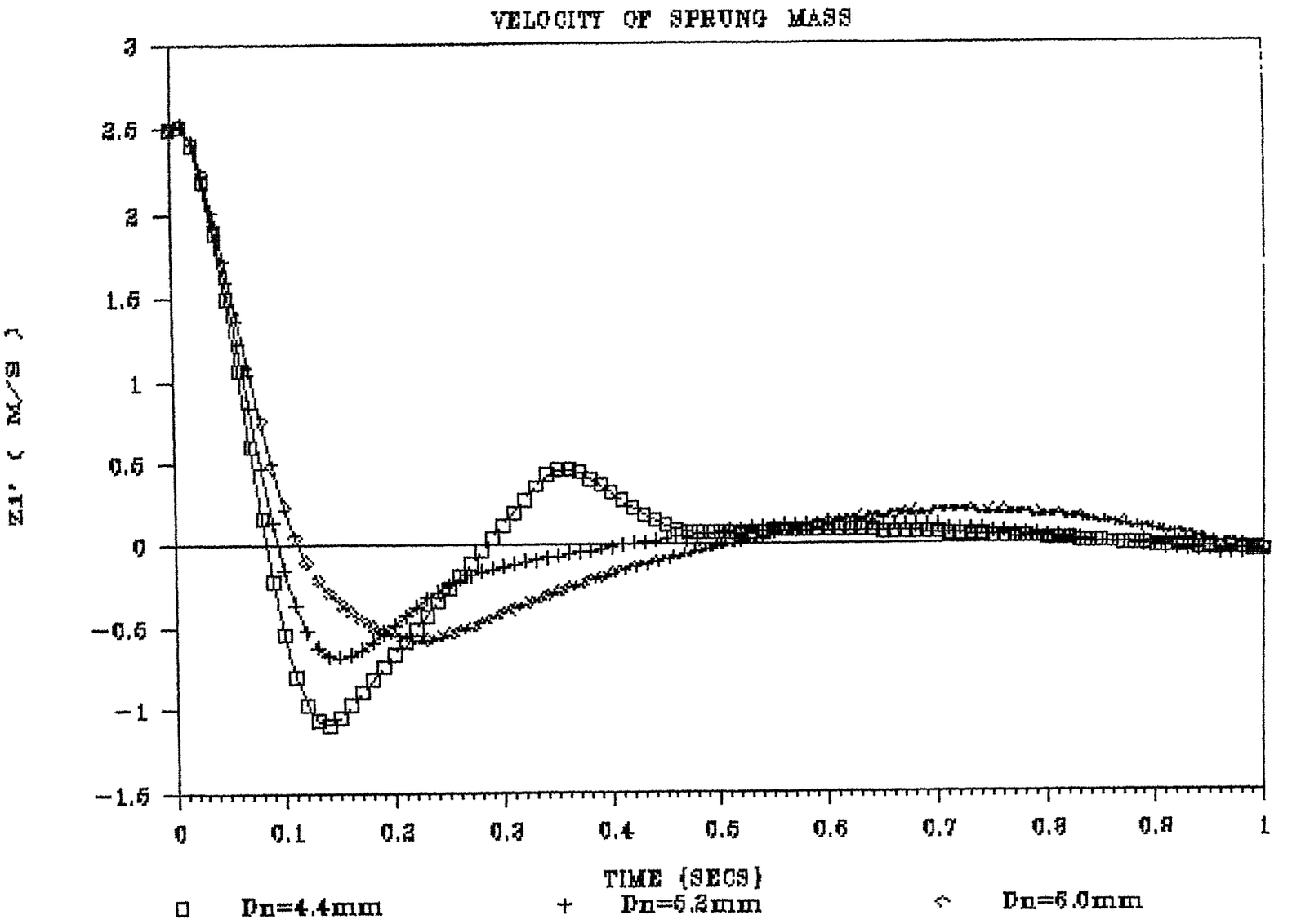

FIG 3.2c VARIATION IN VELOCITY OF THE SPRUNG MASS WITH ORIFICE DIAMETER

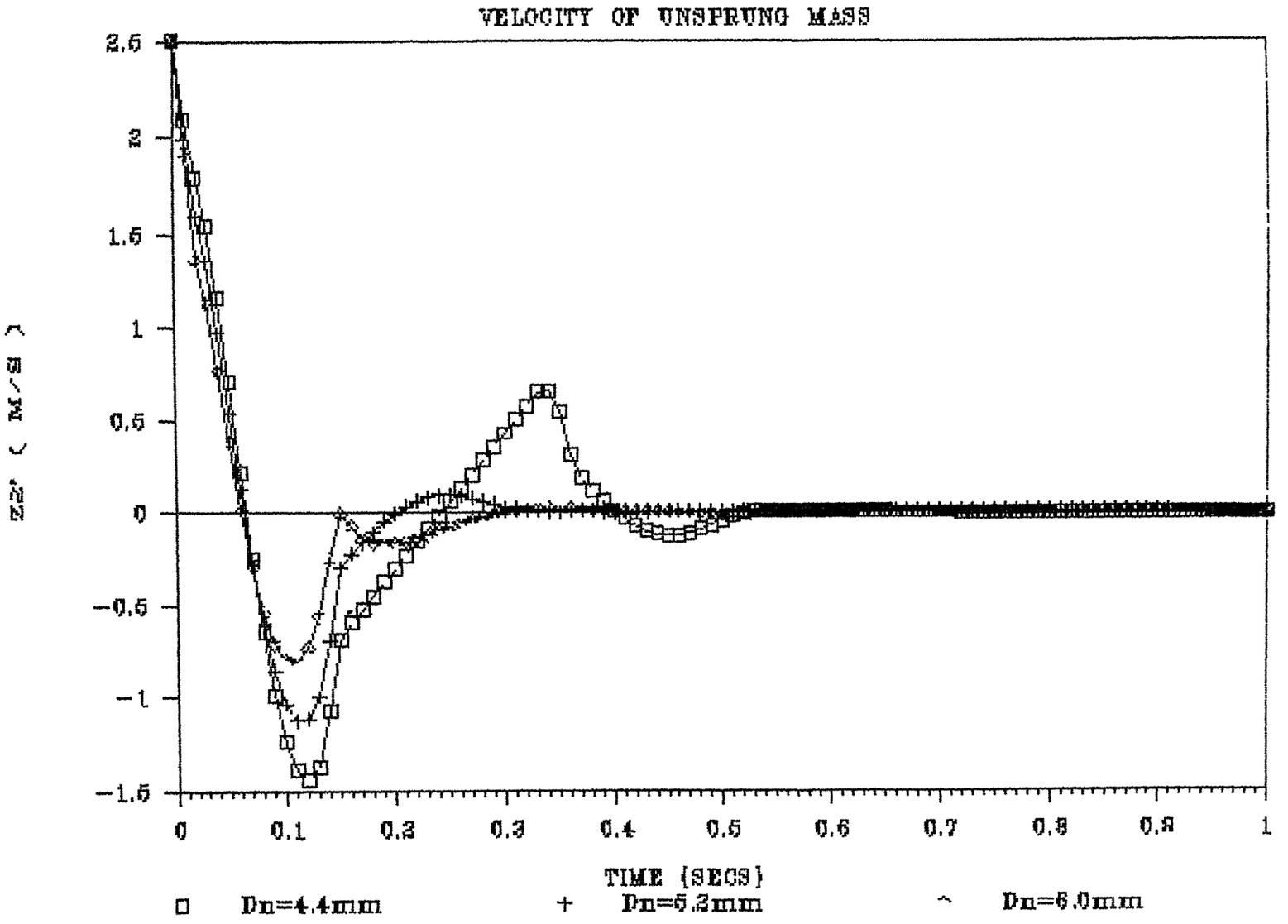

FIG 3.2d VARIATION IN VELOCITY OF THE UNSPRUNG MASS WITH ORIFICE DIAMETER

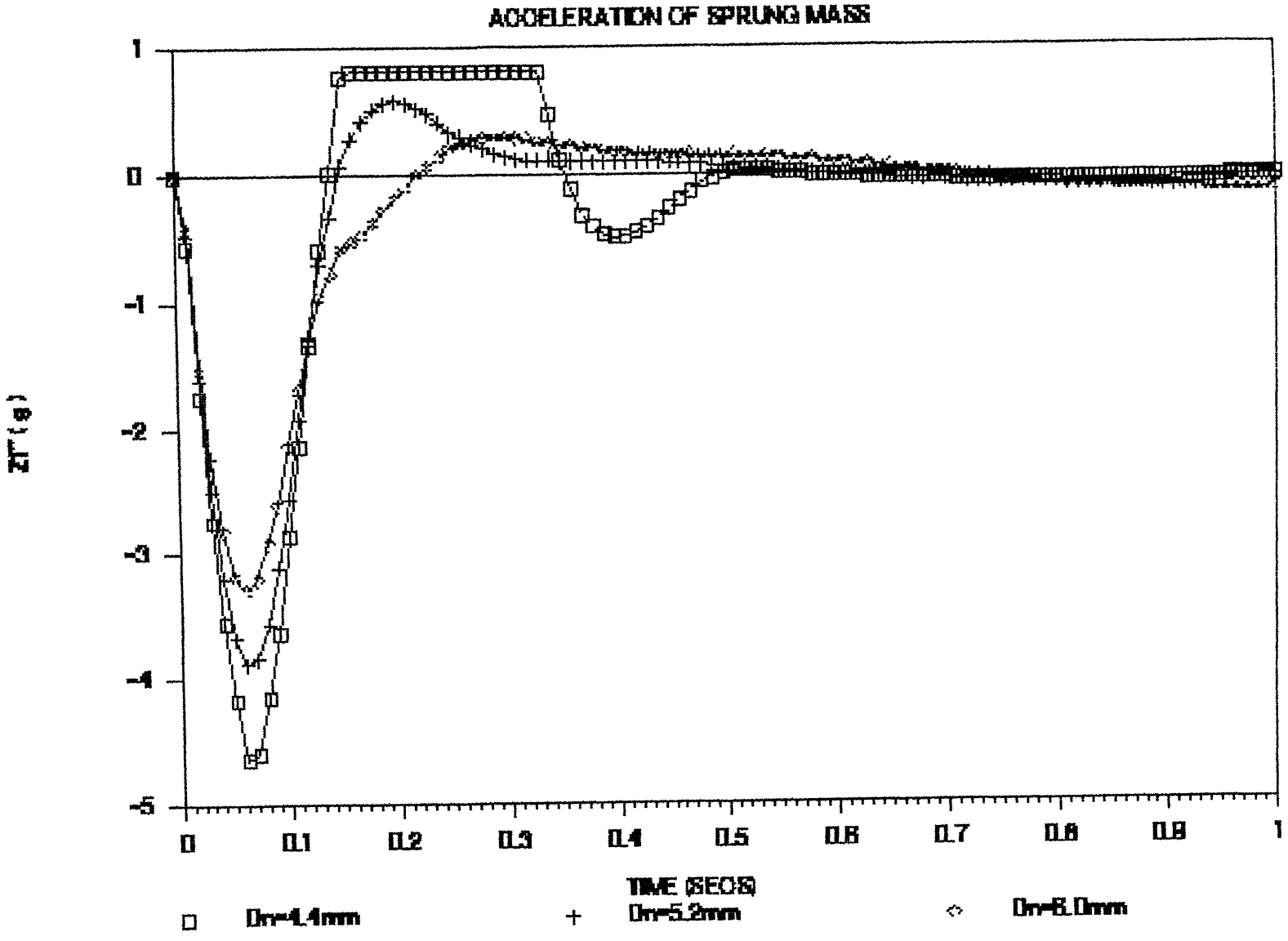

FIG 3.2e VARIATION IN ACCELERATION OF THE SPRUNG MASS WITH ORIFICE DIAMETER

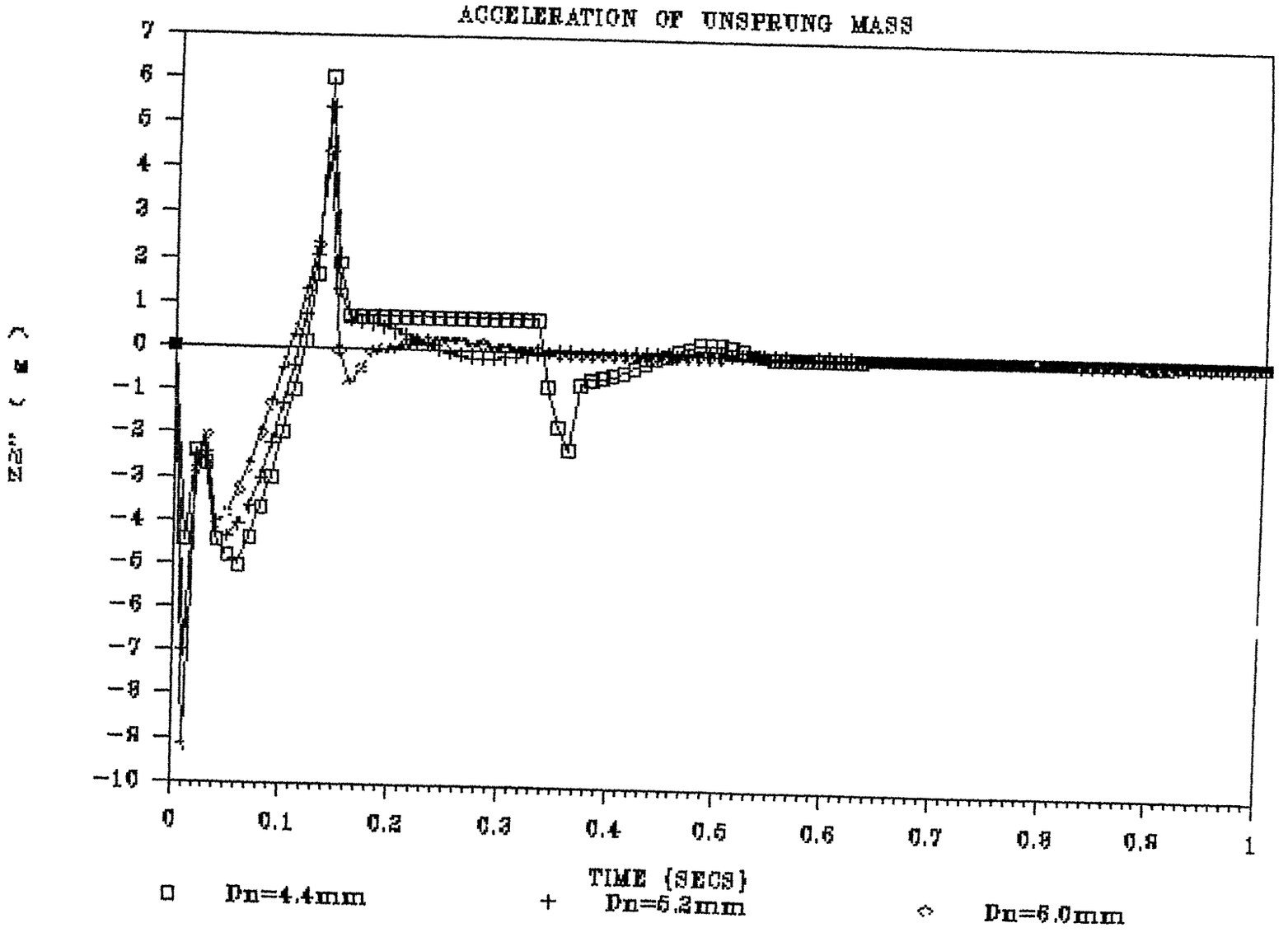

FIG 3.2f VARIATION IN ACCELERATION OF THE UNSPRUNG MASS WITH ORIFICE DIAMETER

Tables 4a and 4b shows the extreme positive and negative displacement and acceleration of the two massee for different values of D_n.

	Maximum Displacement (cm)		Maximum Acceleration (g)	
D_n(mm)	Up	Down	Up	Down
4.4	.	13.5	4.7	0.8
5.2	.	14.6	3.9	0.6
6.0	.	16.1	3.2	0.2

TABLE 4a Variation in the extreme values of displacement and acceleration of the sprung mass with orifice diameter

	Maximum Displacement (cm)		Maximum Acceleration (g)	
D_n(mm)	Up	Down	Up	Down
4.4	3.1	8.8	7.0	6.0
5.2	.	7.8	8.5	5.4
6.0	.	6.9	10.0	4.1

TABLE 4b Variation in the extreme values of displacement and acceleration of the unsprung mass with orifice diameter

3.1.3 Effect of Polytropic Index

As the nature of the air-compression in the shock strut is not well defined, the value of n assumed varied from 1.0 (isothermal) to 1.4 (adiabatic). Figures 3.3a to 3.3f show the influence of n on the aircraft response for the same set of initial conditions. The effect of increase in polytropic index is to increase the pneumatic force in the shock strut. For the present case, variation in air-compression process results in no significant difference in the velocity and acceleration response of the two masses. The sprung mass displacement shows some variation in the rebound after the initial impact, being lower for higher value of n (figure 3.3a).

3.1.4 Effect of Initial Air-Volume

The parametric study for the initial air-volume V_{a_o} is shown in figures 3.4a to 3.4f. The initial air-volume is fixed at 275cc, 350cc and 425cc. A decrease in the value of V_{a_o} results in a higher pneumatic force for the same strut closure -acting upwards on the sprung mass. The displacement of the sprung mass shows some divergence in behaviour after the initial impact. While the frequency and amplitude of oscillation do not have significant changes, their mean values are considerably different. This is due to the fact that oil is less compressible compared to air. Thus the static equilibrium position of the sprung mass is closer to the ground level as

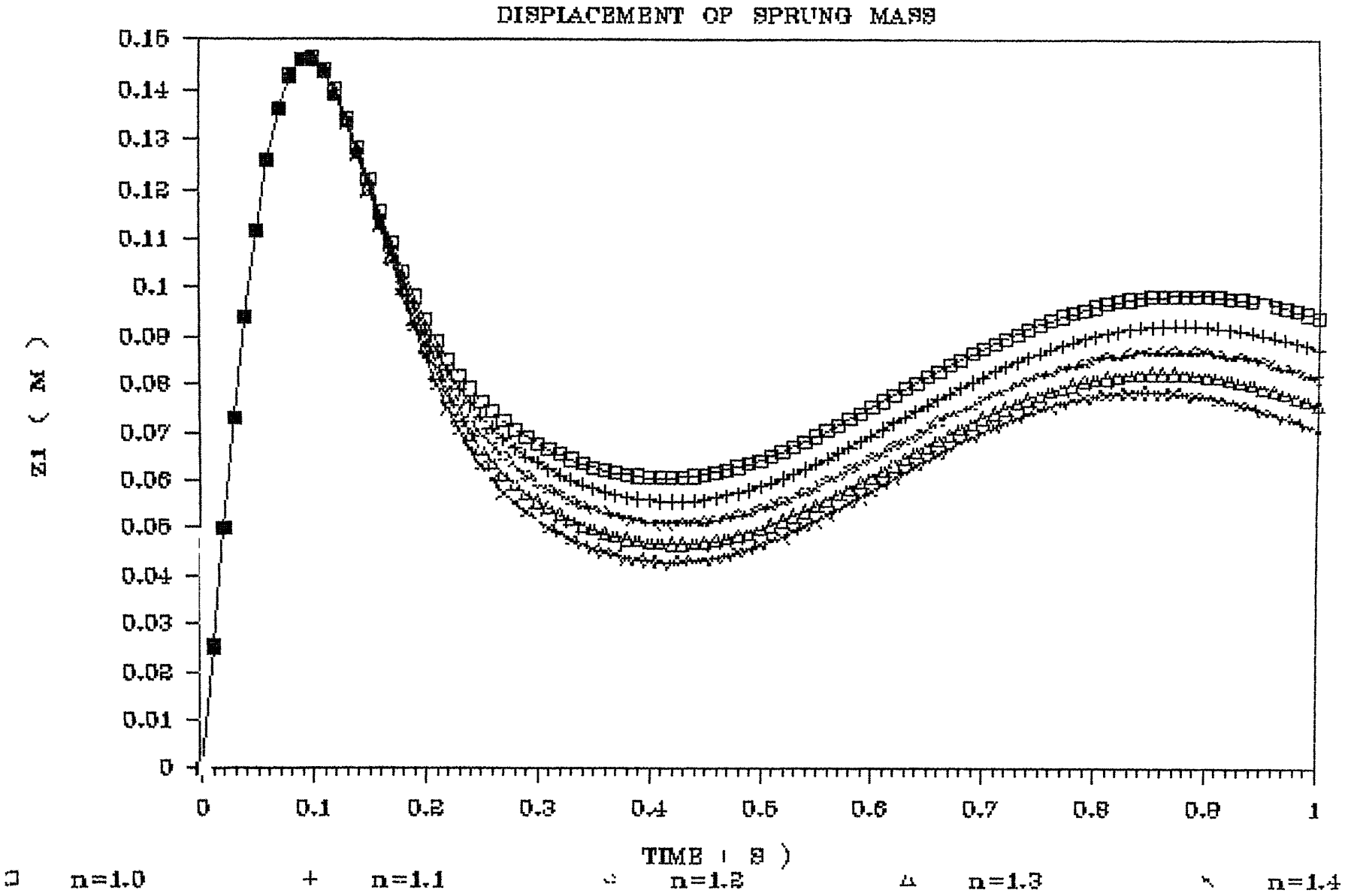

FIG 3.3a VARIATION IN DISPLACEMENT OF THE SPRUNG MASS WITH POLYTROPIC INDEX

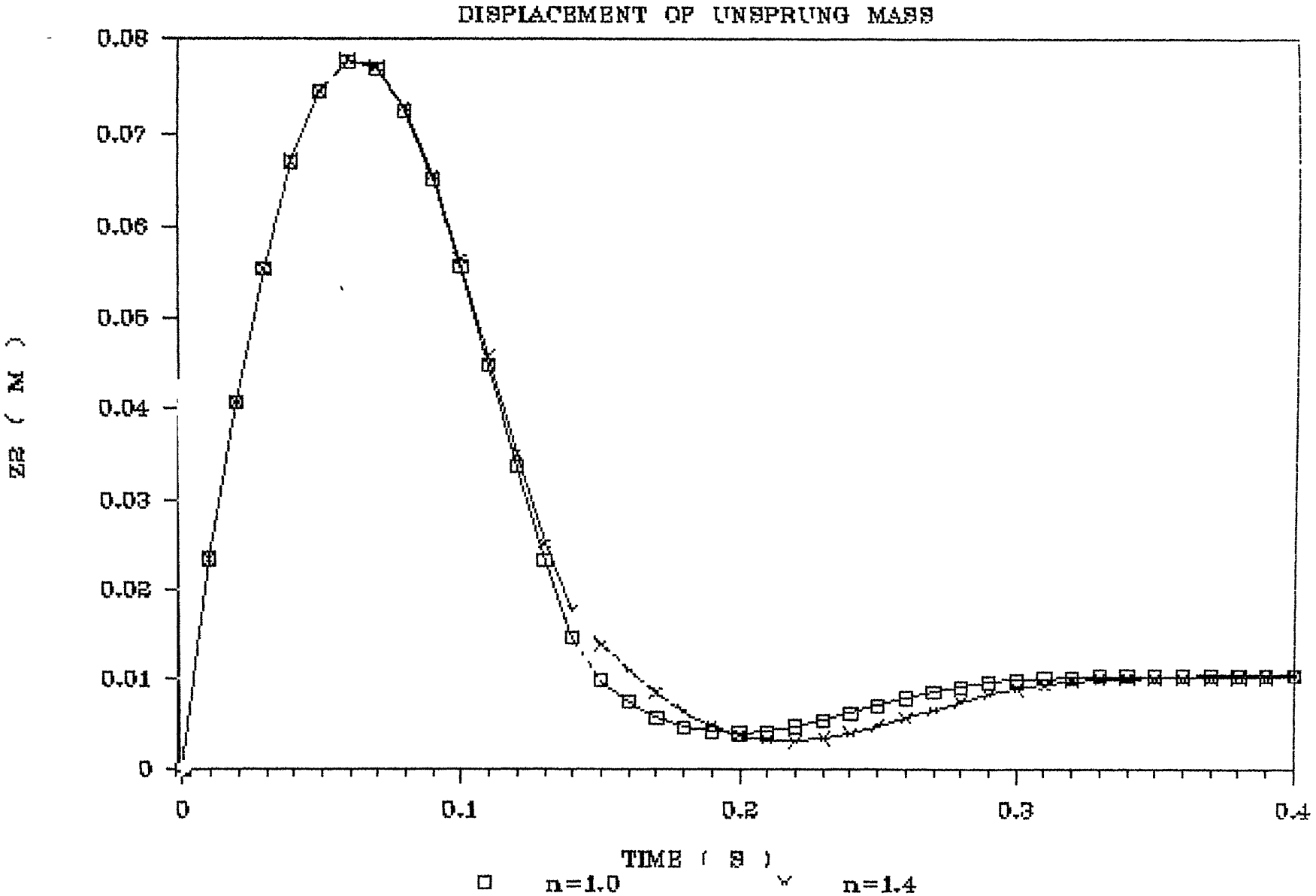

FIG 3.3b VARIATION IN DISPLACEMENT OF THE UNSPRUNG MASS WITH POLYTROPIC INDEX

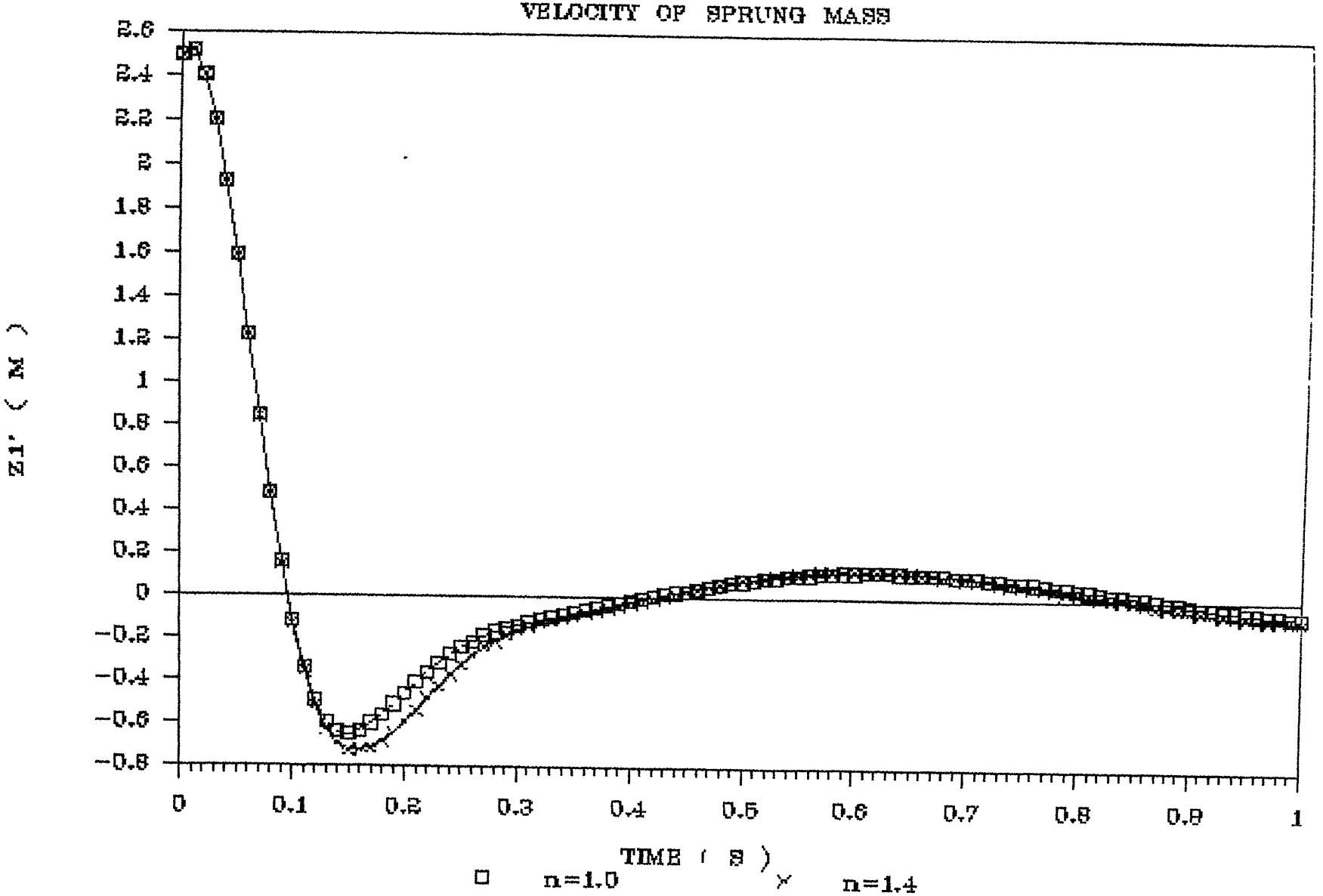

FIG 3.3c VARIATION IN VELOCITY OF THE SPRUNG MASS WITH POLYTROPIC INDEX

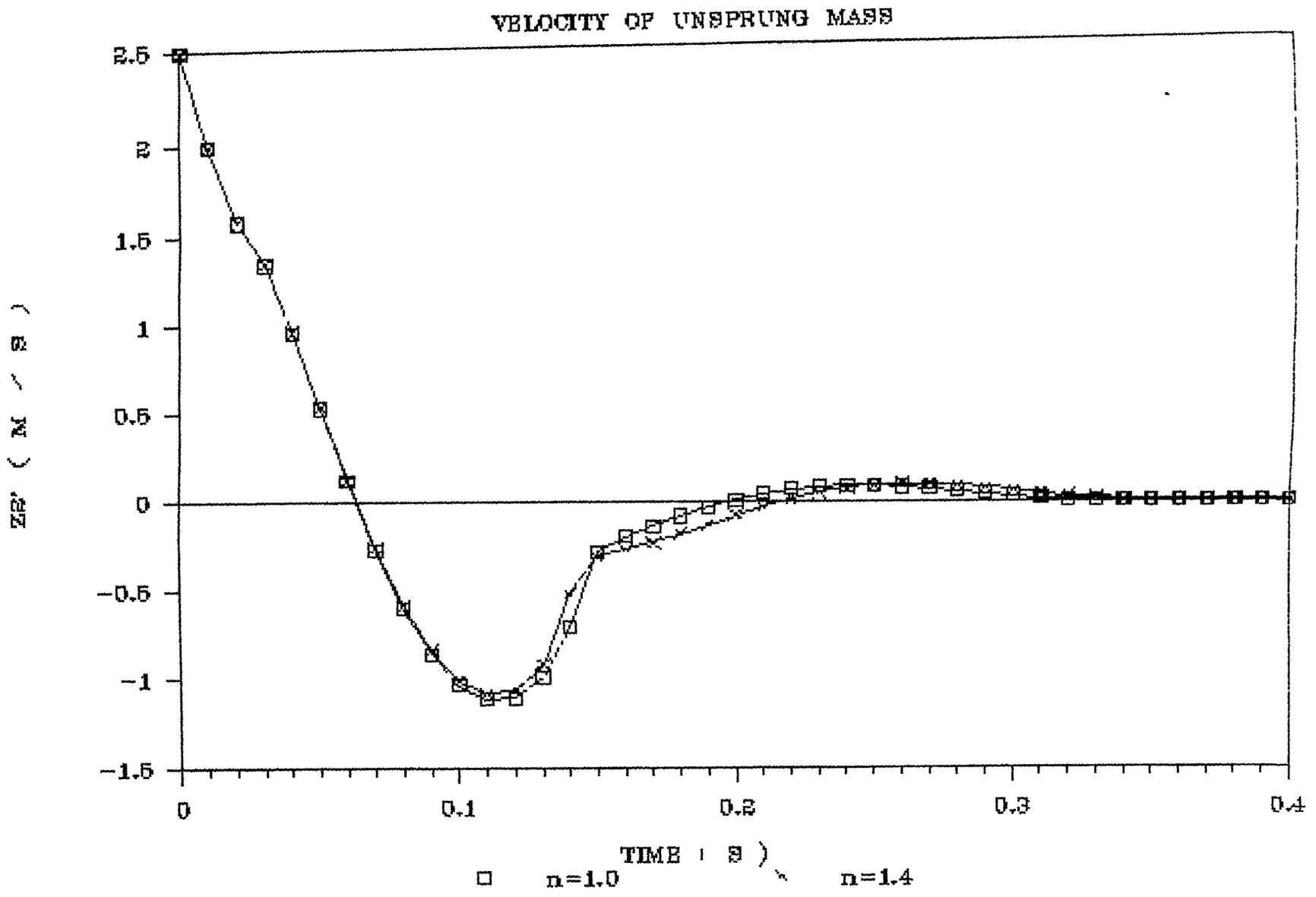

FIG 3.3d VARIATION IN VELOCITY OF THE UNSPRUNG MASS WITH POLYTROPIC INDEX

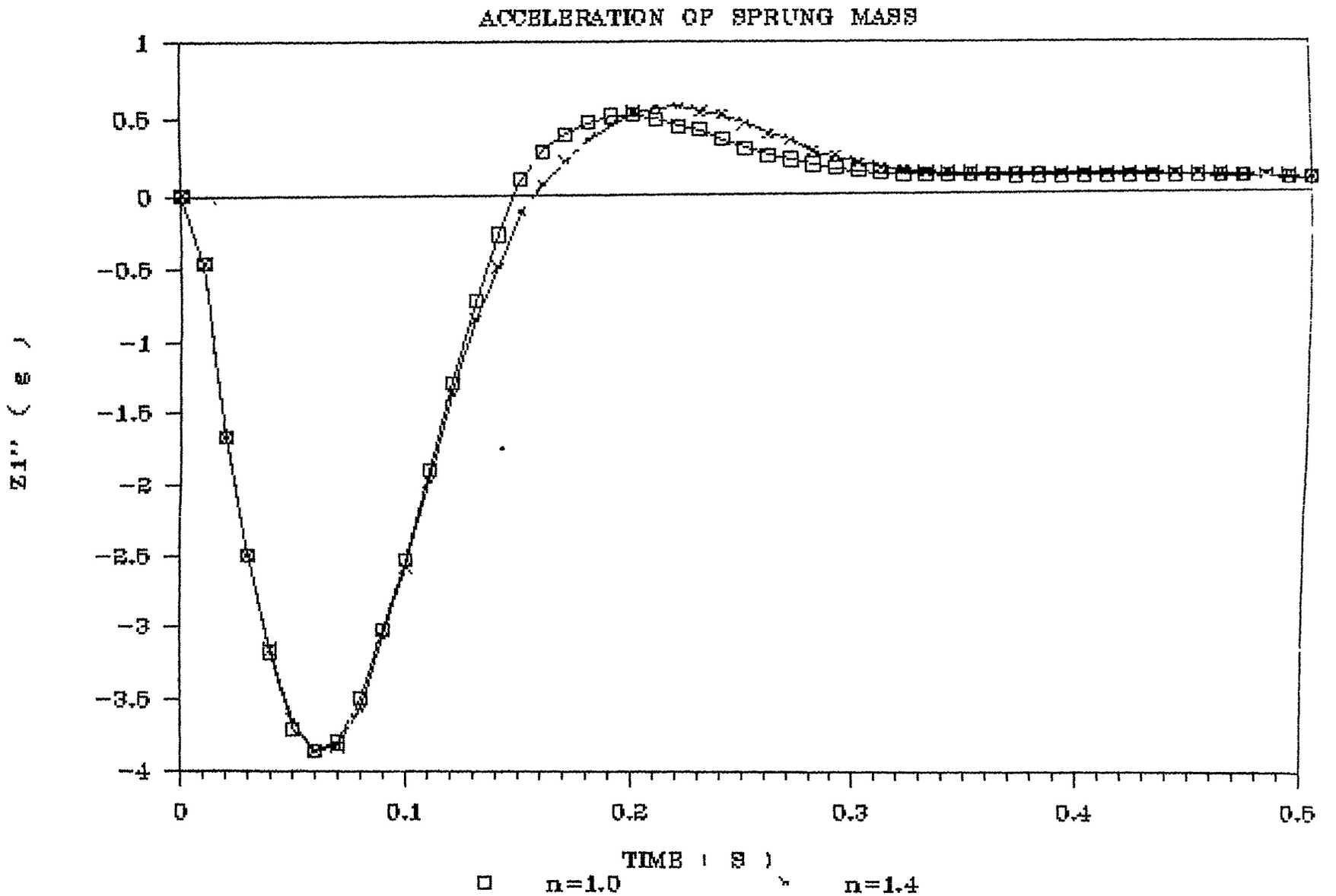

FIG 3.3e VARIATION IN ACCELERATION OF THE SPRUNG MASS WITH POLYTROPIC INDEX

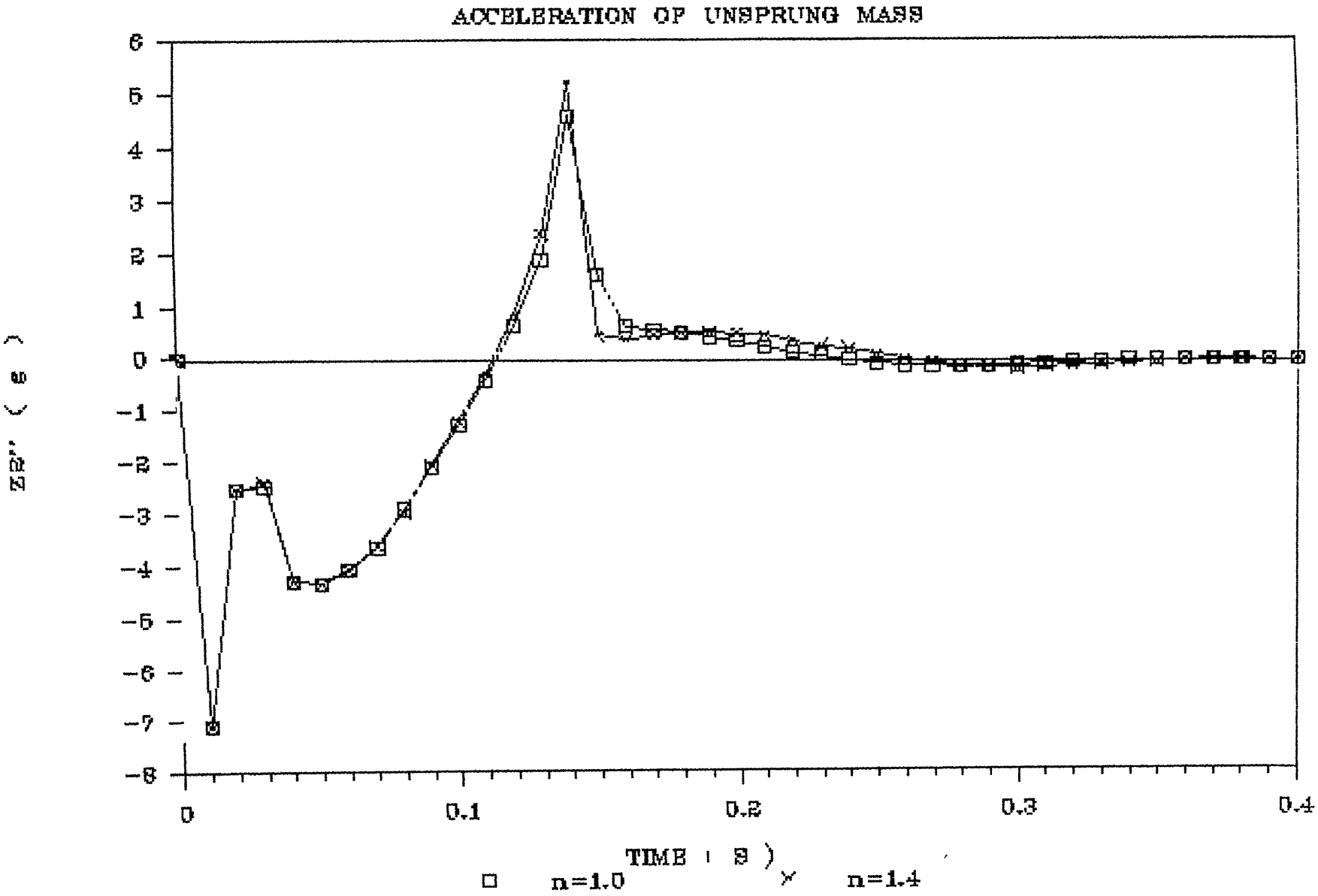

FIG 3.3f VARIATION IN ACCELERATION OF THE UNSPRUNG MASS WITH POLYTROPIC INDEX

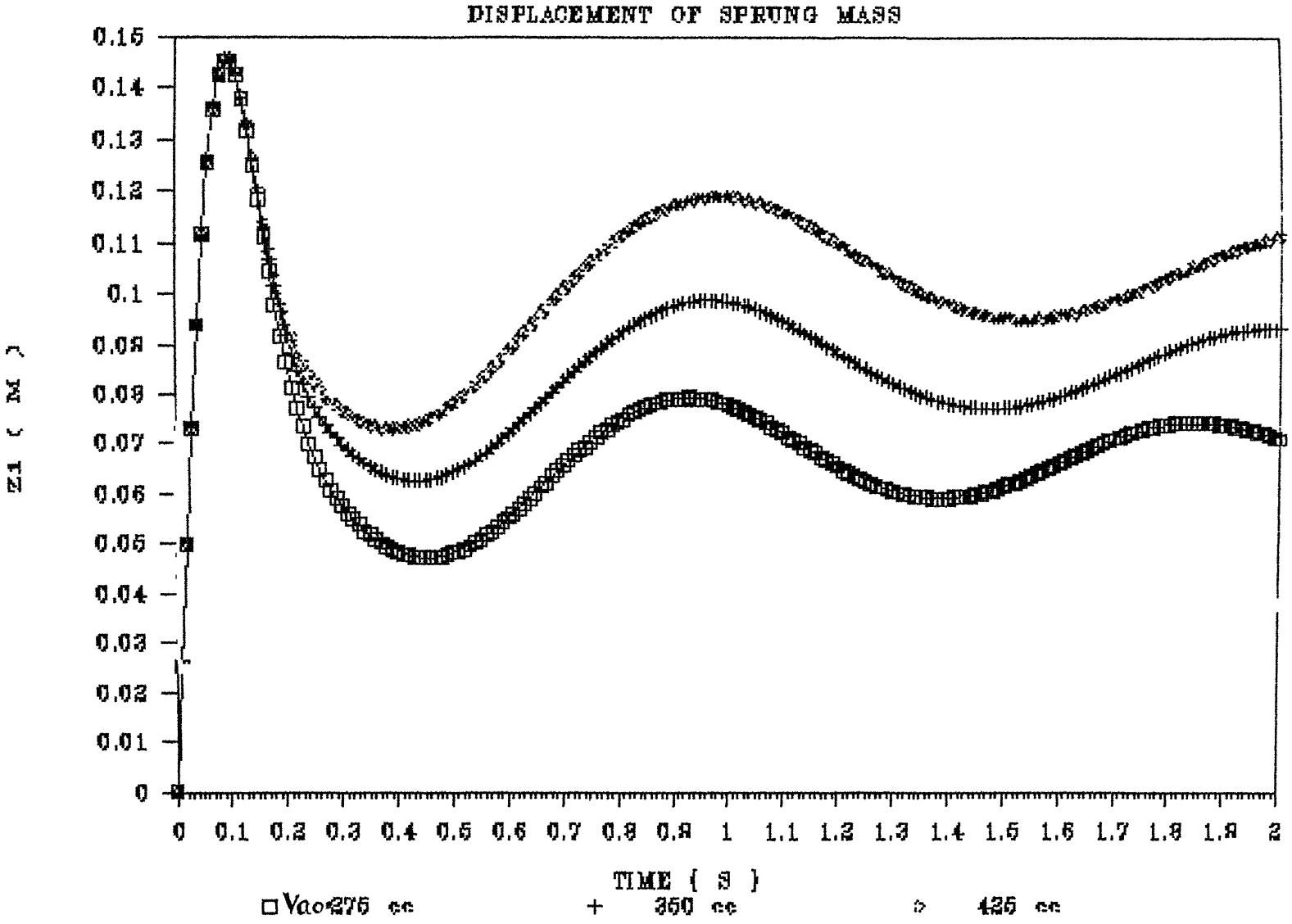

FIG 3.4a VARIATION IN DISPLACEMENT OF THE SPRUNG MASS WITH INITIAL AIR VOLUME

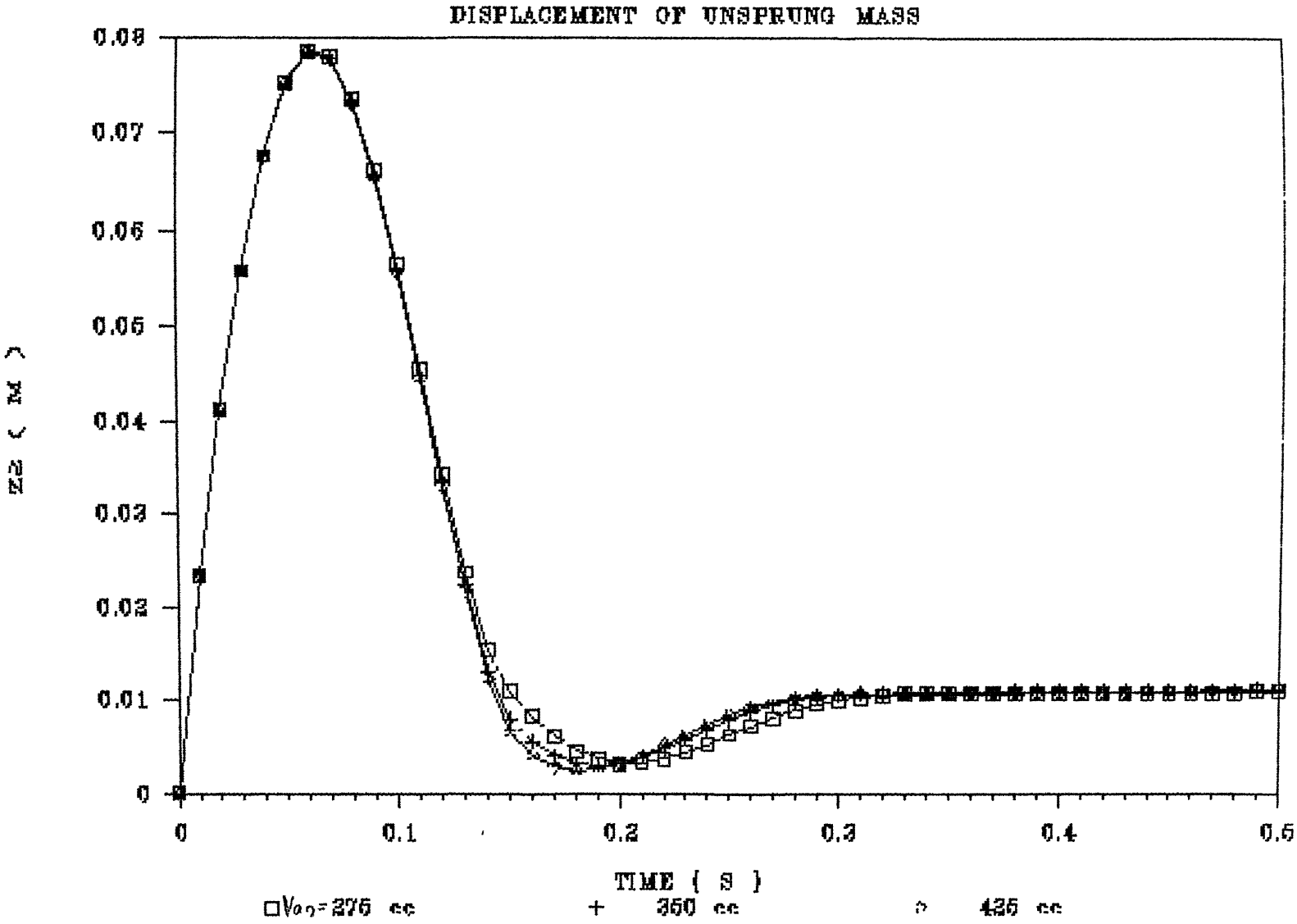

FIG 3.4b VARIATION IN DISPLACEMENT OF THE UNSPRUNG MASS WITH INITIAL AIR VOLUME

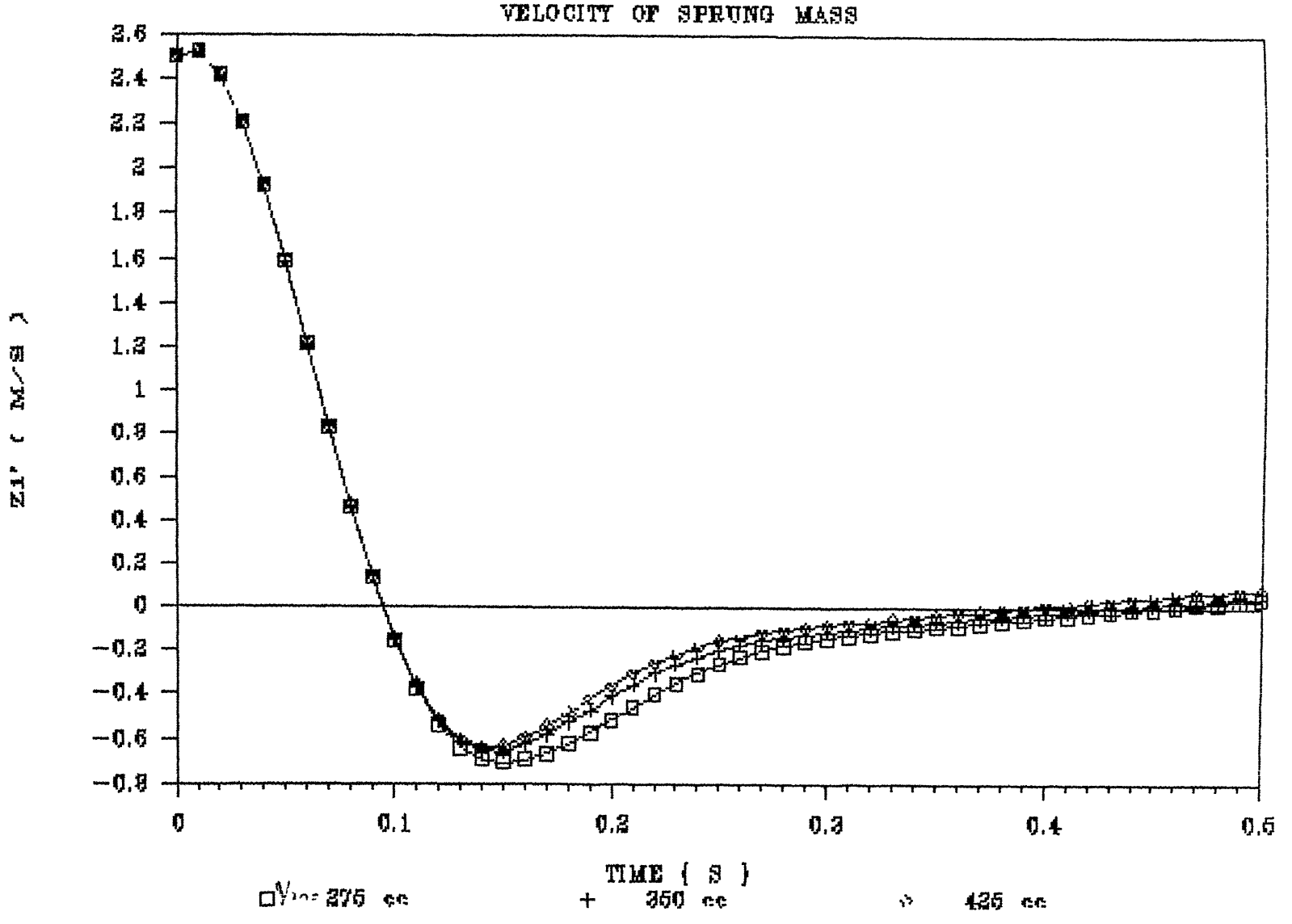

FIG 3.4c VARIATION IN VELOCITY OF THE SPRUNG MASS WITH INITIAL AIR VOLUME

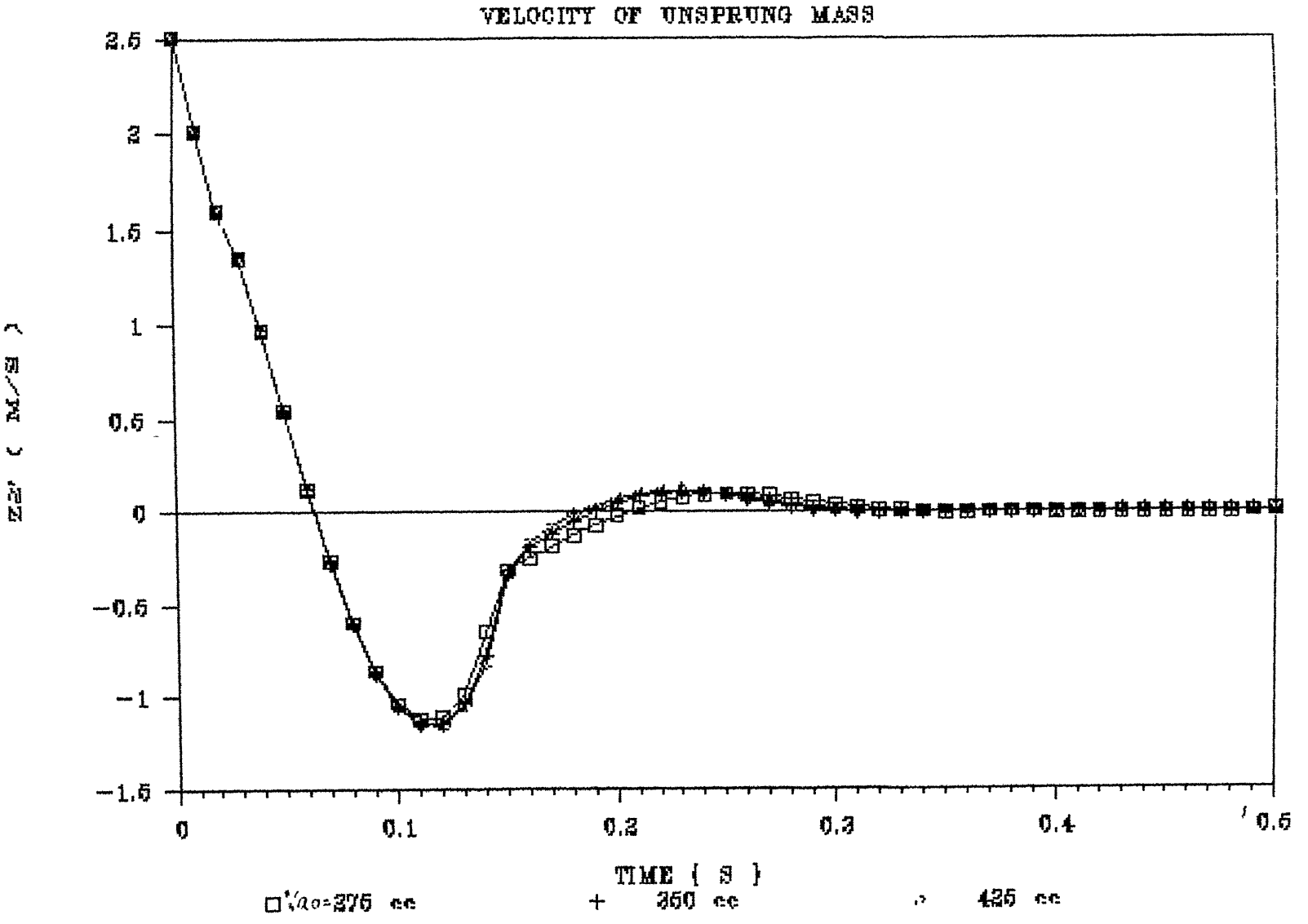

FIG 3.4d VARIATION IN VELOCITY OF THE UNSPRUNG MASS WITH INITIAL AIR VOLUME

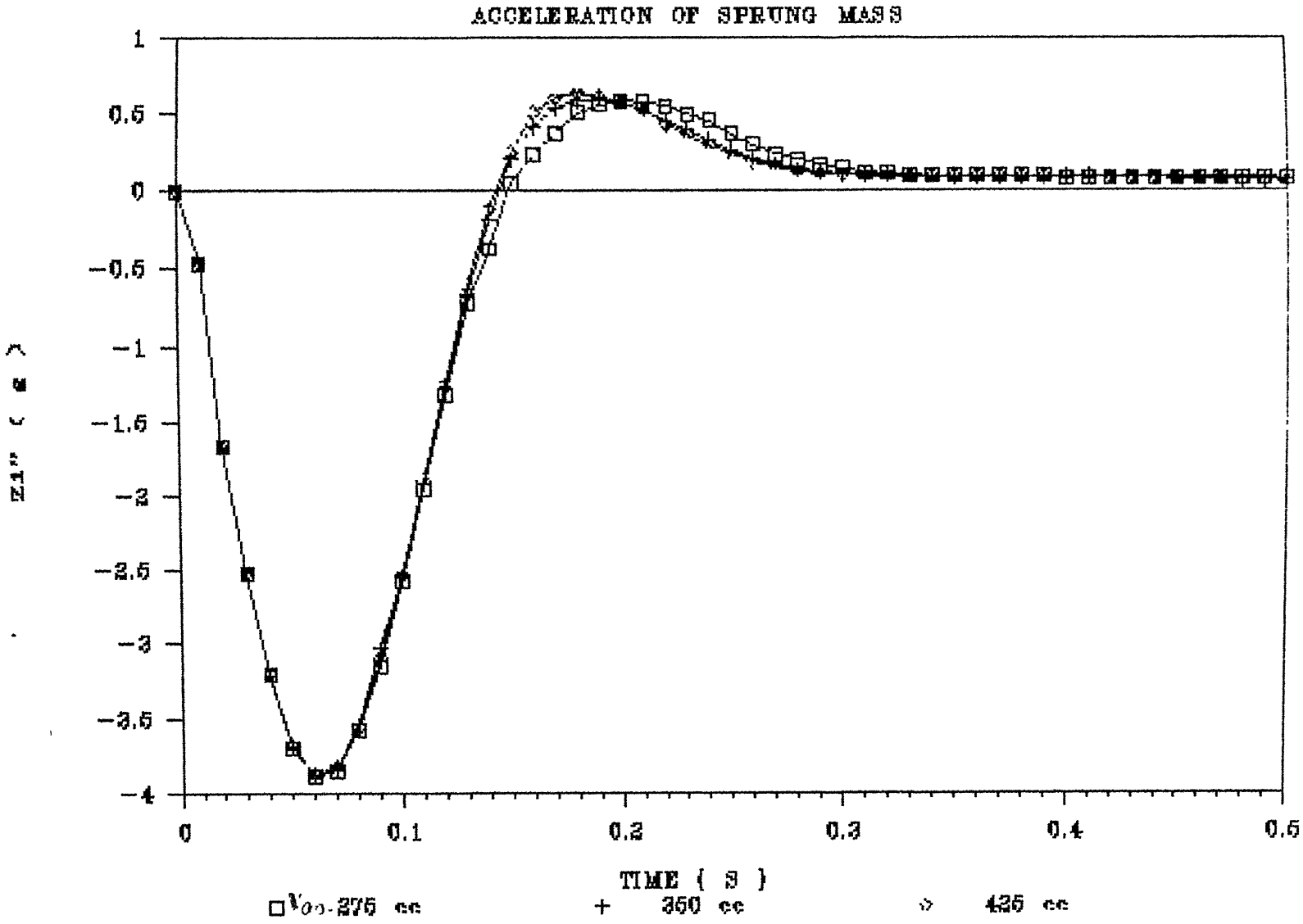

FIG 3.4e VARIATION IN ACCELERATION OF THE SPRUNG MASS WITH INITIAL AIR VOLUME

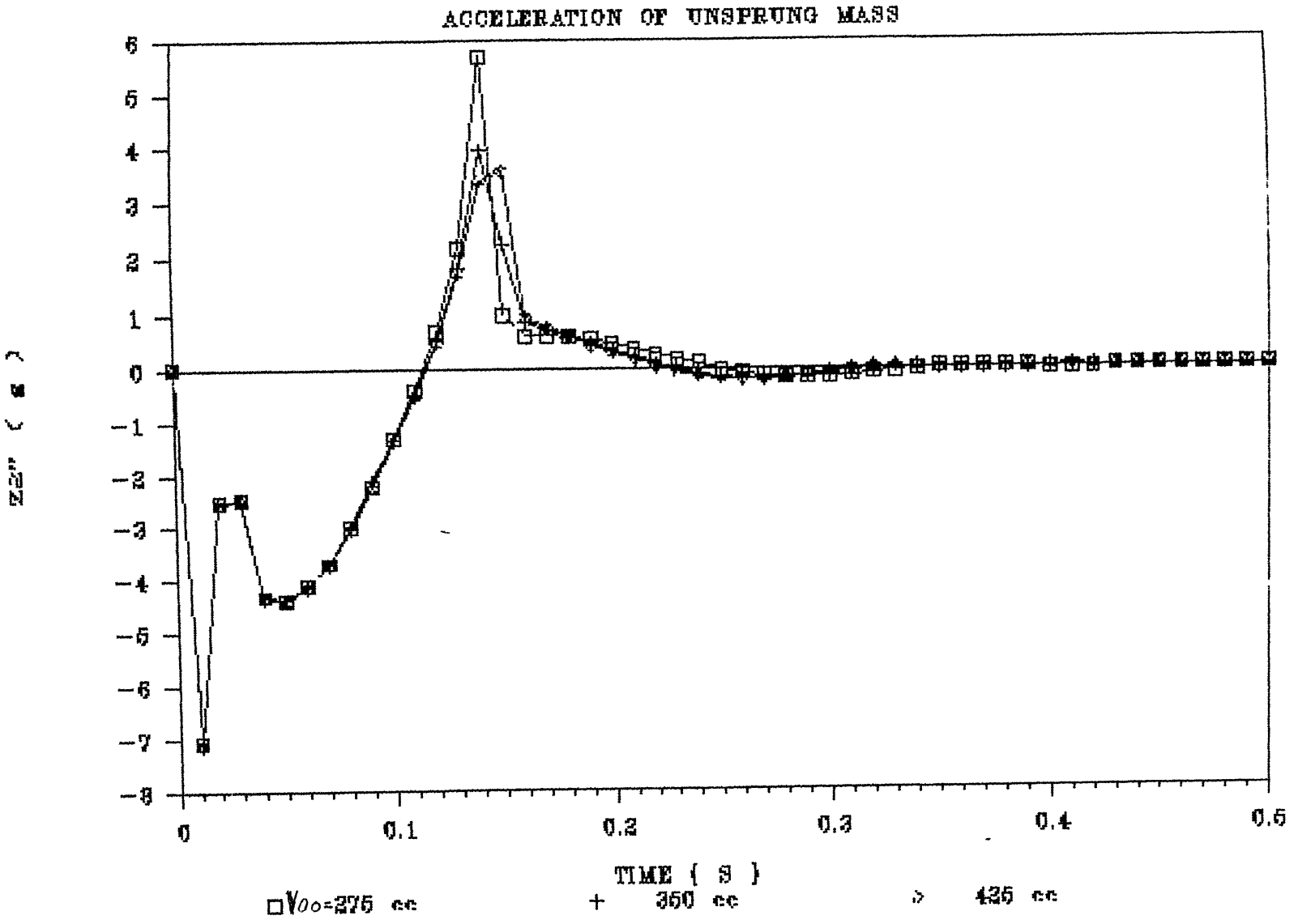

FIG 3.4f VARIATION IN ACCELERATION OF THE UNSPRUNG MASS WITH INITIAL AIR VOLUME

V_{a_o} increases (figure 3.4a) The peak acceleration of the unsprung mass also shows some variation. However on the whole it appears that for the present case the behaviour of the landing gear is not appreciably affected with variations in initial air volume.

3.1.5 Effect of Initial Air - Pressure

The influence of the initial air pressure on the response of the system are shown in figures 3.5a to 3.5f. Initial air pressures of 1 M Pa, 2 M Pa and 3 M Pa were used for generating system responses. An increased initial air pressure produces an increase in the pneumatic force in the shock strut. Thus the sprung mass displaces more for lower values of P_{a_o} (figure 3.5a). As the aircraft is supported by the force in the shock strut at the static equilibrium position the shock strut closure will be more for lower values of P_{a_o}. Thus with decreasing initial air pressure, the sprung mass rests closer to the ground level (figure 3.5a). The velocity and acceleration responses of the sprung mass (figure 3.5c and 3.5e) and the unsprung mass (3.5d and 3.5f) and the displacement of the unsprung mass (figure 3.5b) are not considerably affected by the initial air pressure in the present case, except that the amplitude of the responses is higher for lower P_{a_o}. In conclusion the effect of initial air pressure is only marginal.

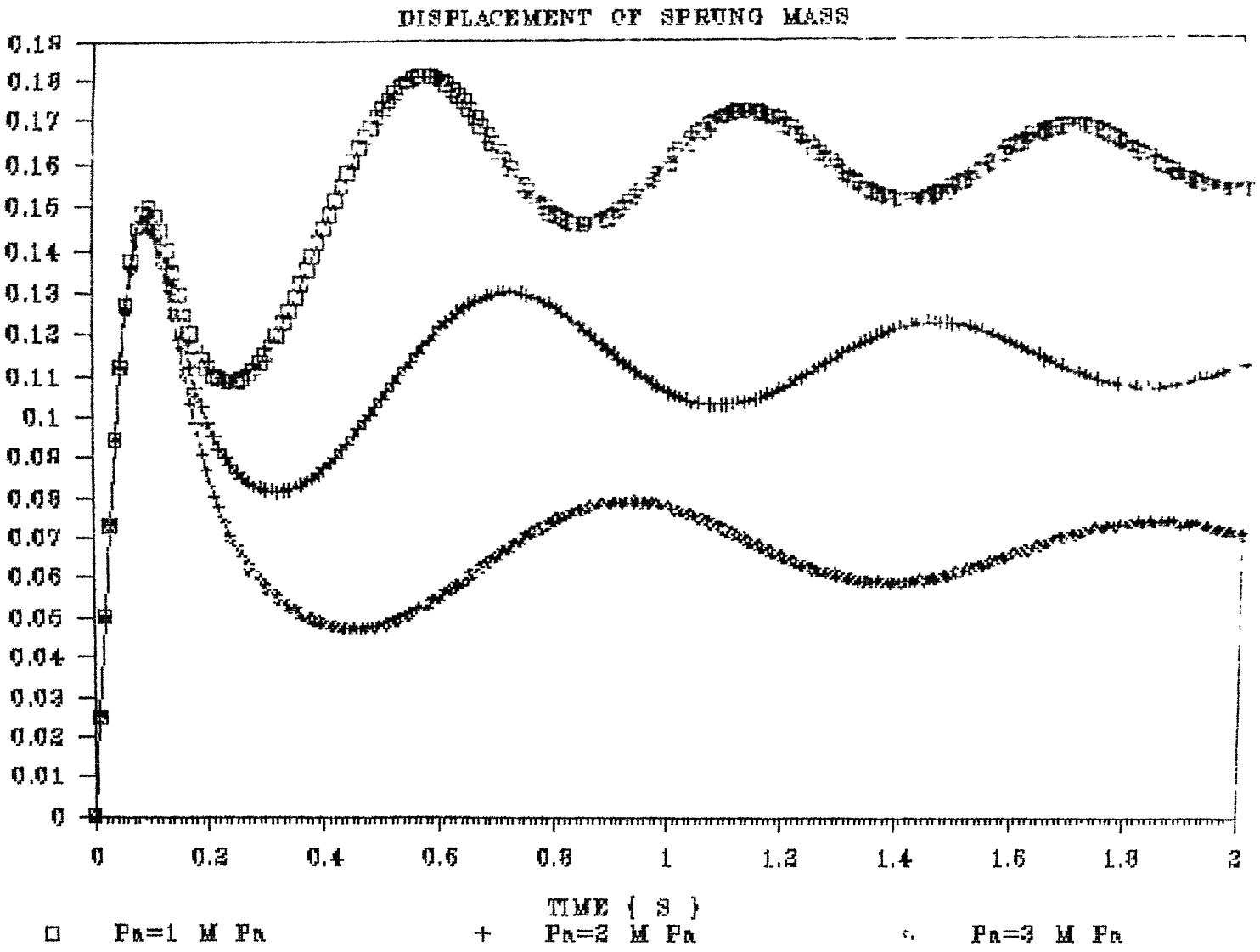

FIG 3.5a VARIATION IN DISPLACEMENT OF THE SPRUNG MASS WITH INITIAL AIR PRESSURE

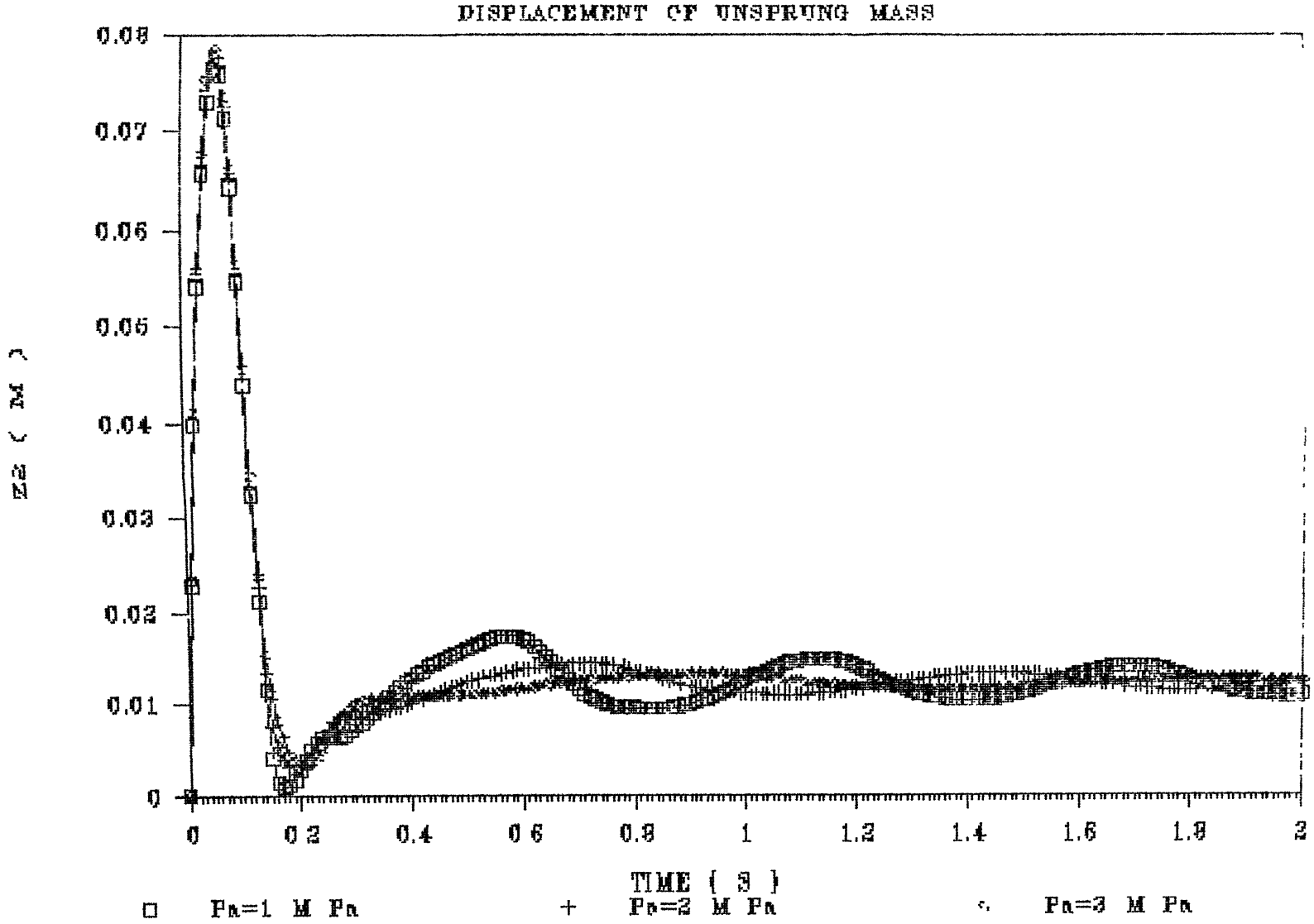

FIG 3.5b VARIATION IN DISPLACEMENT OF THE UNSPRUNG MASS WITH INITIAL AIR PRESSURE

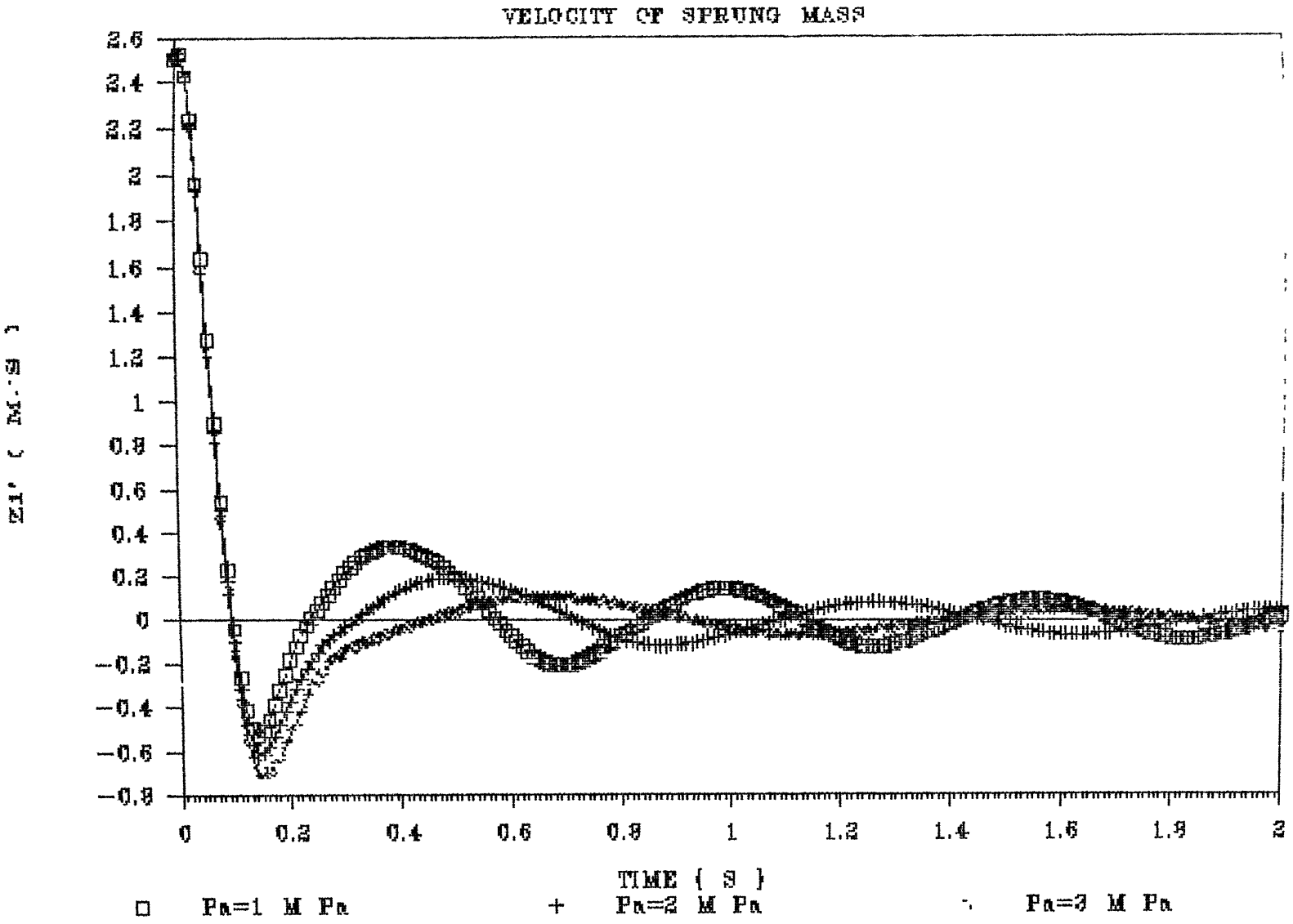

FIG 3.5c VARIATION IN VELOCITY OF THE SPRUNG MASS WITH INITIAL AIR PRESSURE

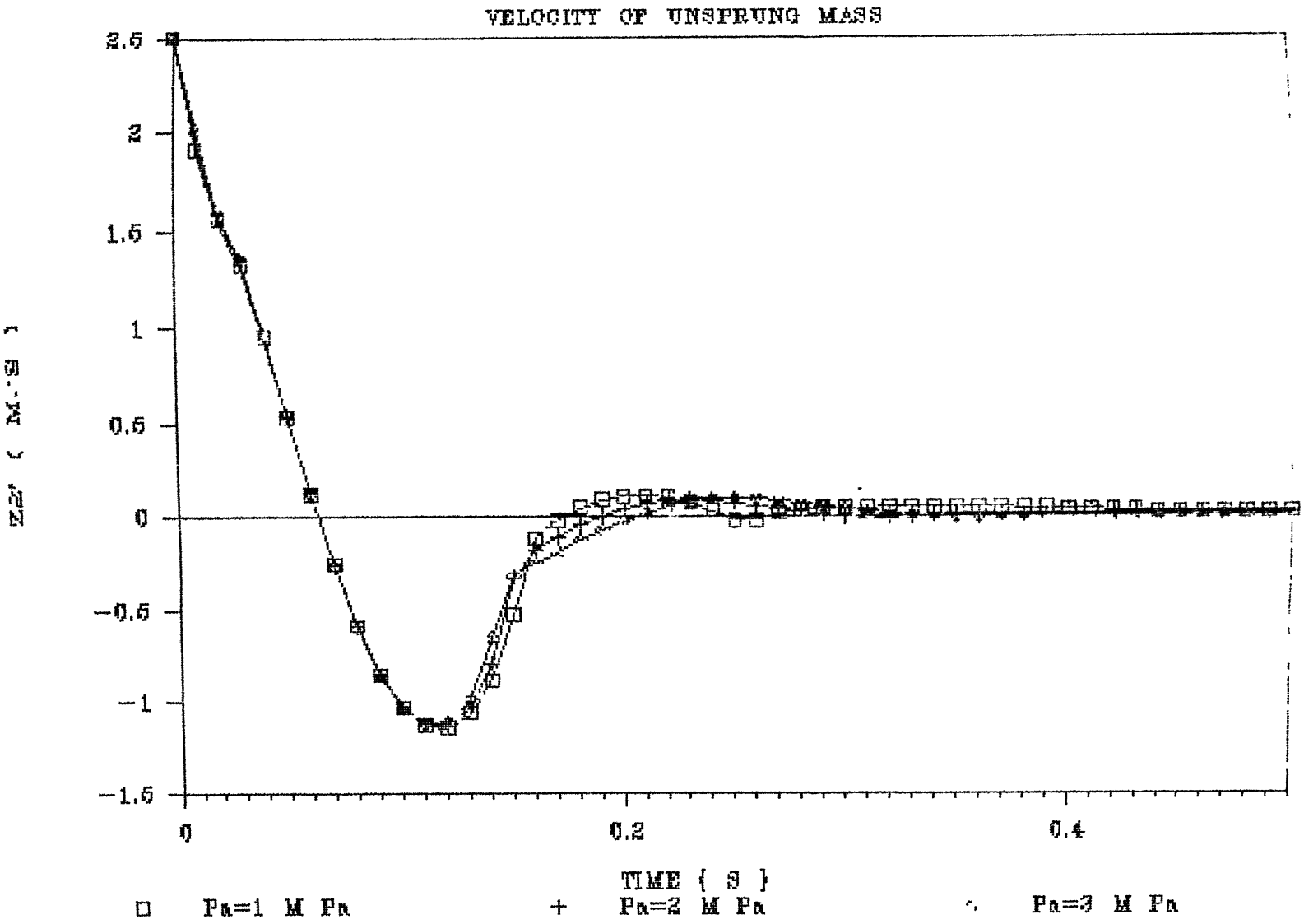

FIG 3.5d VARIATION IN VELOCITY OF THE UNSPRUNG MASS WITH INITIAL AIR PRESSURE

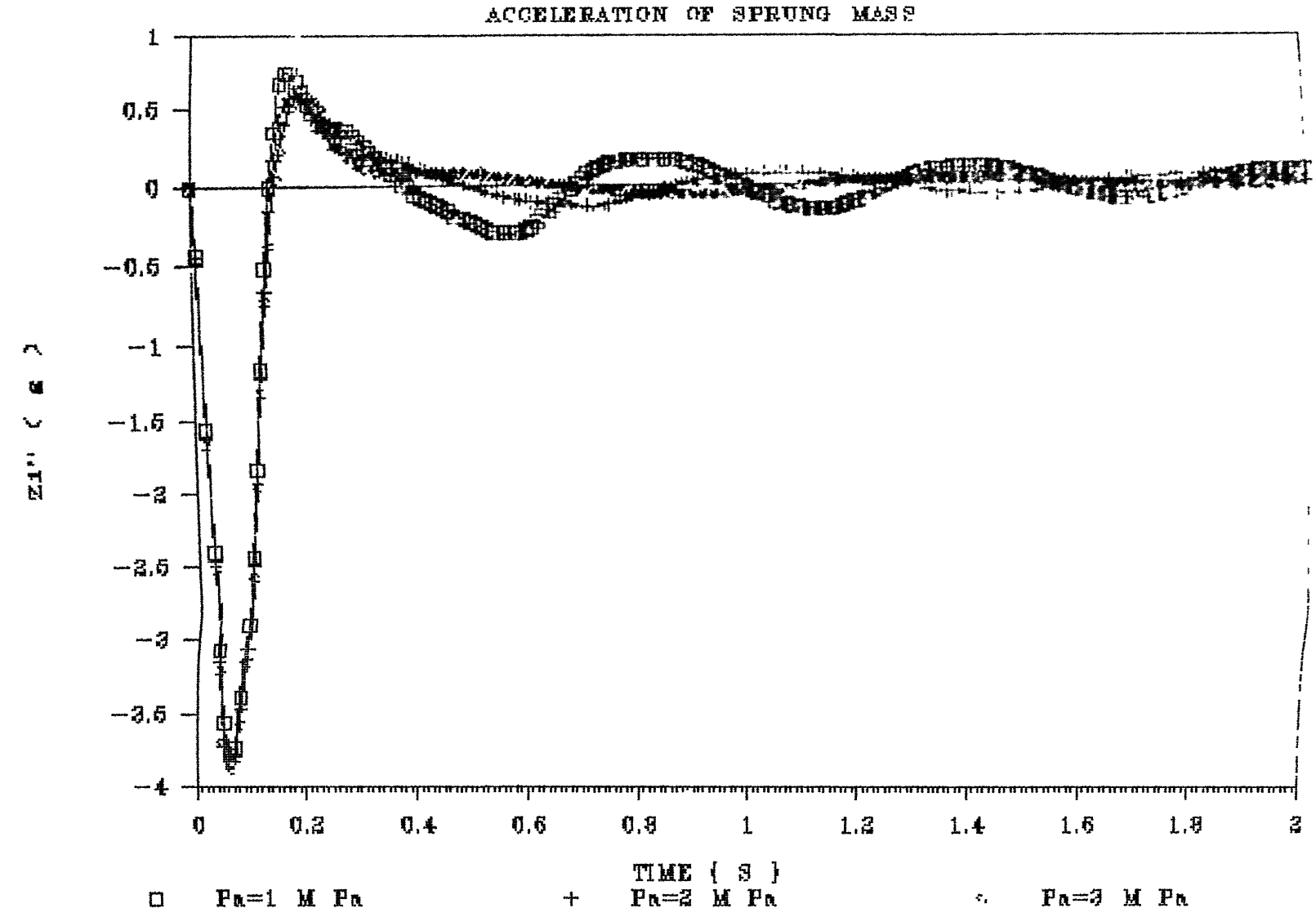

FIG 3.5e VARIATION IN ACCELERATION OF THE SPRUNG MASS WITH INITIAL AIR PRESSURE

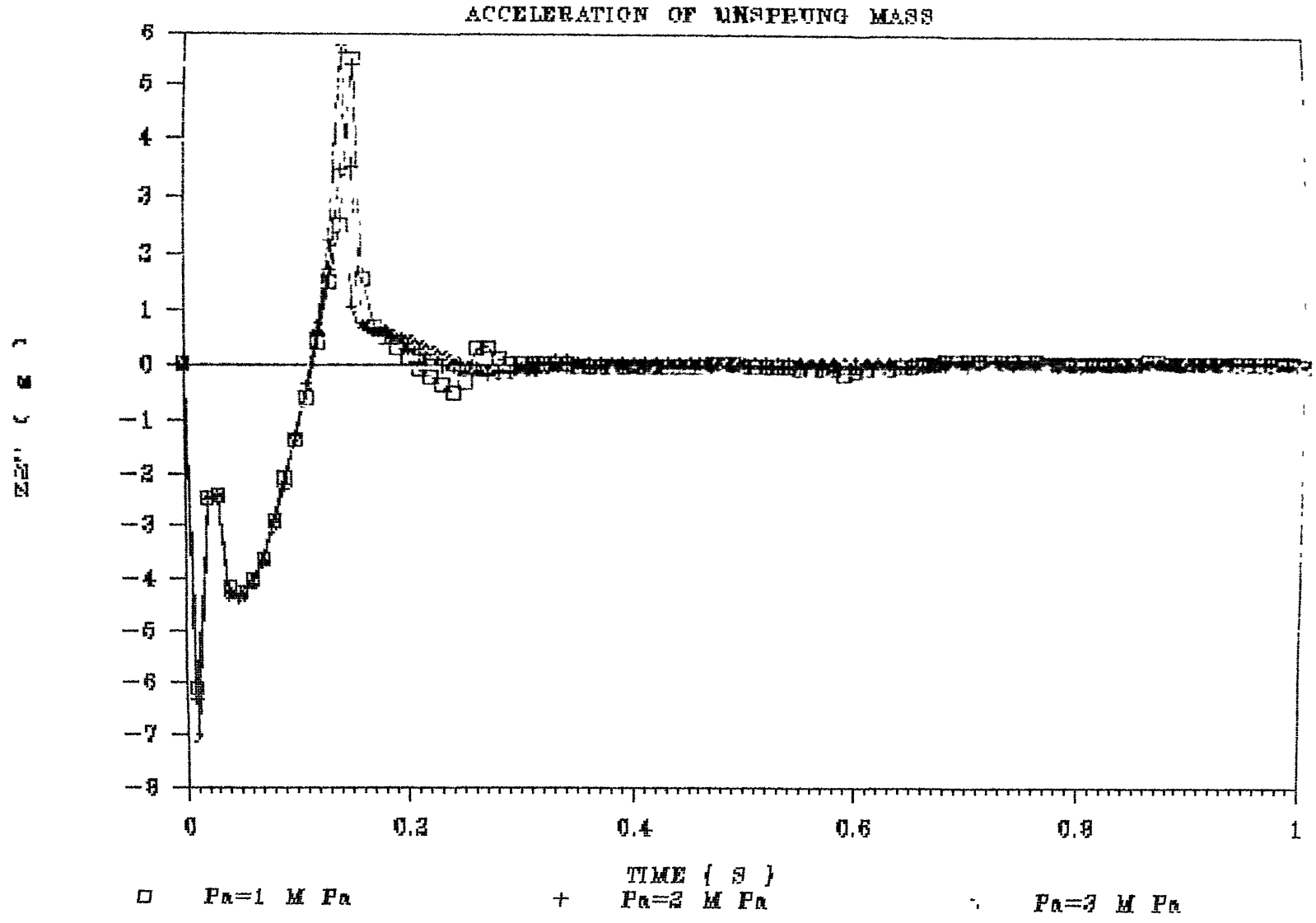

FIG 3.5f VARIATION IN ACCELERATION OF THE UNSPRUNG MASS WITH INITIAL AIR PRESSURE

3.2 PARAMETRIC STUDY OF THE HEAVE-PITCH MODEL

3.2.1 Effect of the Pitching Moment on Inertia of the Aircraft

Figures 3.6a to 3.6l explains the effect of the pitching moment of inertia I_{yy} of the aircraft for the same set of initial conditions. An increase in I_{yy} for the same mass of the aircraft produces a large inertia force in pitching. Thus,

(a). The displacement, velocity and acceleration of the airframe are not significantly influenced by I_{yy} (figures 3.6a, 3.6e and 3.6i)

(b). The pitching response of the aircraft is considerably affected by changes in the value of I_{yy} (figures 3.6b, 3.6f and 3.6j)

(c). Time history curves for the rigid body rotation show that the frequency of rotation is less as I_{yy} is increased (figures 3.6b, 3.6f and 3.6j)

(d). The response of the main wheels which are closer to the aircraft center of gravity are not significantly affected (figures 3.6d, 3.6h and 3.6l)

(e). The nose wheel responses are appreciably affected as they are at some distance from the center of gravity of the aircraft (figures 3.6c, 3.6g and 3.6h)

(f). It can be concluded that the cockpit acceleration may also be considerably affected because of the long rotation arm

Thus, while the effect of I_{yy} may not be significant at

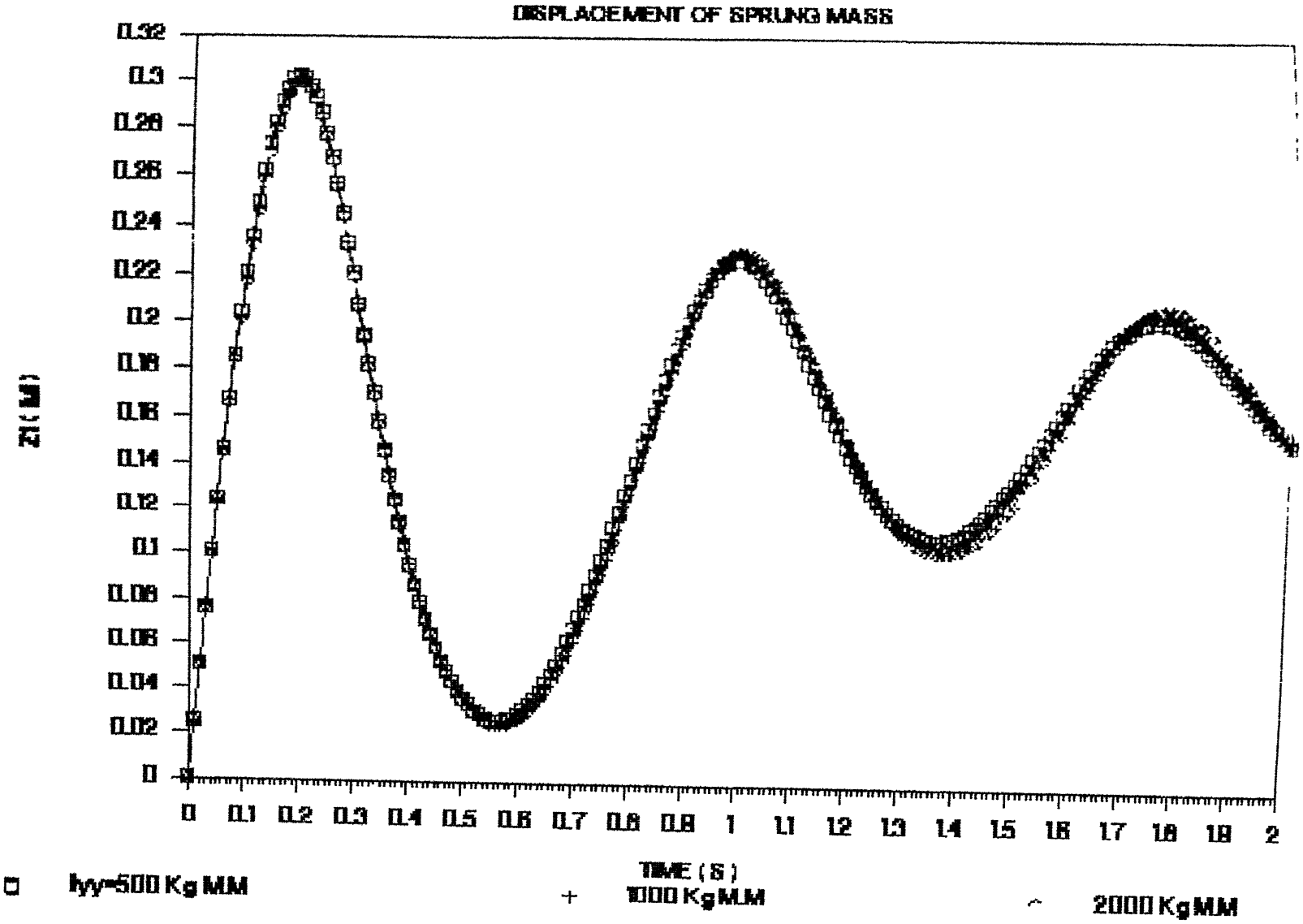

FIG 3.6a VARIATION IN DISPLACEMENT OF THE SPRUNG MASS WITH THE PITCHING MOMENT OF INERTIA

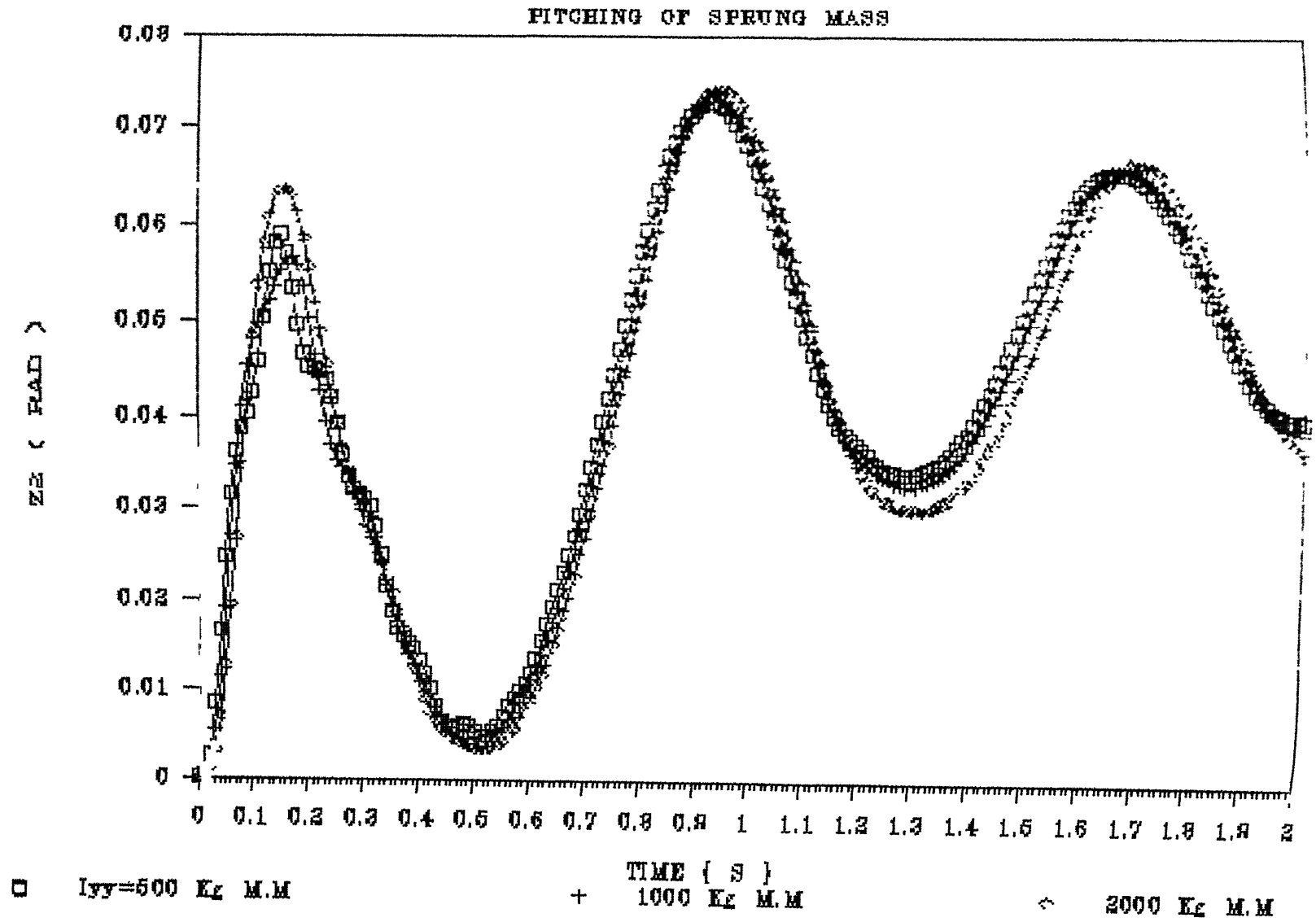

FIG 3.6b VARIATION IN PITCHING RESPONSE OF THE SPRUNG MASS WITH THE PITCHING MOMENT OF INERTIA

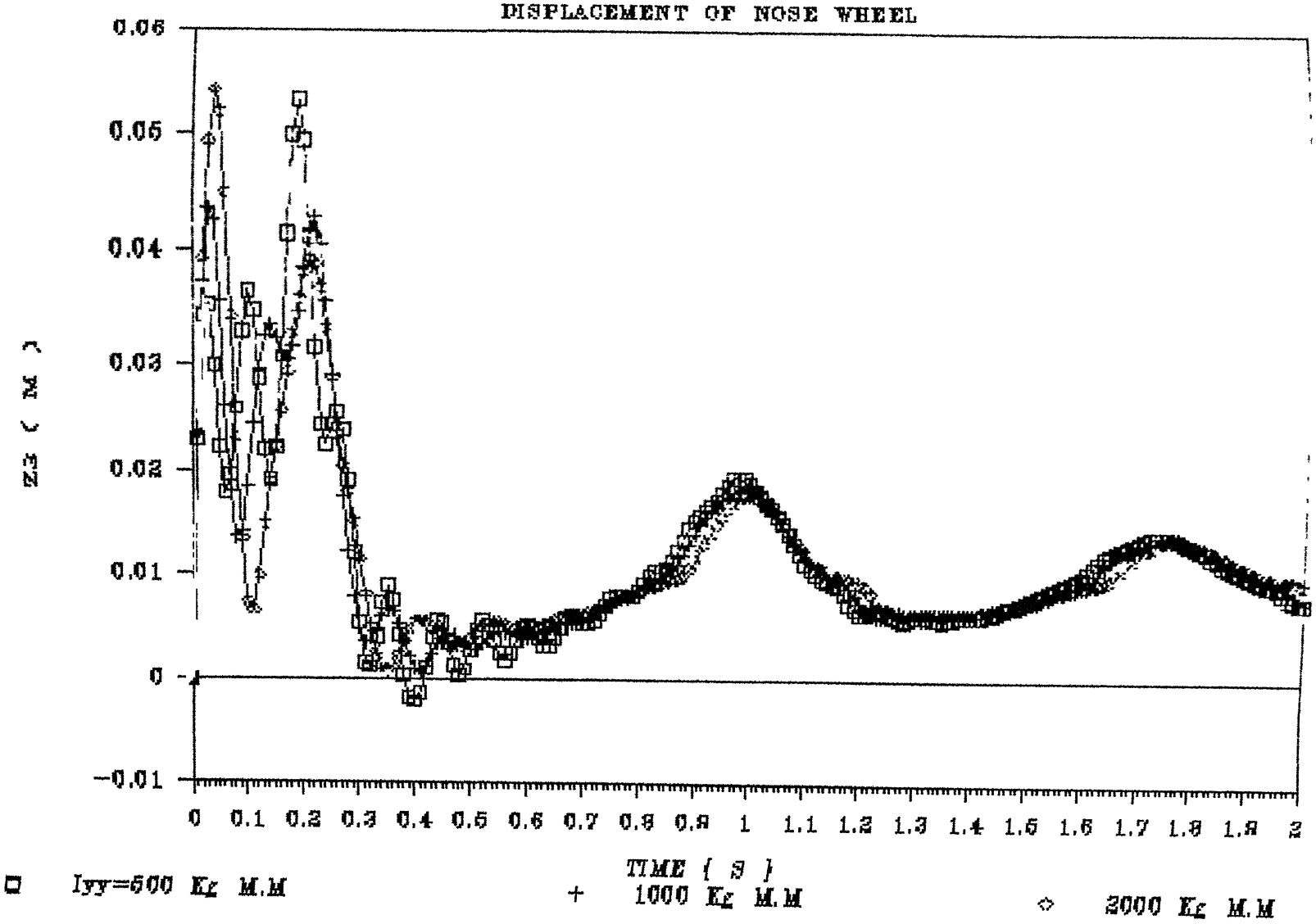

FIG 3.6c VARIATION IN DISPLACEMENT OF THE NOSE WHEEL WITH THE PITCHING MOMENT OF INERTIA

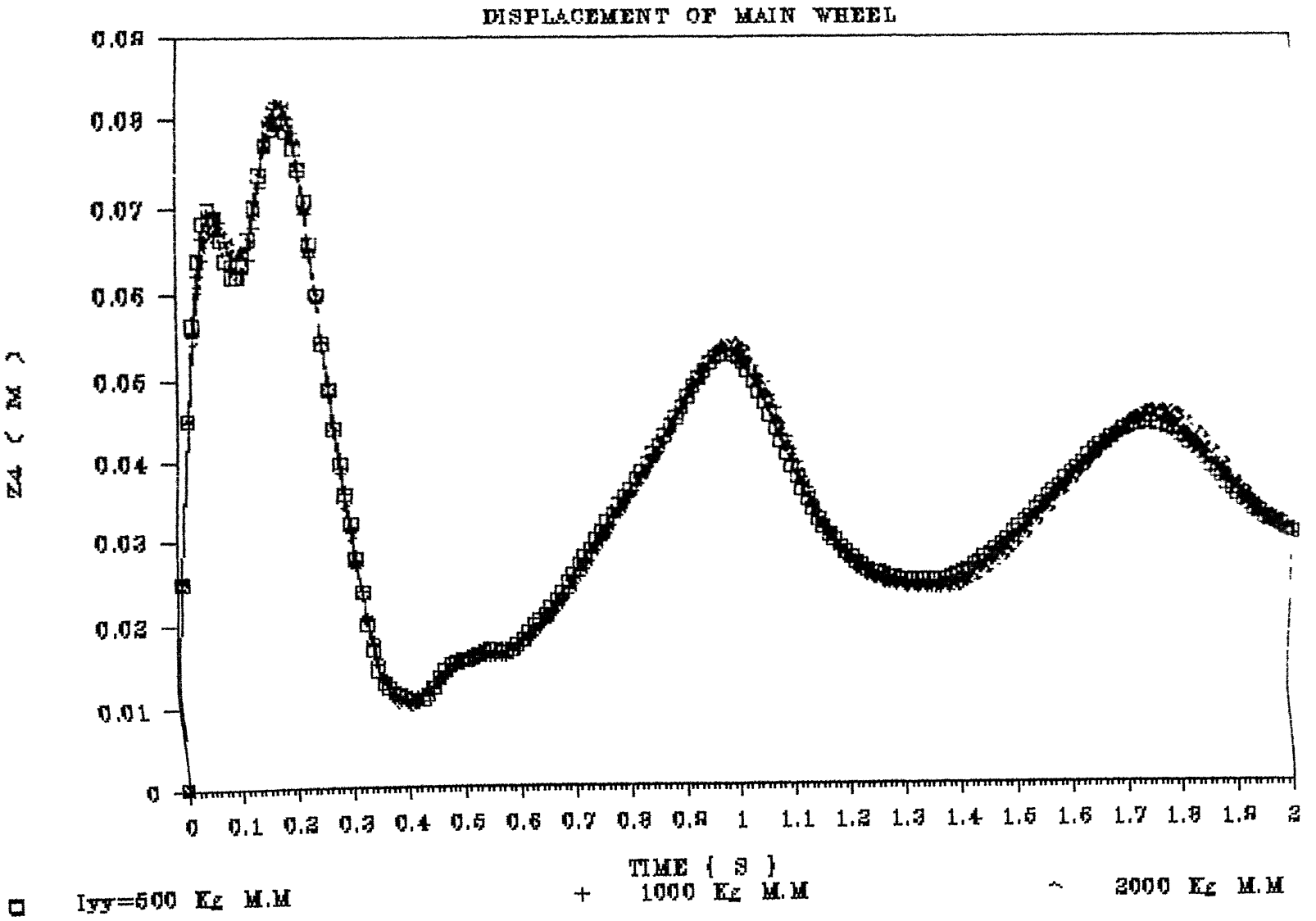

FIG 3.6d VARIATION IN DISPLACEMENT OF THE MAIN WHEEL WITH THE PITCHING MOMENT OF INERTIA

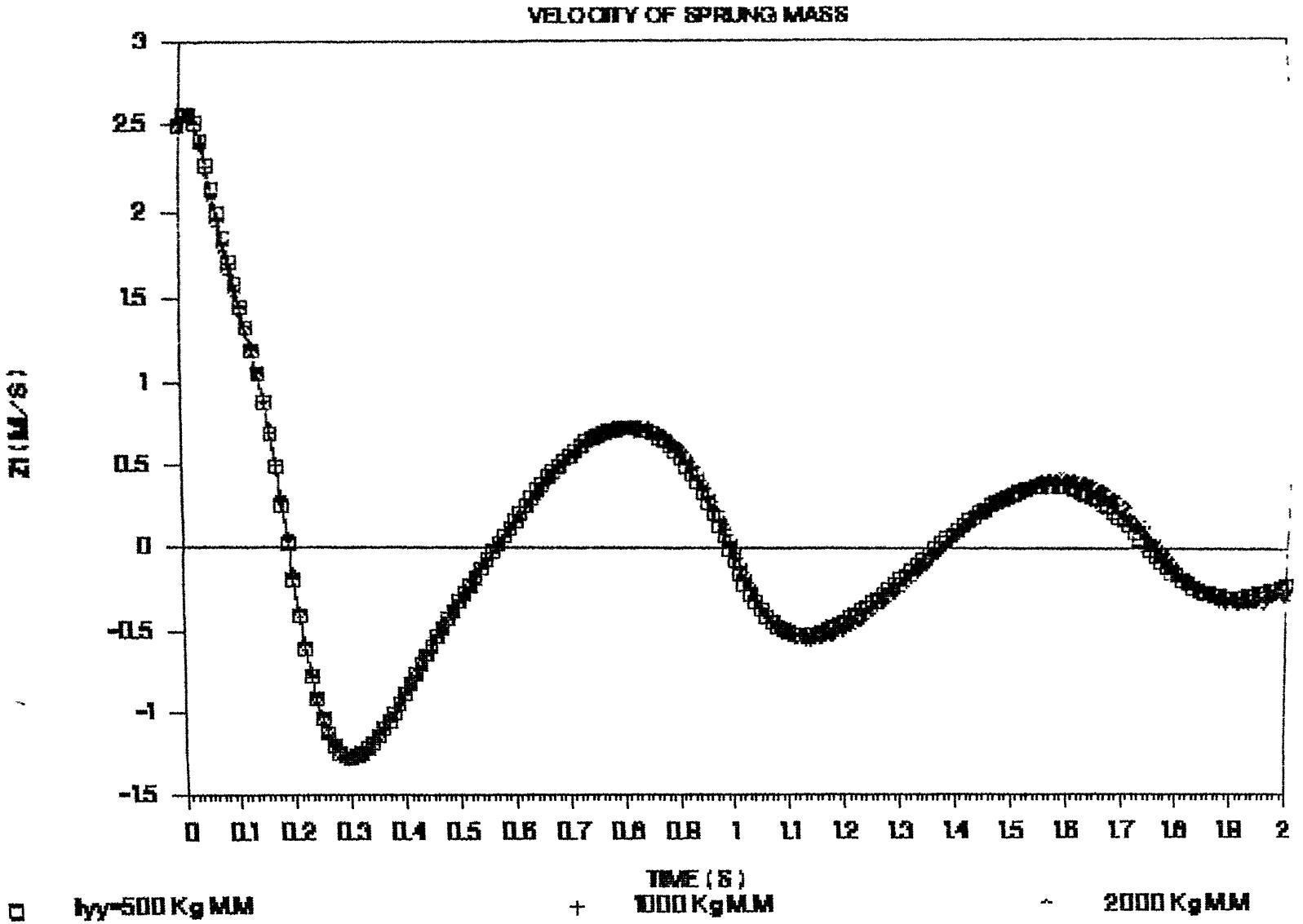

FIG 3.6e VARIATION IN VELOCITY OF THE SPRUNG MASS WITH THE PITCHING MOMENT OF INERTIA

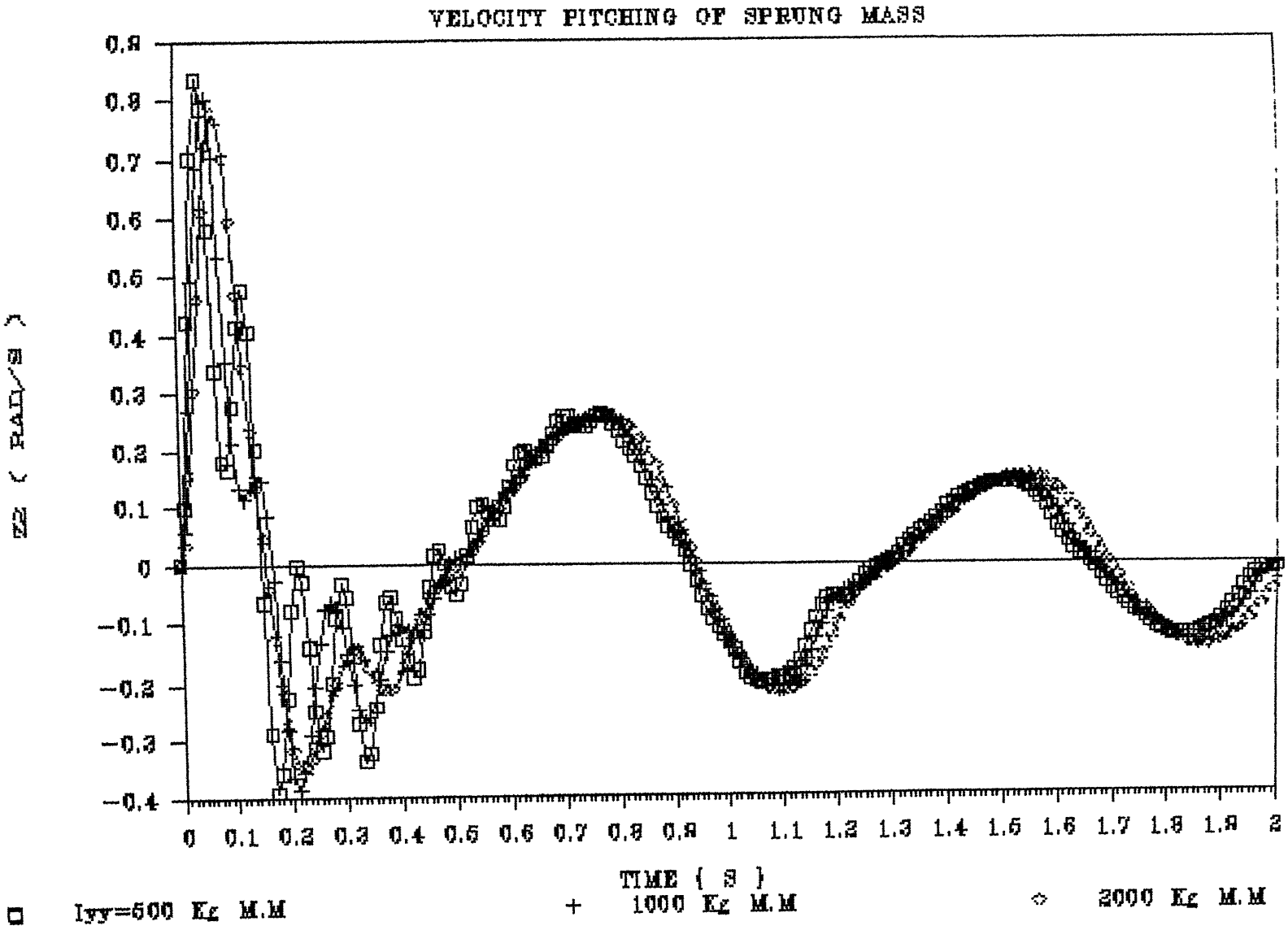

FIG 3.6f VARIATION IN VELOCITY OF PITCHING OF THE SPRUNG MASS WITH THE PITCHING MOMENT OF INERTIA

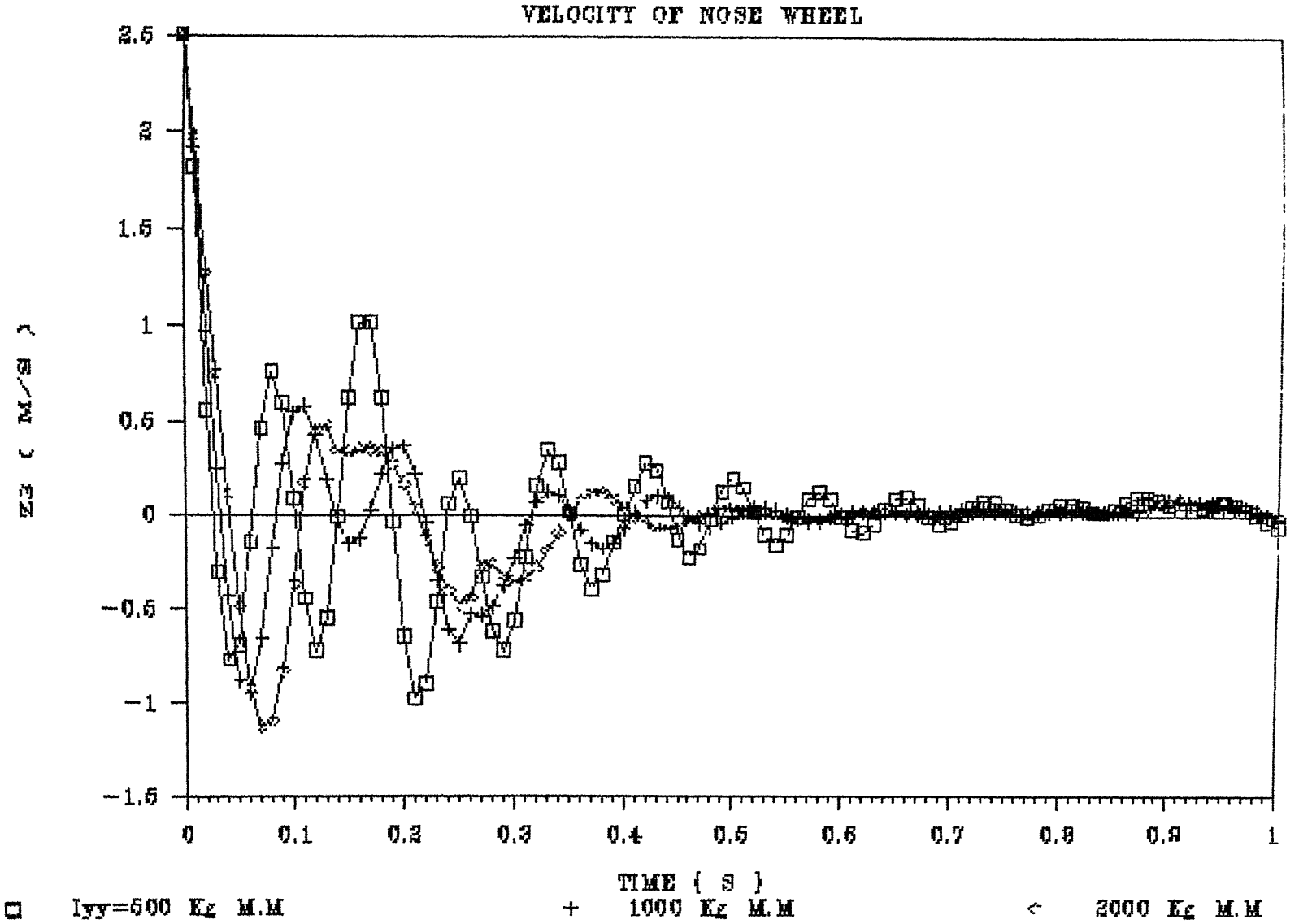

FIG 3.6g VARIATION IN VELOCITY OF THE NOSE WHEEL WITH THE PITCHING MOMENT OF INERTIA

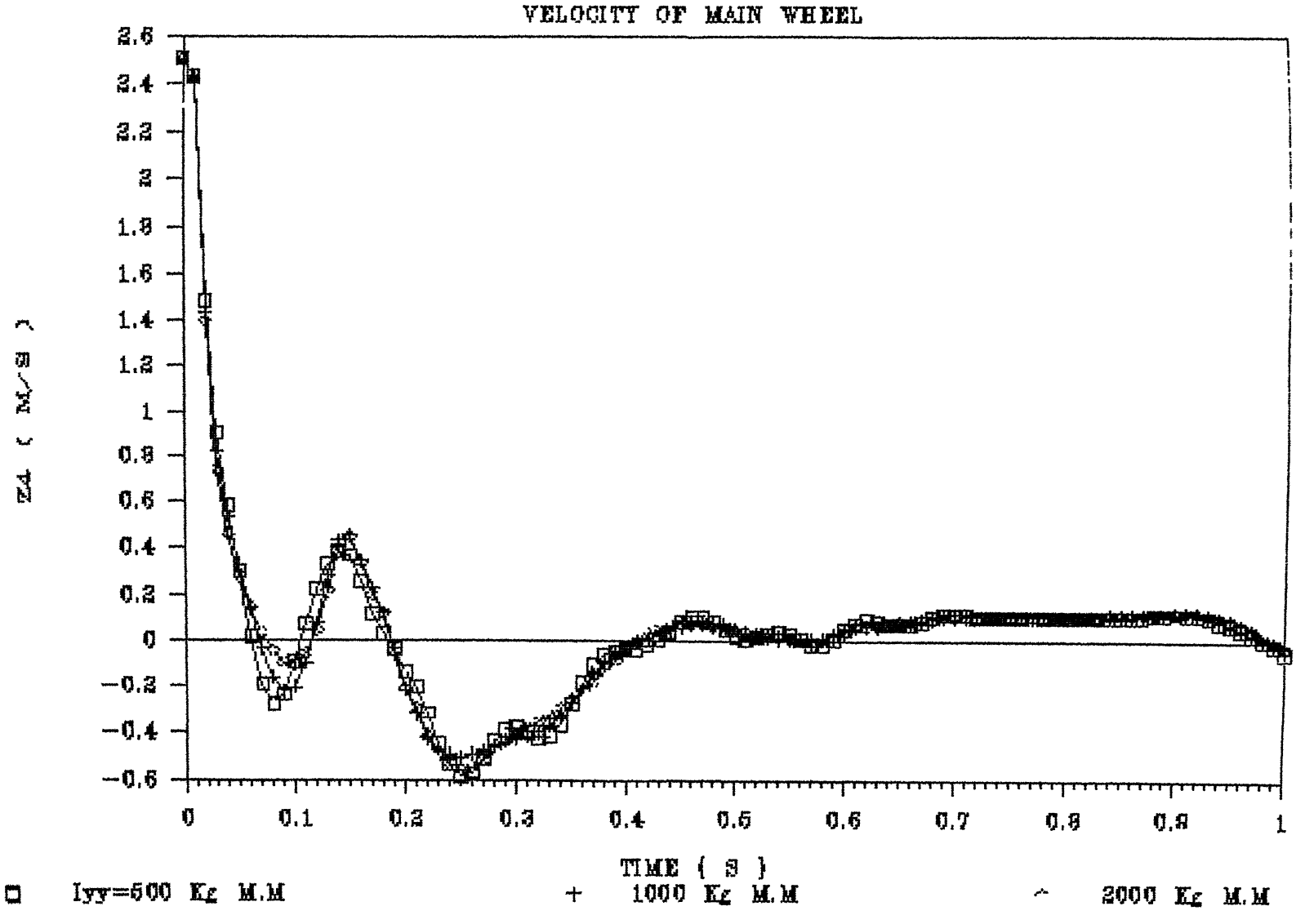

FIG 3.6h VARIATION IN VELOCITY OF THE MAIN WHEEL WITH THE PITCHING MOMENT OF INERTIA

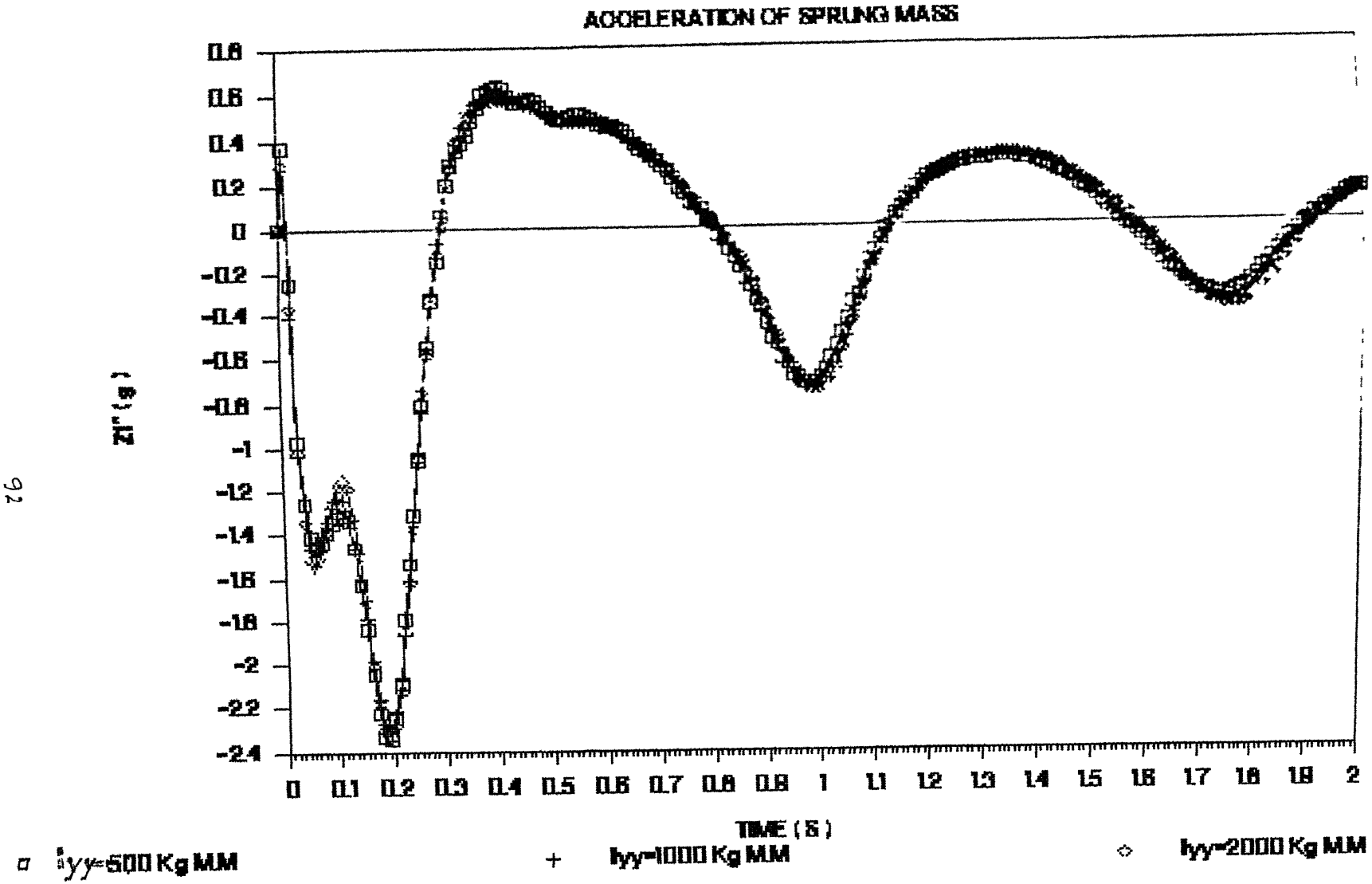

FIG 3.6i VARIATION IN ACCELERATION OF THE SPRUNG MASS WITH THE PITCHING MOMENT OF INERTIA

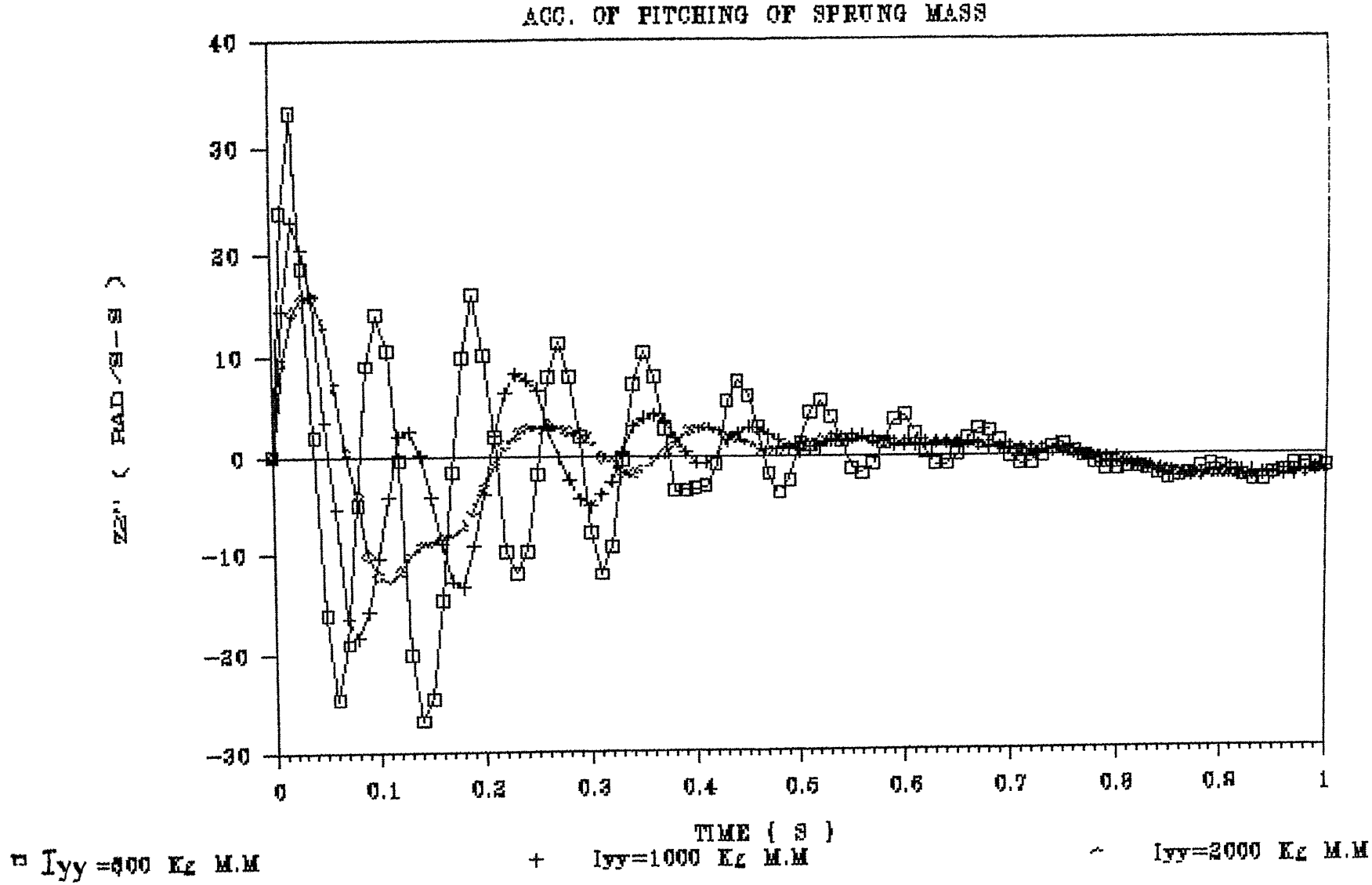

FIG 3.6j VARIATION IN ACCELEARTION OF PITCHING OF THE SPRUNG MASS WITH THE PITCHING MOMENT OF INERTIA

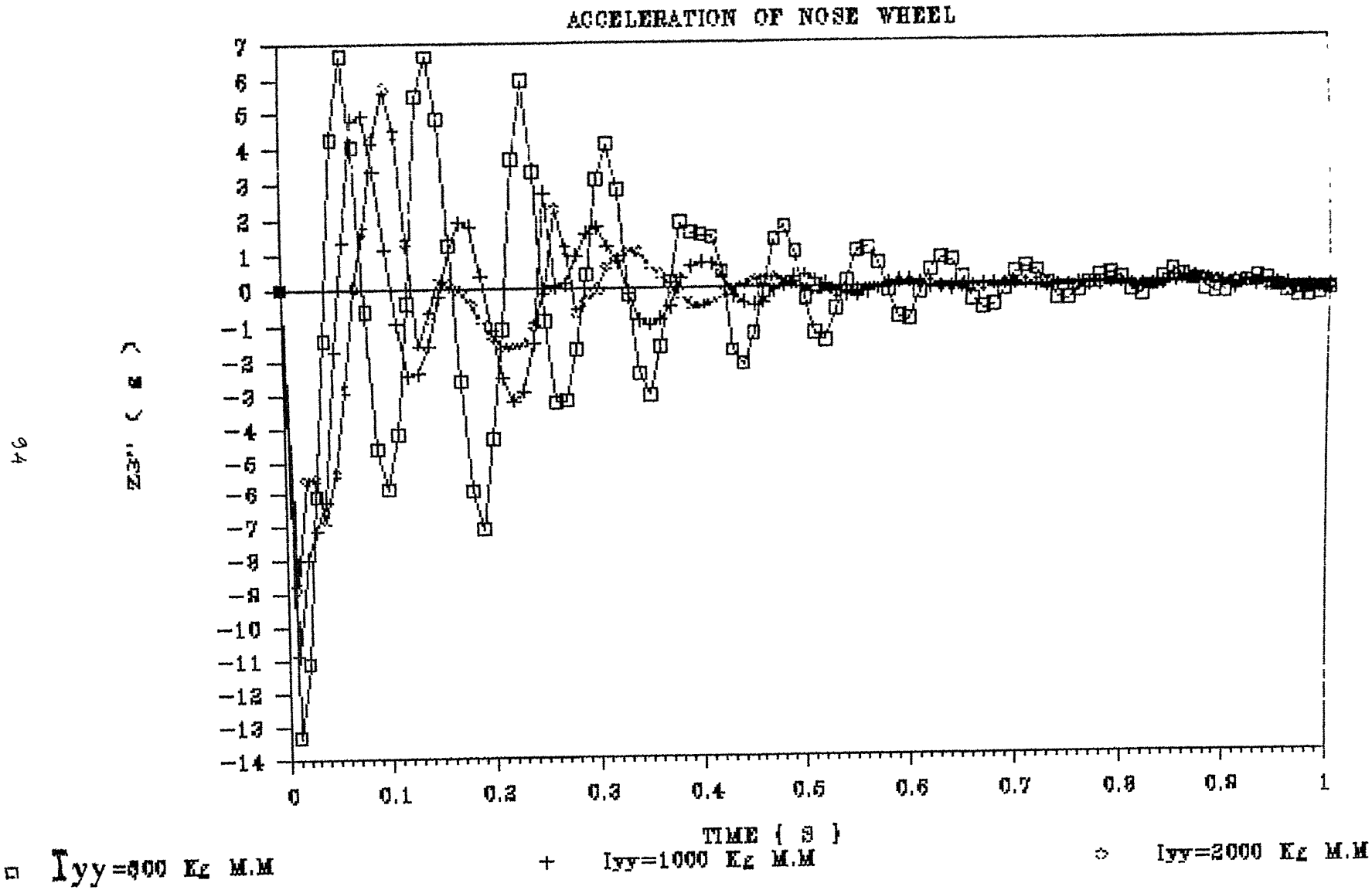

FIG 3.6k VARIATION IN ACCELERATION OF THE NOSE WHEEL WITH THE PITCHING MOMENT OF INERTIA

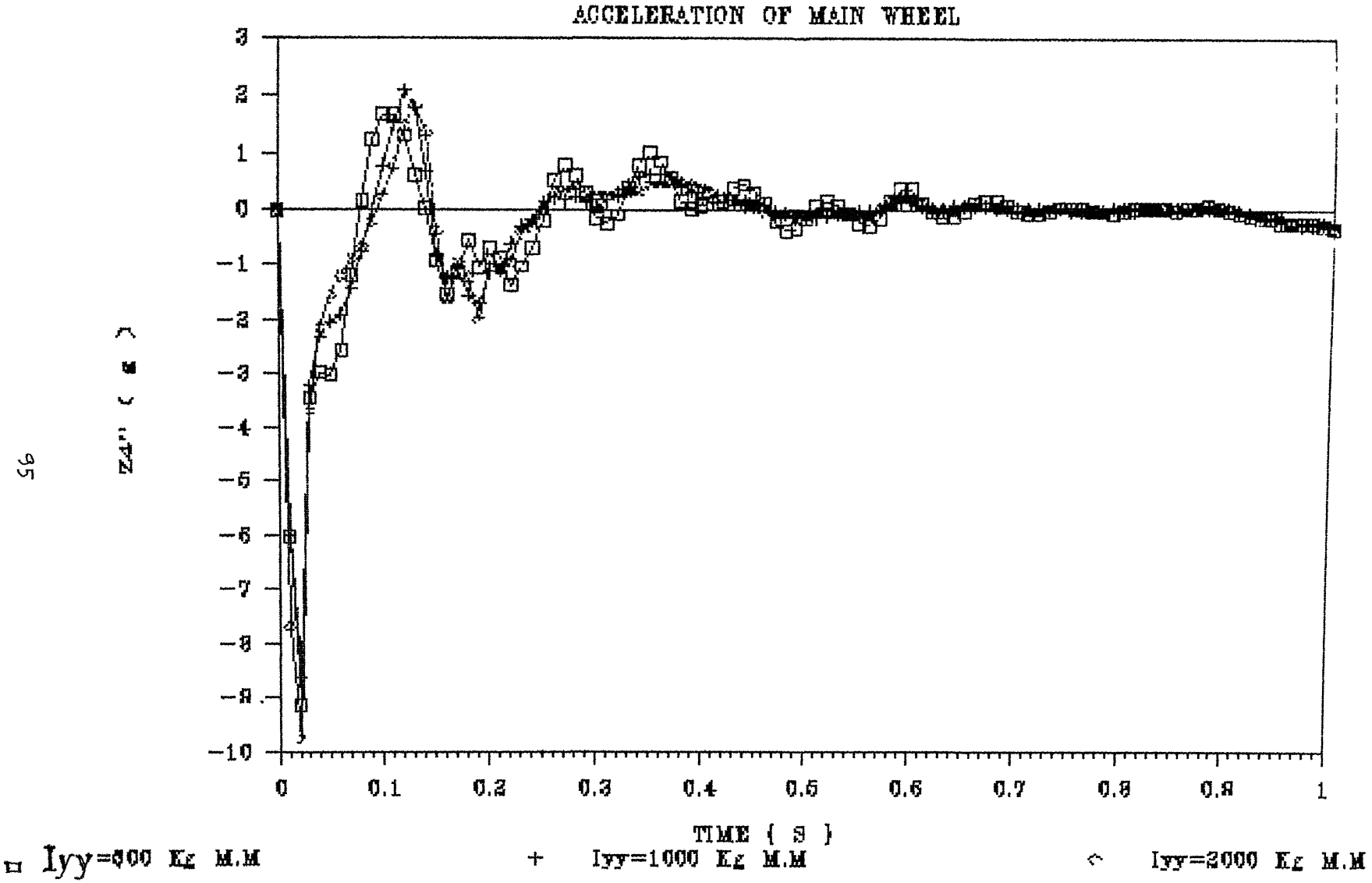

FIG 3.61 VARIATION IN ACCELERATION OF THE MAIN WHEEL WITH THE PITCHING MOMENT OF INERTIA

locations close to the aircraft center of gravity, its effect at points farther from aircraft center of gravity can be critical

3.2.2 Effect of Landing Gear Location with respect to the Aircraft center of Gravity

The changes in aircraft dynamic response with variations in landing gear layout is shown in figures 3.7a to 3.7l. While the wheel-base is kept constant at 3.45 meters for the present study, three values 40 cm, 56 cm and 70 cm, for the distance l_m of the main wheel from the aircraft center of gravity were used in generating the response data. From the figures,

(a). Relative location of landing gears do not have considerable effect on the airframe response except at peak values. For the case studied, closer the location of the main gear to the aircraft center of gravity higher the peak displacement (3.7a), the peak velocity (3.7e), peak acceleration (3.7i). The main wheel response is also found to be similar to that of the airframe (3.7d, 3.7h and 3.7l)

(b). Displacement, velocity and acceleration response of the aircraft in pitching is observed to be higher for lower value of l_m (figures 3.7b, 3.7f and 3.7j)

(c). For the lowest value of l_m, the nose wheel of the aircraft is found to leave the runway during rebound (figure 3.7c)

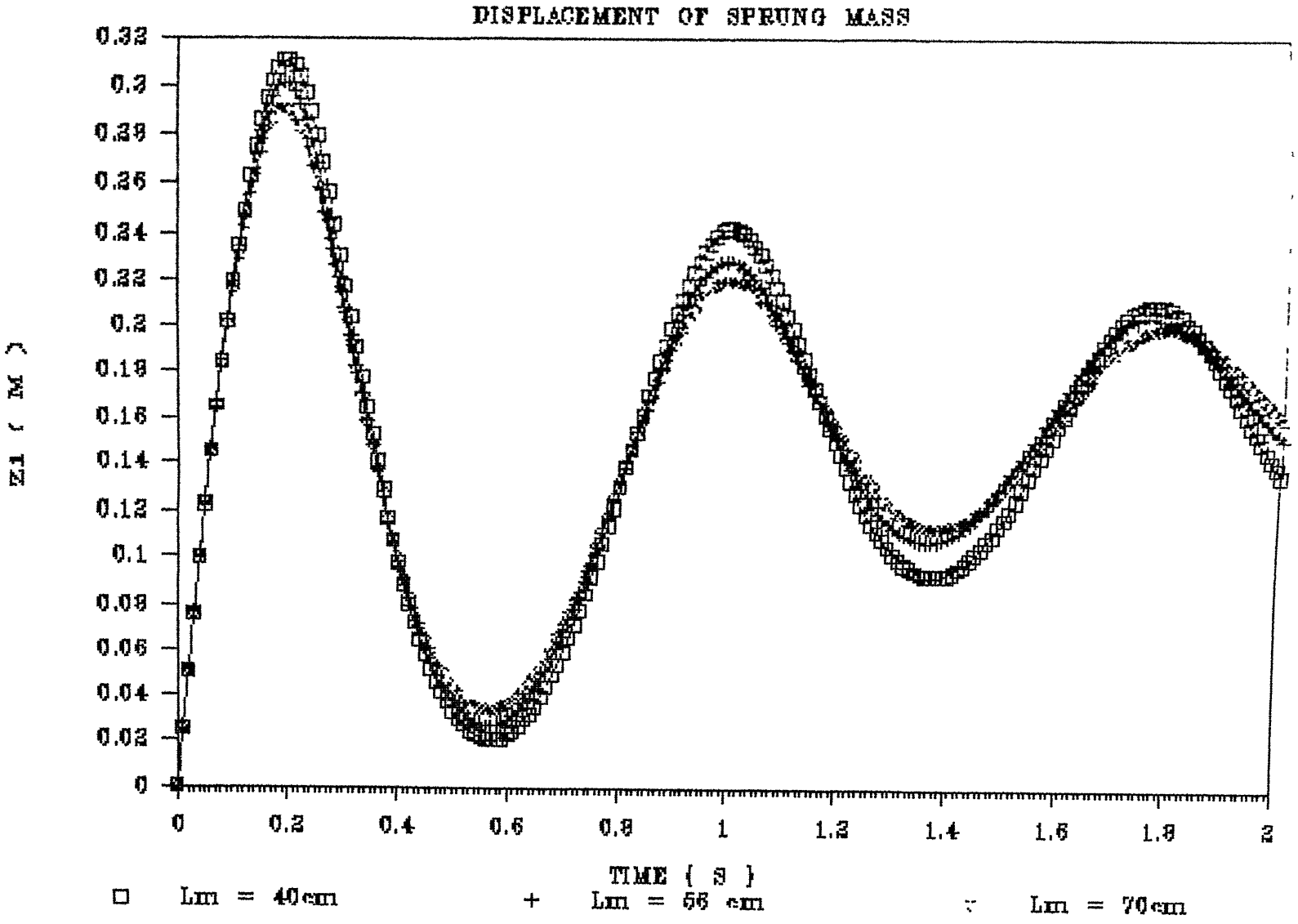

FIG 3.7a VARIATION IN DISPLACEMENT OF THE SPRUNG MASS WITH THE DISTANCE OF AIRCRAFT C.G FROM THE MAIN GEARS

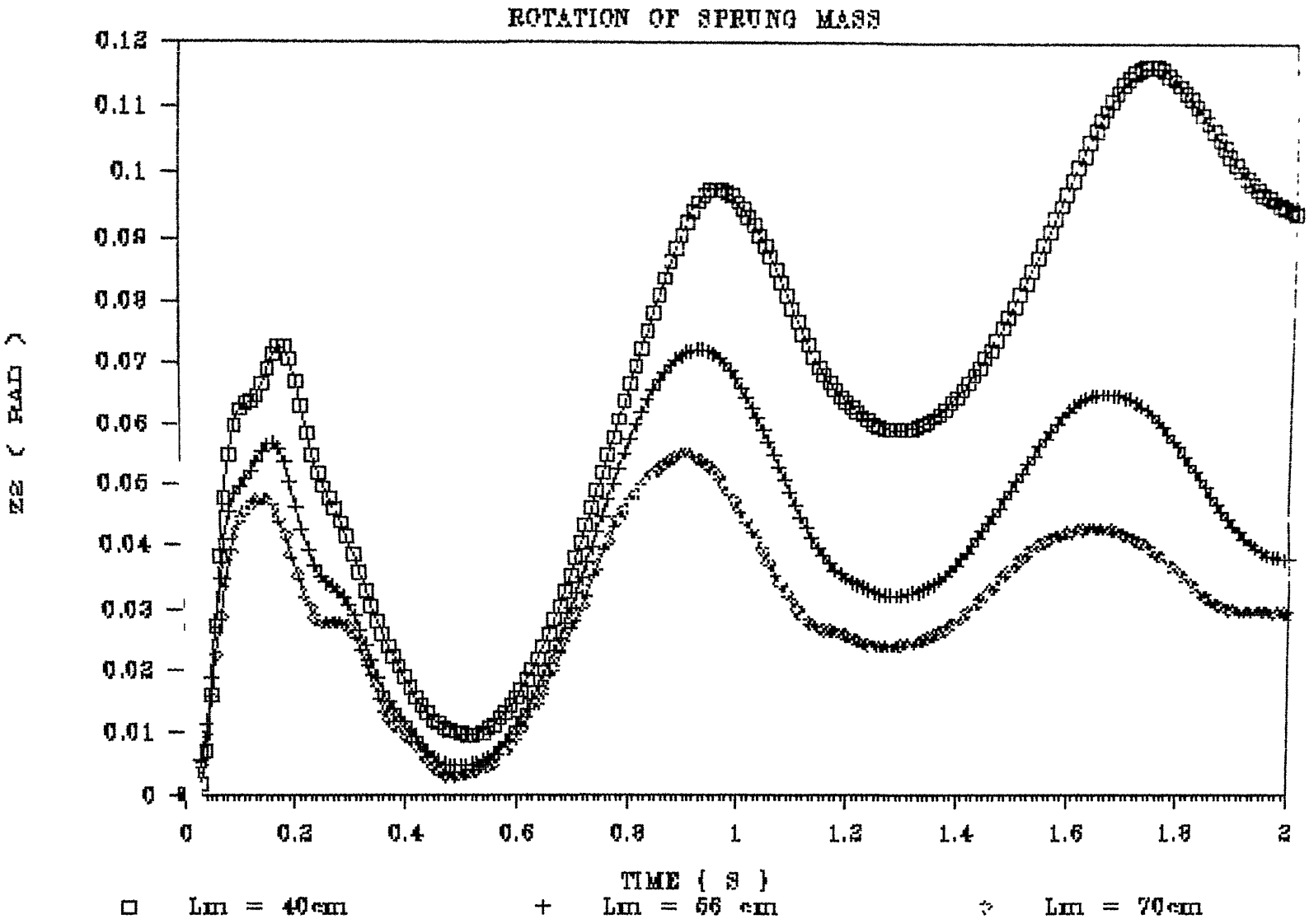

FIG 3.7b VARIATION IN PITCHING RESPONSE OF THE SPRUNG MASS WITH THE DISTANCE OF AIRCRAFT C.G FROM THE MAIN GEARS

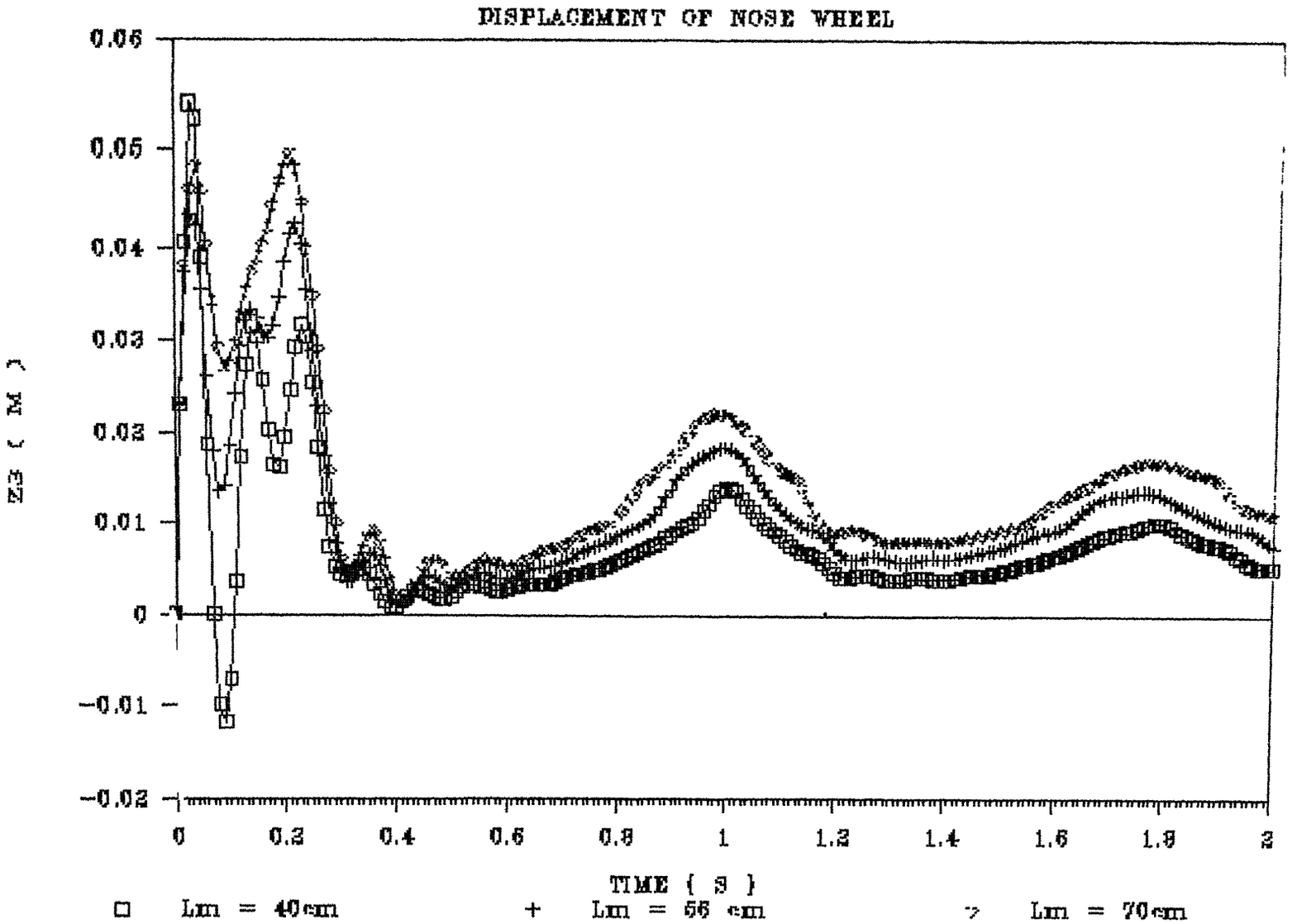

FIG 3.7c VARIATION IN DISPLACEMENT OF THE NOSE WHEEL WITH THE DISTANCE OF AIRCRAFT C.G FROM THE MAIN GEARS

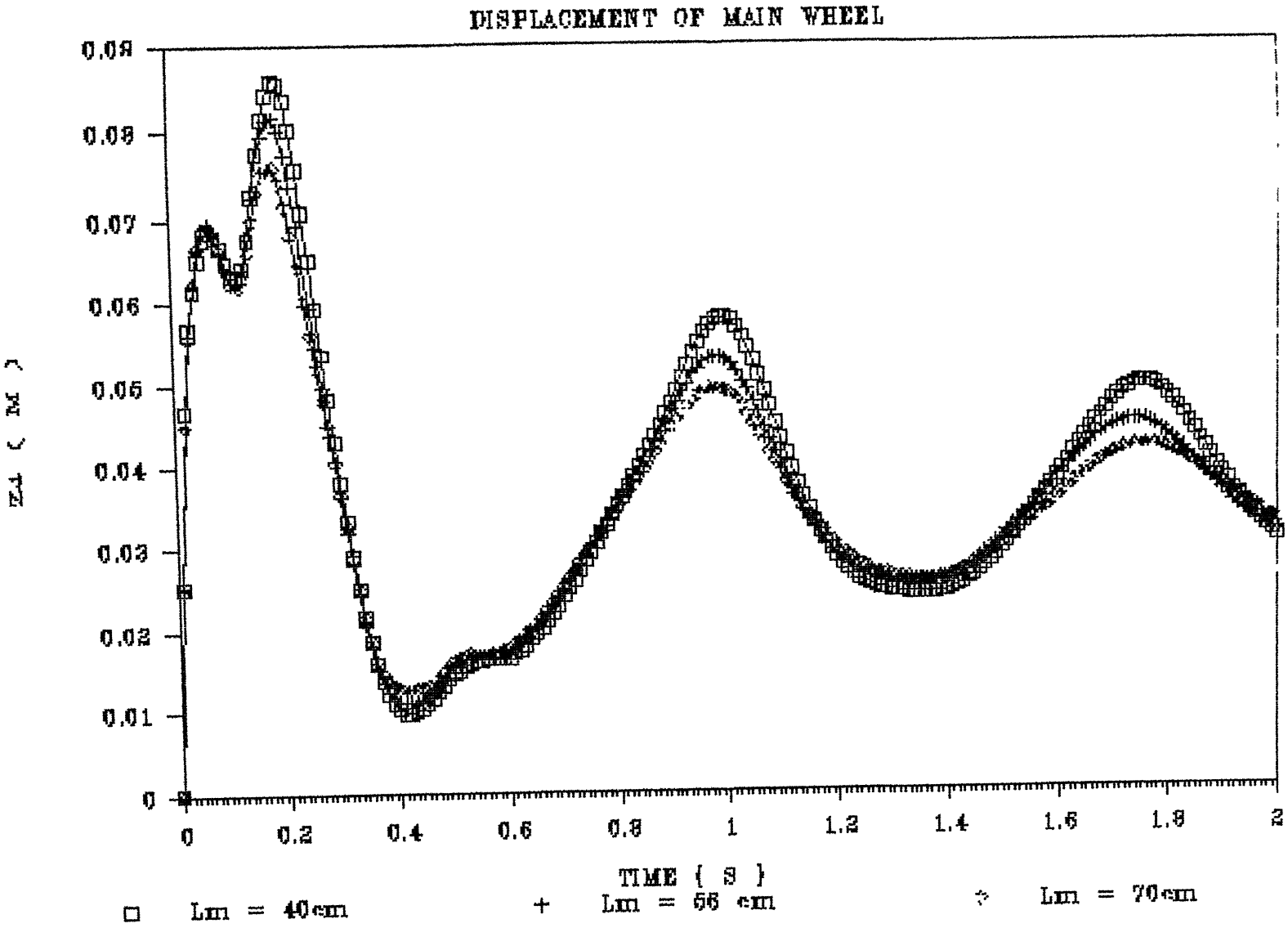

FIG 3.7d VARIATION IN DISPLACEMENT OF THE MAIN WHEEL WITH THE DISTANCE OF AIRCRAFT C.G FROM THE MAIN GEARS

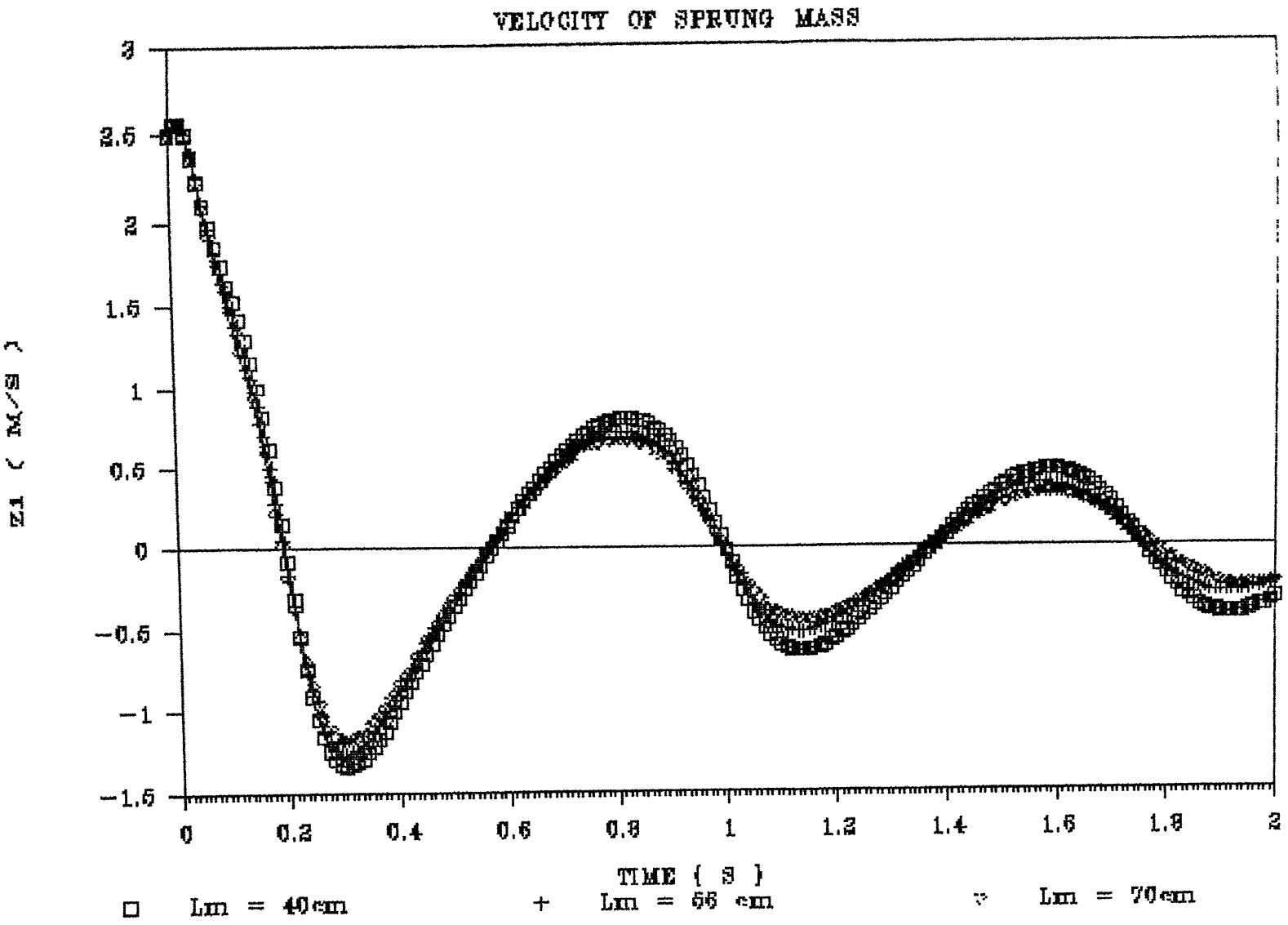

FIG 3.7e VARIATION IN VELOCITY OF THE SPRUNG MASS WITH THE DISTANCE OF AIRCRAFT C.G FROM THE MAIN GEARS

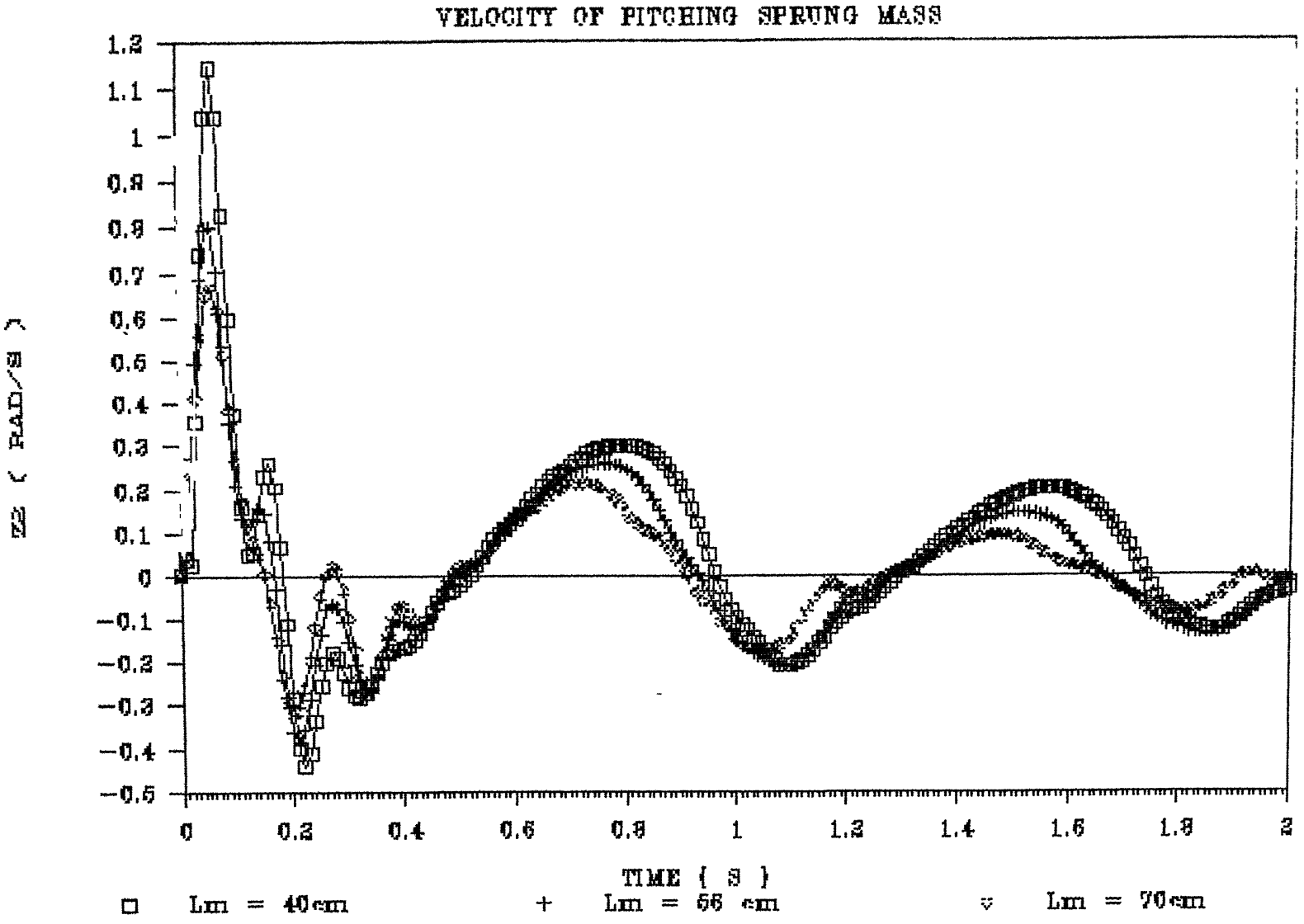

FIG 3.7f VARIATION IN VELOCITY OF PITCHING OF THE SPRUNG MASS WITH THE DISTANCE OF AIRCRAFT C.G FROM THE MAIN GEARS

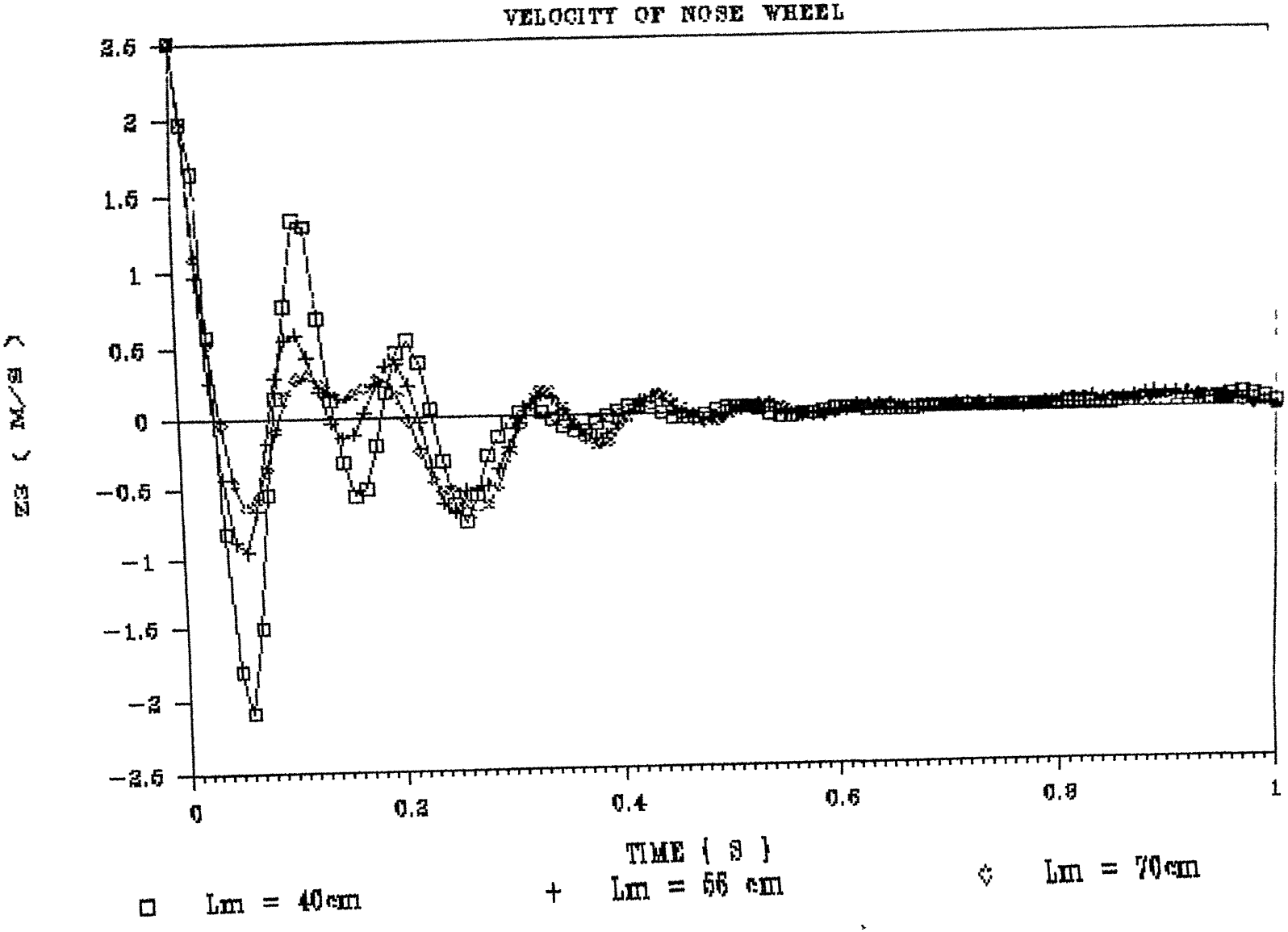

FIG 3.7a VARIATION IN VELOCITY OF THE NOSE WHEEL WITH THE DISTANCE OF AIRCRAFT C.G FROM THE MAIN GEARS

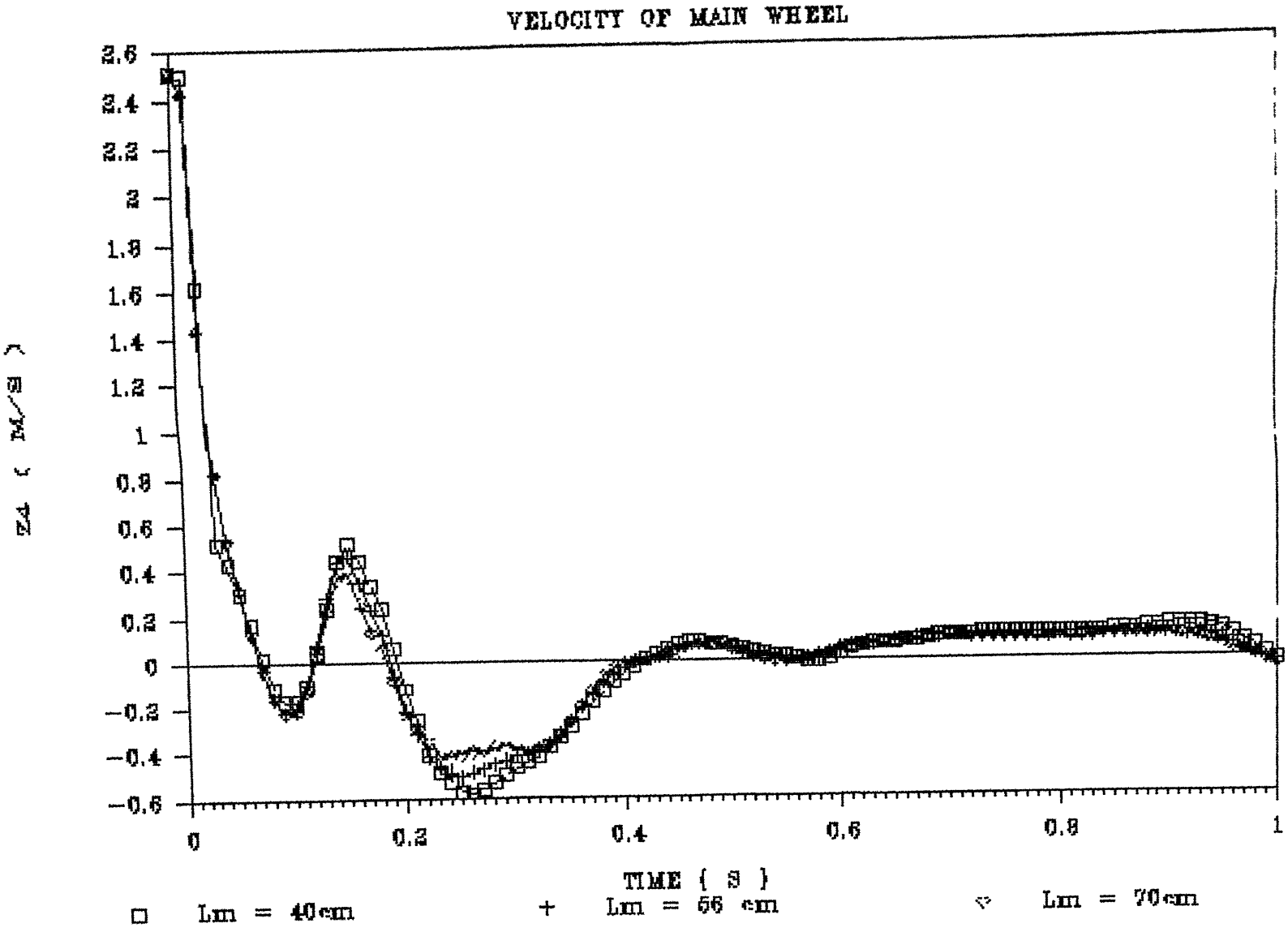

FIG 3.7h VARIATION IN VELOCITY OF THE MAIN WHEEL WITH THE DISTANCE OF AIRCRAFT C.G FROM THE MAIN GEARS

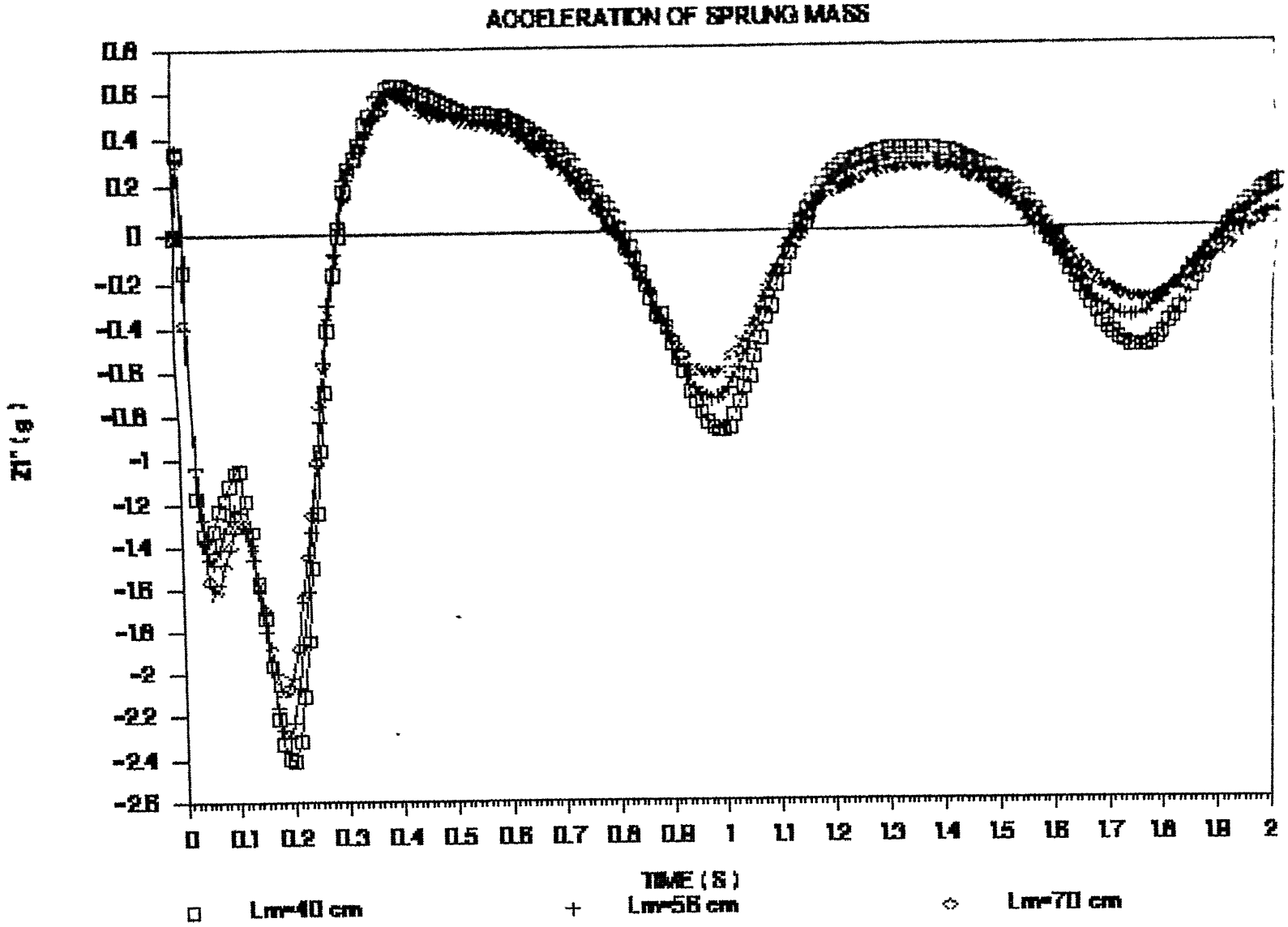

FIG 3.7i VARIATION IN ACCELERATION OF THE SPRUNG MASS WITH THE DISTANCE OF AIRCRAFT C.G FROM THE MAIN GEARS

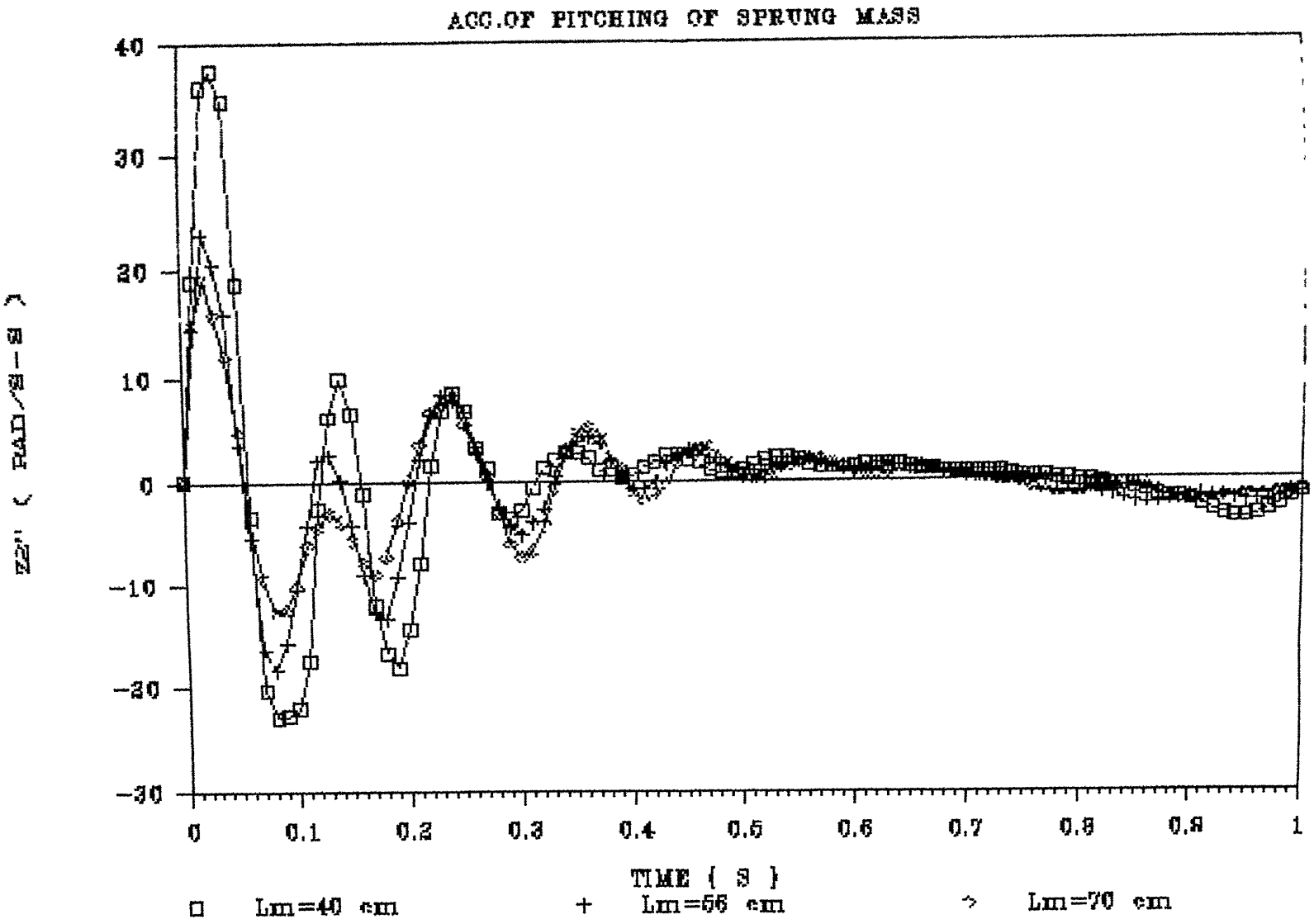

FIG 3.7j VARIATION IN ACCELEARTION OF PITCHING OF THE SPRUNG MASS WITH THE DISTANCE OF AIRCRAFT C.G FROM THE MAIN GEARS

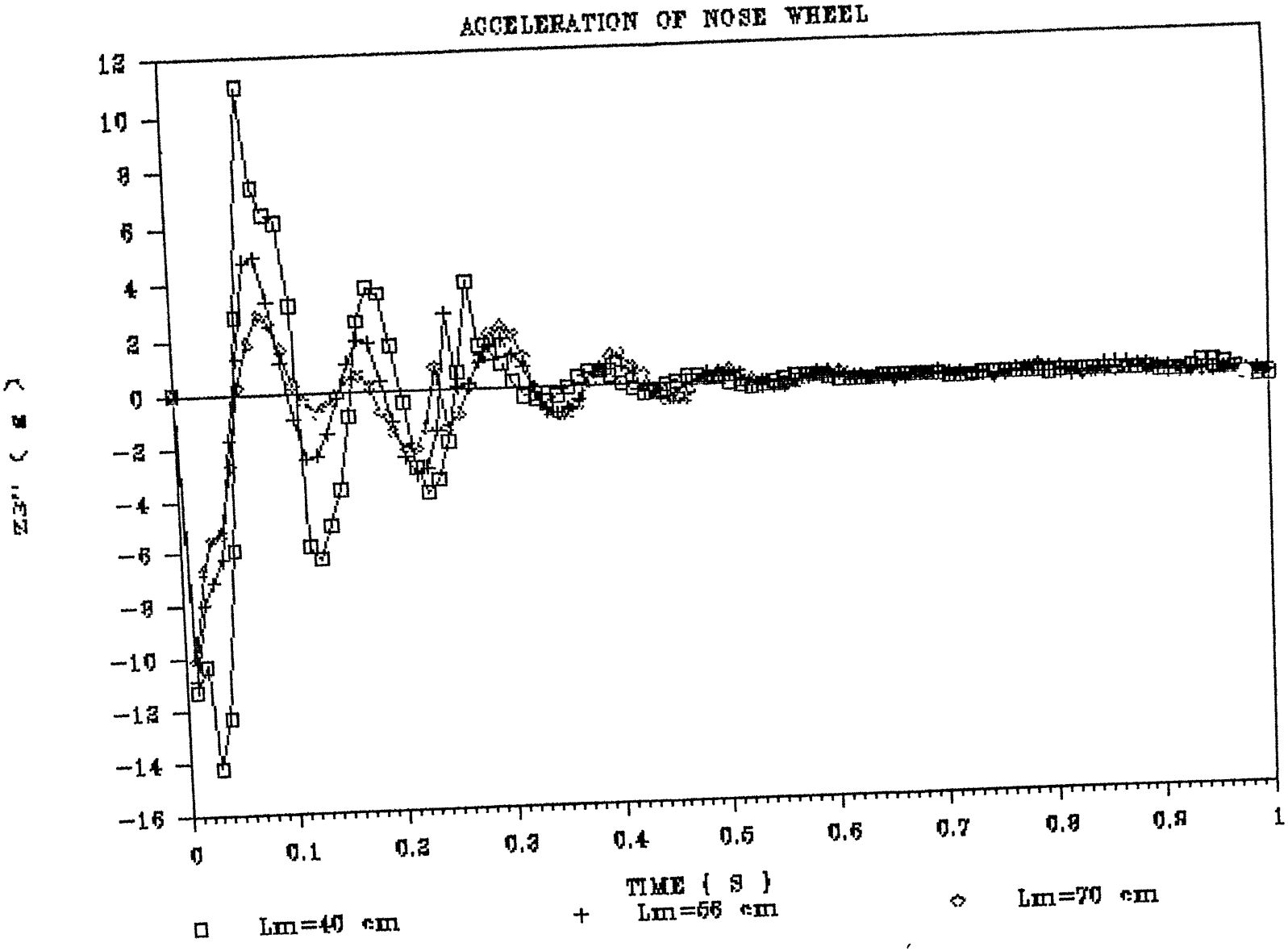

FIG 3.7k VARIATION IN ACCELERATION OF THE NOSE WHEEL WITH THE DISTANCE OF AIRCRAFT C.G FROM THE MAIN GEARS

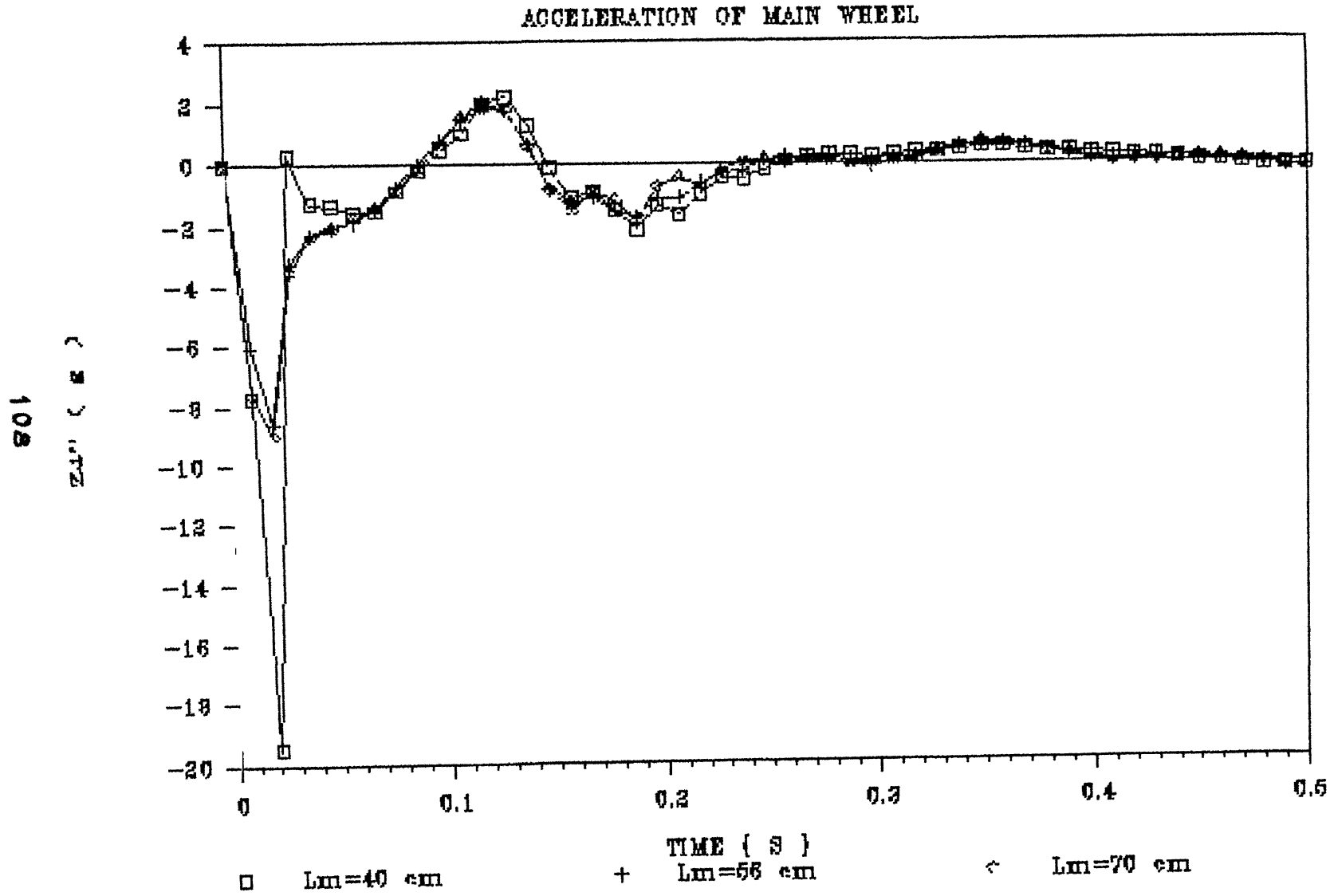

FIG 3.71 VARIATION IN ACCELERATION OF THE MAIN WHEEL WITH THE DISTANCE OF AIRCRAFT C.G FROM THE MAIN GEARS

(d).Considerable difference in the peak value of acceleration of the main and nose wheel can be observed with changes in l_m (figures 3.7k and 3.7l)

Tables 5a, 5b and 5c gives the peak values of displacement and acceleration of the sprung mass, the nose wheel and main wheel with variations in the distance of the main gear from the aircraft center of gravity.

	Maximum Displacements			
L_m cm	a/c c.g cm	pitching rad	nose-wheel cm	main-wheel cm
40.0	30.9	0.118	5.4	8.6
56.0	30.0	0.074	4.8	8.2
70.0	28.8	0.053	4.8	7.5

TABLE 5a Variation in the extreme values of displacement with the distance of the main gear from the aircraft center of gravity

L_m	Maximum Acceleration of the airframe			
	vertical translation		pitching of c.g	
	positive	negative	positive	negative
cm	g	g	rad/s.s	rad/s.s
40.0	0.68	2.4	37.0	23.0
56.0	0.60	2.3	23.0	18.0
70.0	0.58	2.1	19.0	14.0

TABLE 5b Variation in the extreme values of acceleration of the airframe with the distance of the main gear from the aircraft center of gravity

L_m	Maximum Acceleration of the wheels			
	Nose wheel		Main wheel	
	positive	negative	positive	negative
cm	g	g	g	g
40.0	11.0	14.0	2.2	19.5
56.0	4.9	11.0	2.1	8.8
70.0	2.9	10.0	2.1	8.4

TABLE 5c Variation in the extreme values of acceleration of the wheels with the distance of the main gear from the aircraft center of gravity

Thus even for the same mass of the aircraft and for the same initial conditions the relative location of the main and nose gears with respect to the aircraft center of gravity has a considerable influence on the dynamic response of the aircraft.

CHAPTER 4

CONCLUSIONS AND RECOMMENDATIONS

An analysis of a two degrees of freedom heave model of an articulated landing gear has been presented The variation in the dynamic response of the system to changes in the orifice discharge coefficient, polytropic index of air compression process, diameter of the orifice, initial air volume and initial air pressure have been studied.

The study on the heave model has been extended to a heave-pitch model of an aircraft with articulated nose landing gear and telescopic main gears. The effect of the radius of gyration and the landing gear layout configuration also has been included.

4.1 CONCLUSIONS

The main conclusions obtained regarding the landing gear behaviour at touch-down from this study on the heave and the heave-pitch models are presented below.

4.1.1 The Heave model

The conclusions drawn from the study of this model are :

1. The aircraft response is strongly affected by the orifice diameter and the coefficient of discharge. The changes in their values influence the response characteristics in a similar fashion. The peak displacement response increases

with increase in the values of these parameters.

2. Even though the thermodynamic law of air compression process in the shock strut is not well known, it has only a marginal influence on the dynamic response of the aircraft.
3. Initial air volume and air pressure do not have appreciable effect on the aircraft response. However the static equilibrium position of the airframe is affected to some extent.
4. The performance parameters for a landing gear are usually difficult to evaluate accurately. Some extra allowance should be made in the shock strut to take into account the variable nature of some of these parameters.

4.1.2 The Heave - Pitch Model

The study of the heave-pitch model helps in drawing the following conclusions :

1. Even for the same mass of the aircraft its relative distribution plays an important part in landing performance especially at locations farther from the aircraft center of gravity.
2. The layout of the landing gear with the aircraft center of gravity significantly alters the peak values of response. Landing gear locations may be optimized for improving performance.

4.2 SUGGESTIONS FOR FURTHER INVESTIGATION

The following suggestions are made for further study in this area.

1. A more realistic estimate of aircraft response can be obtained by accounting for the flexibility of airframe.
2. In practice the landing may not be perfectly symmetric. The effect of aircraft roll and that of the cross wind on the airframe may be considerable and should be studied to obtain the maximum landing stresses.
3. The influence of runway unevenness on the aircraft during its ground roll in landing can be studied and their effect on structural fatigue and fatigue of undercarriage load attachment points determined.
4. Pilot's input to the system at touch-down can also be included.

REFERENCES

1.Mitchell,C.G.B.," Some Measured and Calculated Effects of Runway Unevenness on a Supersonic Transport Aircraft " , *Aeronautical Journal*, V.75, No:725, May 1971, pp.339-343.

2.Woods,A.G.," Human Response to Low Frequency Sinusoidal and Random Vibrations ", Aircraft Engineering, V.39, No:7, July 1967, pp.6-14.

3.Conway,H.G., *Landing gear Design*, Chapman & Hall, 1958.

4.Schlaefke,K.," On Force-Deflection Diagrams of Airplane Shock Absorber Struts ", *NACA* TM 1373, 1944.

5.Milwitzky,B. and Cook,F.E.," Analysis of Landing Gear Behavior ", *NACA* TR 1154, 1963.

6.Wahi,M.K.," Oleopneumatic Shock-Strut Dynamic Analysis and its Real Time Simulation ", *Journal of Aircraft*, V.13, No:4, April 1976, pp.303-308.

7.Wahi,M.K.," Oil Compressibility and Polytropic Air Compression Analysis of Oleopneumatic Shock-Struts " *Journal of Aircraft*, V.13, No:7, July 1976, pp.527-530.

8.Nightingale,J.," The Determination of Orifice Parameters for Shock-Absorbers ", *Aircraft Engineering*, V.23, No:271, Sept. 1951, pp.261-262 .

9.Jayarami Reddy,P., Nagaraj,V.T. and Ramamurthi,V.," Analysis of Articulated Landing Gear Behavior ", *Sixth IFTOMM Congress on Theory of Machines and Mechanisms*, New Delhi, Dec. 1983.

10.Jayarami Reddy,P., Nagaraj,V. and Ramamurthi,V.," Analysis of Semi-Levered Suspension Landing Gear with Some Parametric Study", *Journal of Dynamic Systems, Measurements and Control*,V.106,No.3,Sept.1984,pp.218-224.

APPENDIX

AIRCRAFT DATA

I. GENERAL

1. Gross weight of the aircraft	= 40750.7 Newtons
2. Weight of the main wheels	= 627.0 Newtons
3. Weight of the nose wheels	= 55.0 Newtons
4. Wheel base	= 3.45 m
5. Distance of aircraft c.g from main wheels	= 0.56 m
6. Distance of aircraft c.g from nose wheel	= 2.89 m
7. Distance of aerodynamic center from aircraft c.g	= 0.2m
8. Moment of inertia of the aircraft in pitching	= 1000 kg-m^2
9. Landing velocity of aircraft	= 54 m/s

II. CHARECTERISTICS OF THE SHOCK STRUT OF THE MAIN GEAR

1. Coefficient of discharge	= 0.6
2. Coefficient of seal friction	= 0
3. Mass density of fluid	= 850 kg/cu.m
4. Orifice area	= 2.405 sq.cm

5.Hydraulic area	= 63.6 sq.cm
6.Pneumatic area	= 49.5 sq.cm
7.Extended air pressure	= 140 psi
8.Extended air volume	= 1462.0 c.c
9.Index for air compression	= 1.3
10.Initial oil volume	= 1950.0 c.c
11.Full stroke	= 26.4 cm
12.Coefficient of friction at bearings	= 0.05 to 0.1
13.Axial distance between bearings	= 20.0 cm
14.Coulomb friction	= Ω
15.Preload	= 4780.8 Newtons

III.CHARECTERISTICS OF THE SHOCK STRUT OF THE NOSE GEAR

1.Coefficient of discharge	= 0.6
2.Coefficient of seal friction	= Ω
3.Mass density of fluid	= 850 kg/cu.m
4.Orifice area	= 0.216 sq.cm
5.Hydraulic area	= 42.0 sq.cm
6.Pneumatic area	= 27.2 sq.cm
7.Extended air pressure	= 400 psi
8.Extended air volume	= 273.6 c.c
9.Index for air compression	= 1.3
10.Initial oil volume	= 400.0 c.c
11.Full stroke	= 9.3 cm

12.Coefficient of friction at bearings = 0.05 to 0.1

13.Axial distance between bearings = 5.0 cm

14.Coulomb friction = Ω

15.Preload = 7512.4 Newtons

IV. MAIN TYRES

1.Radius = 25.0 cm

2.Spin-up time = 0.038 secs

3.Polar moment of inertia = 3217 kg-cm^2

4.Load-deflection curve given

V. NOSE TYRE

1.Radius = 20.0 cm

2.Spin-up time = 0.030 secs

3.Polar moment of inertia = 1173 kg-cm^2

4.Load-deflection curve given

V. DIMENSIONS OF THE NOSE GEAR (refer fig 2.1)

A_1 = 6.0 cm

A_2 = 20.0 cm

A_3 = 40.0 m

A_4 = 3.0 cm

A_5 = 50.0 cm

θ = 30°

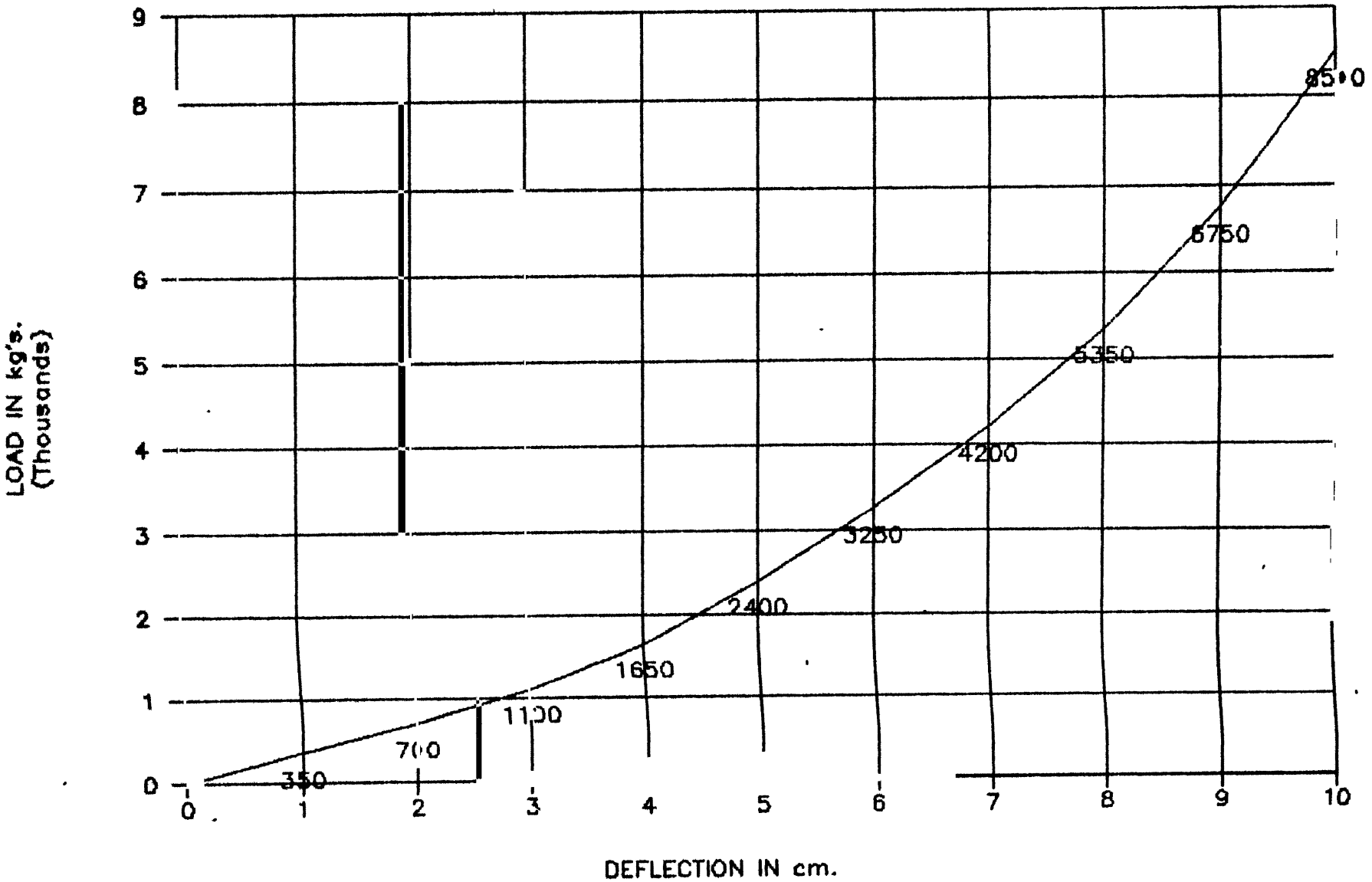

Fig. A1 Load - deflection curve for the main wheel.

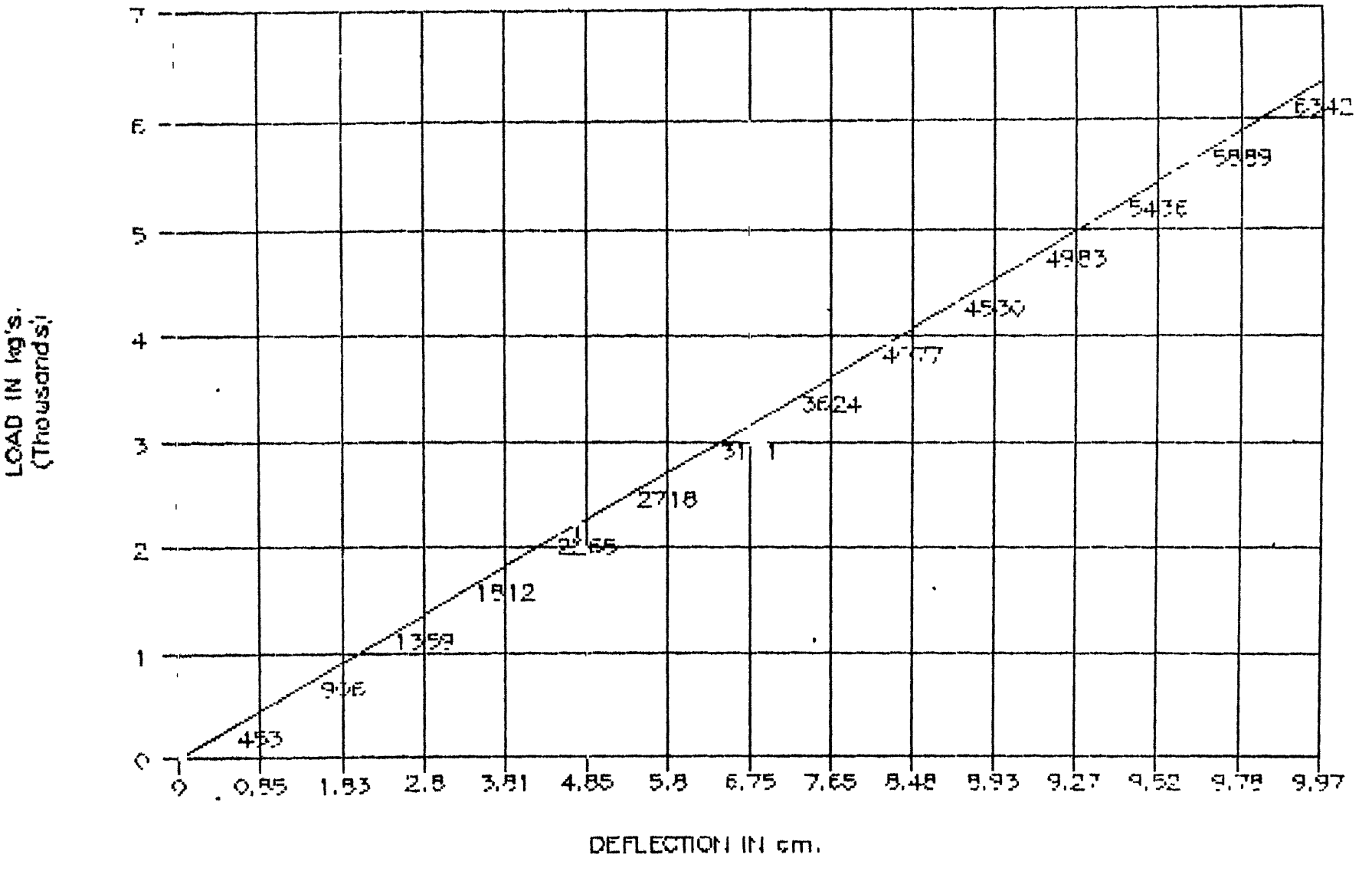

Fig. A2 Load - deflection curve for the nose wheel.